USC–SIPI REPORT #222

EVAM: An Eigenvector-Based Algorithm for Multichannel Blind Deconvolution of Input Colored Signals

by

M. I. Gurelli and C. L. Nikias

September 1992

Signal and Image Processing Institute
UNIVERSITY OF SOUTHERN CALIFORNIA
Department of Electrical Engineering-Systems
3740 McClintock Avenue, Room 400
Los Angeles, CA 90089-2564 U.S.A.

EVAM: AN EIGENVECTOR-BASED ALGORITHM FOR MULTICHANNEL BLIND DECONVOLUTION OF INPUT COLORED SIGNALS

M. İ. GÜRELLİ, Student Member, IEEE, and C. L. NIKIAS, Fellow, IEEE

Signal and Image Processing Institute, Department of Electrical Engineering-Systems,
University of Southern California,
3740 McClintock Ave., Los Angeles, CA 90089-2564

ABSTRACT

In this paper, the development of a new algorithm is presented for the deconvolution of an unknown, possibly colored signal which is observed through two or more unknown channels described by rational system transfer functions. The algorithm not only reconstructs the input signal but also determines the roots (poles and zeros) of the multipath channels with enhanced accuracy, even in the presence of additive Gaussian noise at the channel outputs. This algorithm can also be used in multichannel system identification problems. In this paper, it is assumed that the additive noise processes at the outputs of the unknown channels are white. Results are presented for both noise-free and noisy cases.

This work was supported by the National Science Foundation under grant MIP-9206829 and the Office of Naval Research under contract N00014-92-J-1034.

1. Introduction

The problem of deconvolving signals observed through two or more unknown multipath channels arises in many signal processing applications (see, for example, [1]). The unknown channels are usually modeled by rational system transfer functions with additive noise at their outputs. The problem of recovering the input of the channels is based on the determination of the orders and roots (poles and zeros) of the channel transfer functions.

Several of the existing multichannel adaptive system identification algorithms, generally fail in determining the orders and roots of the channels with sufficient accuracy. The reason is mainly twofold: First, the performance surface may be highly ill-conditioned which leads to very slow convergence rates for stochastic gradient type algorithms [2]-[4]. Secondly, the possible presence of additive colored noise (with generally unknown variances) leads to a bias in the root locations determined by any algorithm based on the minimization of a mean-squared error cost function. These include the RLS-type algorithms [5]-[8].

The aforementioned limitations of the existing algorithms motivated us to develop a new algorithm for determining the orders and the roots of the unknown channels with enhanced accuracy. The algorithm is based on eigenvalue decomposition of the data matrix. It also employs a balancing technique to compensate the different noise levels at the channel outputs in order to reduce the bias of the estimated root locations. In this paper, the noise processes at the channel outputs are assumed to be white. The analysis for colored noise is currently under investigation, and will be reported in the future.

The organization of the paper is as follows. In Section 2, a detailed problem formulation is given. Also the adaptive system employed by the algorithm is described. In Section 3, basic lemmas used in the development of the algorithm are given and their possible utilizations are explained. In Section 4, the basic framework utilized in the development of the algorithm is described. In Section 5, some experimental results are given. Finally, some conclusions are given in Section 6. The proofs of several lemmas stated in this paper may be found in the Appendices.

2. Problem Formulation

2.1. The Unknown System Model

The block diagram of the unknown system model is shown in Figure 1(a). It is assumed that the number of channels, p, is greater than one.

All channels are fed by the same unknown signal $x(t)$ which needs to be recovered from the observations $\{ u_i(t) ; i = 1,2,...,p \}$. It is assumed that $x(t)$ is a wide-sense stationary and possibly colored signal with

$$E\{x(t)\} = 0 \quad \forall t \tag{1}$$

where $E\{.\}$ denotes the statistical expectation operator.

The channels of the unknown system are described by the rational system transfer functions $C_i(z^{-1})$, given by,

$$C_i(z^{-1}) = \frac{\mathcal{N}_i(z^{-1})}{\mathcal{D}_i(z^{-1})} \qquad i = 1,...,p \tag{2}$$

where $\mathcal{N}_i(z^{-1})$ and $\mathcal{D}_i(z^{-1})$ are polynomials in z^{-1} of orders N_i and D_i, respectively. Although the powers of z appearing in $\mathcal{D}_i(z^{-1})$ are strictly non-positive, they are allowed to be both negative and positive in $\mathcal{N}_i(z^{-1})$. It is assumed that the channel transfer functions $C_i(z^{-1})$ have no common poles or zeros. Furthermore, we assume that the roots (poles and zeros) as well as the orders of the channels are unknown and that there are no roots at the origin.

The channel output signals, denoted by $r_i(t)$, $i = 1,...,p$, are corrupted by additive noise processes $n_i(t)$, $i = 1,...,p$. The following assumptions are made about the noise processes,

$$E\{n_i(t)\} = 0 \;\; i = 1,...,p \tag{3}$$

$$E\{n_i(t)n_i(t+\tau)\} = \begin{cases} \sigma_i^2 & \text{for } \tau = 0, \\ 0 & \text{for } \tau \neq 0 \end{cases} \qquad i = 1,...,p \;\; ; \tag{4}$$

that is the noise processes are zero mean white sequences with variances σ_i^2. We have assumed different noise variances for each channel to set up a more realistic model. Furthermore, we assume that,

$$E\{x(t)n_i(t+\tau)\} = 0 \;\; i = 1,...p \;\text{ and }\; \forall t,\tau \tag{5}$$

and

$$E\{n_i(t)n_j(t+\tau)\} = 0 \;\; i \neq j \;\text{ and }\; \forall t,\tau. \tag{6}$$

The noisy channel output signals given by,

$$u_i(t) = r_i(t) + n_i(t) \;\; i = 1,...,p \tag{7}$$

are the only observations of this multichannel system. Our aim is to recover the unknown signal $x(t)$ from observations $u_i(t)$, $i = 1,...,p$. More specifically, we want to determine the

orders N_i and D_i, and the roots of the multipath channel transfer functions $C_i(z^{-1})$, $i = 1, ..., p$, with enhanced accuracy.

For simplicity, but without loss of generality, we will consider the two-channel case (that is, $p = 2$) in the remaining part of this paper. However, the results will be applicable to the general case where $p > 2$.

2.2. The Adaptive System Model

Consider the two channel adaptive system shown in Figure 1(b). The channel transfer functions are finite order polynomials $\mathcal{W}_1(z^{-1})$ and $\mathcal{W}_2(z^{-1})$ in z^{-1} with orders W_1 and W_2, respectively. That is, we have,

$$\mathcal{W}_1(z^{-1}) = w_{1,0} + w_{1,1}z^{-1} + ... + w_{1,W_1}z^{-W_1} \tag{8}$$

$$\mathcal{W}_2(z^{-1}) = w_{2,0} + w_{2,1}z^{-1} + ... + w_{2,W_2}z^{-W_2} \tag{9}$$

where the polynomial coefficients $w_{1,i}$ $i = 0, ..., W_1$ and $w_{2,i}$ $i = 0, ..., W_2$ are assumed to be adaptable via some algorithm. A convenient way to represent the polynomials in (8) and (9) is to put the polynomial coefficients into a vector form. That is,

$$\underline{w}_1 = [\, w_{1,0},\ w_{1,1},\ \ldots,\ w_{1,W_1}\,]^T \tag{10}$$

$$\underline{w}_2 = [\, w_{2,0},\ w_{2,1},\ \ldots,\ w_{2,W_2}\,]^T \quad . \tag{11}$$

In other words, the polynomials $\mathcal{W}_1(z^{-1})$ and $\mathcal{W}_2(z^{-1})$ are the *equivalent polynomials* of the vectors $\underline{w}_1$ and $\underline{w}_2$, respectively. The composite tap weight vector is defined as,

$$\underline{w} = [\, \underline{w}_1^T \ \ \underline{w}_2^T \,]^T_{(W_1+W_2)\times 1} \quad . \tag{12}$$

The two channels of the adaptive system are fed by the observation signals $u_1(t)$ and $u_2(t)$, respectively. For convenience, we define the following composite regressor,

$$\underline{u}(t) = [\, u_1(t),\ u_1(t-1),\ \ldots,\ u_1(t-W_1),\ u_2(t),\ u_2(t-1),\ \ldots,\ u_2(t-W_2)\,]^T \quad . \tag{13}$$

Therefore, the error signal $e(t)$ is given by,

$$e(t) = \underline{w}^T \underline{u}(t) \quad . \tag{14}$$

Many of the existing multichannel system identification algorithms such as the stochastic gradient type algorithms [2]-[4], and the RLS based algorithms [5]-[8], aim to minimizing

the mean-squared error (MSE) defined by,

$$\mathcal{E}(\underline{w}) = \sum_{t=0}^{T} |e(t)|^2 \tag{15}$$

(or a weighted version of it) where T is the length of the time interval.

Assuming that the observation signals $u_1(t)$ and $u_2(t)$ are noiseless (that is, $\sigma_1 = \sigma_2 = 0$), and assuming that the adaptive channel orders are chosen such that,

$$W_1 = N_2 + D_1 \tag{16}$$

$$W_2 = N_1 + D_2 \quad , \tag{17}$$

the unique family of solutions for $\mathcal{W}_1(z^{-1})$ and $\mathcal{W}_2(z^{-1})$ that minimize $\mathcal{E}(\underline{w})$ is given by,

$$\mathcal{W}_1(z^{-1}) = \alpha \mathcal{N}_2(z^{-1}) \mathcal{D}_1(z^{-1}) \tag{18}$$

$$\mathcal{W}_2(z^{-1}) = -\alpha \mathcal{N}_1(z^{-1}) \mathcal{D}_2(z^{-1}) \tag{19}$$

where α is an arbitrary constant. With the above family of solutions, we have,

$$\mathcal{E}(\underline{w}) = 0 \quad . \tag{20}$$

Thus, if we can find some vector $\underline{w}$ for which $\mathcal{E}(\underline{w}) = 0$, then the set of roots of the channel transfer functions, $C_1(z^{-1})$ and $C_2(z^{-1})$, can be obtained by factorizing $\mathcal{W}_1(z^{-1})$ and $\mathcal{W}_2(z^{-1})$.

A similar result can be obtained if one of the orders, W_1 or W_2, is chosen as in (16) or (17), and the other is overestimated. Without loss of generality, assume that $W_1 = N_2 + D_1$ and $W_2 > N_1 + D_2$. More specifically, let $W_2 = N_1 + D_2 + \Delta K$. Then the unique family of solutions for $\mathcal{W}_1(z^{-1})$ and $\mathcal{W}_2(z^{-1})$ for which $\mathcal{E}(\underline{w}) = 0$ is given by,

$$\mathcal{W}_1(z^{-1}) = \alpha \mathcal{N}_2(z^{-1}) \mathcal{D}_1(z^{-1}) \tag{21}$$

$$\mathcal{W}_2(z^{-1}) = -\alpha \mathcal{N}_1(z^{-1}) \mathcal{D}_2(z^{-1}) \theta_{\Delta K}(z^{-1}) \tag{22}$$

where $\theta_{\Delta K}(z^{-1})$ is a polynomial of order ΔK having all of its roots at the origin, and α is an arbitrary constant.

The minimization of $\mathcal{E}(\underline{w})$ can be achieved by employing an adaptive control method such as the LMS algorithm or the multichannel RLS algorithms (conventional or modular). Computer experiments have revealed that the stochastic gradient type algorithms (such as LMS) may have extremely poor performance in such applications. This is mainly due to

large eigenvalue spread which leads to very slow convergence rates [2]-[4]. The least-squares based algorithms (such as the conventional or modular multichannel RLS [5]-[8]) are not, in general, affected by the eigenvalue spread. However, it can be shown that the presence of noise in the observation signals $u_1(t)$ and $u_2(t)$ causes a bias in the estimated root locations of the channel transfer functions $C_1(z^{-1})$ and $C_2(z^{-1})$, when $\mathcal{E}(\underline{w})$ is employed.

In this paper, we assume that the orders N_1, N_2, D_1, D_2, of the channel transfer functions, $C_1(z^{-1})$ and $C_2(z^{-1})$, are unknown. Therefore, we may not be able to choose the adaptive system orders W_1 and W_2 as in (16) and (17). However, we assume that the adaptive system orders can be overestimated, in the sense that,

$$W_1 \geq N_2 + D_1 \tag{23}$$

$$W_2 \geq N_1 + D_2 \quad . \tag{24}$$

Our objective is twofold:

i) to determine the *minimal orders* of the adaptive channels, that is,

$$W_{1,m} = N_2 + D_1 \tag{25}$$

$$W_{2,m} = N_1 + D_2 \quad , \tag{26}$$

and

ii) to estimate the root locations of the channel transfer functions $C_1(z^{-1})$ and $C_2(z^{-1})$ with sufficient accuracy.

To achieve these goals, we make use of certain lemmas described in the next section.

3. Basic Lemmas Leading to the New Algorithm

3.1. Extraneous Zeros of the Adaptive Systems

As described in Section 2, if the channel orders are known and the channel noise variances are zero, there is a direct relationship between the roots of the unknown channels and the roots of the adaptive systems. However, in general, the equalities in (16) and (17) do not hold and thus the minimal roots can not be determined by (18) and (19). Therefore, we need a similar relationship between the minimal roots of the unknown channels and the roots of the adaptive systems when the orders are overdetermined (that is, the case where (23) and (24) hold by strict inequality). More specifically, we will assume that,

$$W_1 = N_2 + D_1 + K_1 \tag{27}$$

$$W_2 = N_1 + D_2 + K_2 \tag{28}$$

where K_1 and K_2 account for the extraneous zeros of $\mathcal{W}_1(z^{-1})$ and $\mathcal{W}_2(z^{-1})$, respectively.

Also, we will assume that the channel output noise variances are zero, that is

$$\sigma_1 = \sigma_2 = 0 \implies u_1(t) = r_1(t) \text{ and } u_2(t) = r_2(t) \quad \forall t \quad . \tag{29}$$

For the discussion in this part, we will make use of the following matrix

$$A_u = \begin{bmatrix} \underline{u}^T(T) \\ \underline{u}^T(T-1) \\ \vdots \\ \underline{u}^T(1) \end{bmatrix} \tag{30}$$

where $\underline{u}(t)$ is the composite regressor defined by (13). Also, we define the following sample correlation matrix,

$$R_u = A_u^T A_u \quad . \tag{31}$$

Lemma 1:

Assuming $\sigma_1 = \sigma_2 = 0$ and $x(t)$ is persistently exciting, for sufficiently large T, we have,

$$\dim(\aleph(R_u)) = K + 1 \tag{32}$$

where $\aleph(.)$ denotes the null space of a matrix, and dim(.) denotes the dimension of a vector space. Also,

$$K = \min\{K_1, K_2\}. \tag{33}$$

A proof of the above lemma is given in Appendix A. In Lemma 1 the term *persistently exciting* refers to the fact that the input signal $x(t)$ is such that for sufficiently long time of observations, the matrix A_u achieves the greatest possible rank that is possible for any input signal and for arbitrarily long observation time.

Corollary 1:

With the assumptions in Lemma 1, R_u will have exactly $(K+1)$ zero eigenvalues and $(K+1)$ linearly independent eigenvectors corresponding to these eigenvalues.

The proof of the above corollary is obvious.

In this paper, we will denote the eigenvectors corresponding to the $(K+1)$ zero eigenvalues of R_u as $\underline{q}_i$, $i = 1, ..., (K+1)$.

Lemma 2:

Assuming $\sigma_1 = \sigma_2 = 0$, the error signal $e(t)$ can be made identically zero for all t by the following family of system transfer functions for the adaptive channels,

$$W_1(z^{-1}) = \alpha N_2(z^{-1})\mathcal{D}_1(z^{-1})\theta_1(z^{-1}) \quad (34)$$

$$W_2(z^{-1}) = -\alpha N_1(z^{-1})\mathcal{D}_2(z^{-1})\theta_2(z^{-1}) \quad (35)$$

where the polynomials $\theta_1(z^{-1})$ and $\theta_2(z^{-1})$ have orders K_1 and K_2, respectively, and they have exactly the same factorizations except for the one with the larger order having all of its extraneous zeros at the origin. Also, α appearing in (34) and (35) is an arbitrary constant.

A proof of the above lemma is obvious.

Without loss of generality, assuming that $K_2 \geq K_1$ and defining $\Delta K = (K_2 - K_1)$, we may write the family of solutions given by (34) and (35) as,

$$W_1(z^{-1}) = \alpha N_2(z^{-1})\mathcal{D}_1(z^{-1})\theta_1(z^{-1}) \quad (36)$$

$$W_2(z^{-1}) = -\alpha N_1(z^{-1})\mathcal{D}_2(z^{-1})\theta_1(z^{-1})\theta_{\Delta K}(z^{-1}) \quad (37)$$

where $\theta_{\Delta K}(z^{-1})$ is a polynomial of order ΔK having all of its roots at the origin.

Corollary 2:

Assuming $\sigma_1 = \sigma_2 = 0$ and $x(t)$ is persistently exciting, the error signal $e(t)$ can be made identically zero for all t *if and only if* the transfer functions for the adaptive channels are of the form,

$$W_1(z^{-1}) = \alpha N_2(z^{-1})\mathcal{D}_1(z^{-1})\theta_1(z^{-1}) \quad (38)$$

$$W_2(z^{-1}) = -\alpha N_1(z^{-1})\mathcal{D}_2(z^{-1})\theta_2(z^{-1}) \quad (39)$$

where the polynomials $\theta_1(z^{-1})$ and $\theta_2(z^{-1})$ have orders K_1 and K_2, respectively, and they have exactly the same factorizations except for the one with the larger order having all of its extraneous zeros at the origin. Also, α appearing in (38) and (39) is an arbitrary constant.

A proof of the above corollary is given in Appendix B.

Therefore, any solution for the adaptive channel transfer functions $W_1(z^{-1})$ and $W_2(z^{-1})$ that make $e(t) = 0$ $\forall t$ will have K (where K is as defined in (33)) common zeros appearing exactly at the same locations. The other zeros will be at different locations since we assumed that the unknown channels have no poles or zeros in common. Furthermore, the locations of the K common zeros are completely arbitrary.

The following corollary forms the basis of a root detection algorithm.

Corollary 3:

Assume that the eigenvectors $\underline{q}_i$, $i = 1,...,(K+1)$, corresponding to the $(K+1)$ zero eigenvalues are partitioned as in (12). Let these partitions be denoted as $\underline{q}_{i,1}$, $\underline{q}_{i,2}$ $i = 1,...,K$. Let,

$$Q_{i,1}(z^{-1}) = \underline{q}_{i,1}^T \cdot [1,\ z^{-1},\ ...,\ z^{-W_1}]^T \quad i = 1,...,K \tag{40}$$

$$Q_{i,2}(z^{-1}) = \underline{q}_{i,2}^T \cdot [1,\ z^{-1},\ ...,\ z^{-W_2}]^T \quad i = 1,...,K \quad . \tag{41}$$

That is, $Q_{i,1}(z^{-1})$ and $Q_{i,2}(z^{-1})$ are the *equivalent polynomials* of the vectors $\underline{q}_{i,1}$ and $\underline{q}_{i,2}$, respectively. Then, the minimal roots of $Q_{i,1}(z^{-1})$, $i = 1,...,K$, (or, $Q_{i,2}(z^{-1})$) will be exactly at the same locations. The extraneous roots will, in general, be at different locations. Furthermore, for a given $i \in \{1,...,K\}$, the minimal roots of $Q_{i,1}(z^{-1})$ and $Q_{i,2}(z^{-1})$ will be at completely different locations and the extraneous zeros will be at exactly the same locations.

The proof of the above corollary follows easily from the previous lemmas and corollaries.

3.2. Noise Balancing Method

Our discussion thus far is based on the assumption that $\sigma_1 = \sigma_2 = 0$, which may be unrealistic in practice. In general, there is always noise and, furthermore, the noise variances at each channel may be different; that is, $\sigma_1, \sigma_2 \neq 0$ and $\sigma_1 \neq \sigma_2$.

In this case, we will no longer have the equalities described in (29). To make the preceeding analysis useful in the presence of noise, we will develop in this section a noise balancing method.

We define a noise matrix

$$A_n = \begin{bmatrix} \underline{n}(T) \\ \underline{n}(T-1) \\ \vdots \\ \underline{n}(1) \end{bmatrix} \tag{42}$$

where $\underline{n}(t)$ is the composite noise regressor defined by

$$\underline{n}(t) = [\, n_1(t),\ ...,\ n_1(t-W_1),\ n_2(t),\ ...,\ n_2(t-W_2)\,]^T \quad . \tag{43}$$

The noiseless channel output matrix is defined by

$$A_r = \begin{bmatrix} \underline{r}(T) \\ \underline{r}(T-1) \\ \vdots \\ \underline{r}(1) \end{bmatrix} \tag{44}$$

where the regressor $\underline{r}(t)$ is defined by

$$\underline{r}(t) = [\, r_1(t),\ \ldots,\ r_1(t-W_1),\ r_2(t),\ \ldots,\ r_2(t-W_2)\,]^T \quad . \tag{45}$$

Thus, we have,

$$A_u = A_r + A_n \tag{46}$$

which implies that

$$R_u = R_r + R_n + 2A_r^T A_n \quad , \tag{47}$$

where

$$R_r = A_r^T A_r \quad \text{and} \quad R_n = A_n^T A_n \quad . \tag{48}$$

Note that the matrix R_r obeys all the results obtained for R_u in the previous section. This is because, for $\sigma_1 = \sigma_2 = 0$, we have $R_u = R_r$. Thus, even in the noisy case, R_r will have a total of $(K+1)$ zero eigenvalues (where K is given by (33)) and the corresponding linearly independent eigenvectors will have the properties described in the previous section. However, since $\underline{r}(t)$ is not observable, we have to develop results for $\underline{u}(t)$.

In the forthcoming analysis, we will assume that the data length is sufficiently long so that the assumptions given by (3)-(6) imply that,

$$R_n = \text{diag}(\sigma_1, \ldots, \sigma_1, \sigma_2, \ldots, \sigma_2) \tag{49}$$

and

$$A_r^T A_n \approx \underline{O} \tag{50}$$

where $\underline{O}$ is the zero matrix. Therefore, we have,

$$R_u \approx R_r + \text{diag}(\underbrace{\sigma_1, \ldots, \sigma_1}_{W_1+1}, \underbrace{\sigma_2, \ldots, \sigma_2}_{W_2+1}) \quad . \tag{51}$$

From (51), it is clearly seen that for $\sigma_1 \neq \sigma_2$, the eigenvalues and eigenvectors will not in general obey the conditions established in the preceeding section. However, the following lemma will enable some kind of noise balancing.

Lemma 4:

Assume that R_r has eigenvalues $\lambda_{r,i}$ and corresponding eigenvectors $\underline{v}_{r,i}$ for $i = 1, \ldots, (W_1 + W_2 + 2)$. Consider the matrix,

$$\tilde{R}(\xi) = R_u + P(\xi) \tag{52}$$

where $P(\xi)$ is defined by

$$P(\xi) = \text{diag}(\underbrace{\xi, ..., \xi}_{W_1+1}, \underbrace{0, ..., 0}_{W_2+1}) \quad . \tag{53}$$

If $\xi = \sigma_2 - \sigma_1$, then the matrix $\tilde{R}(\xi)$ will have the eigenvalues $(\lambda_{r,i} + \sigma_2)$ and the corresponding eigenvectors will still be $\underline{v}_{r,i}$ for $i = 1, ..., (W_1 + W_2 + 2)$.

The proof of the above lemma is obvious.

Therefore, for $\xi = \sigma_2 - \sigma_1$, the matrix $\tilde{R}(\xi)$ will have $K + 1$ minimum eigenvalues which will be equal to σ_2 and the corresponding eigenvectors will obey the Corollary 3.

In cases where σ_1 and σ_2 are very different, regardless of the data length, the root locations estimated from the eigenvectors of R_u may be extermely biased. To remove this effect, the noise balancing method described by (52) may be employed. However, since the noise variances are not generally known a priori, an adaptive method for determining the parameter ξ must be developed based on a suitable criterion. The choice of this criterion is currently under investigation.

4. The "Algorithmic Fractals" Framework

The exact formulation in this Section will be carried out for the noiseless case. However, it can be approximated for the noisy case. The minimal systems we are searching for are described by the transfer functions

$$\mathcal{W}_{1,m}(z^{-1}) = \alpha \mathcal{N}_2(z^{-1}) \mathcal{D}_1(z^{-1}) \tag{54}$$

$$\mathcal{W}_{2,m}(z^{-1}) = -\alpha \mathcal{N}_1(z^{-1}) \mathcal{D}_2(z^{-1}) \quad . \tag{55}$$

These solutions may be obtained from (36)-(37) by letting $\theta_1(z^{-1}) = 1$. It should be reminded that the transfer function $\theta_{\Delta K}(z^{-1})$ may appear either in $\mathcal{W}_{1,m}(z^{-1})$ or $\mathcal{W}_{2,m}(z^{-1})$. Its presence in the final solution is not a problem since it represents a system with all of its roots appearing at $z = 0$.

Each polynomial pair $\mathcal{Q}_{i,1}(z^{-1})$ and $\mathcal{Q}_{i,2}(z^{-1})$ obtained from the eigenvectors $\underline{q}_i$ for $i = 1, ..., K$ can be written as

$$\mathcal{Q}_{i,1}(z^{-1}) = \mathcal{W}_{1,m}(z^{-1}) \theta_{i,1}(z^{-1}) \tag{56}$$

$$\mathcal{Q}_{i,2}(z^{-1}) = \mathcal{W}_{2,m}(z^{-1}) \theta_{i,1}(z^{-1}) \quad , \tag{57}$$

These equations represent K pairs of system transfer functions each of which is a minimum mean-squared error solution of the two channel system identification problem. Each pair,

$i = 1, ..., K$, of transfer functions will only differ from another by $\theta_{i,1}(z^{-1})$; the polynomials $\mathcal{W}_{1,m}(z^{-1})$, $\mathcal{W}_{2,m}(z^{-1})$ will always be the same, whatever the value of i.

These observations lead to an "algorithmic fractals framework": Each pair of transfer functions $\mathcal{Q}_{i,1}(z^{-1})$, $\mathcal{Q}_{i,2}(z^{-1})$ can be thought of as the output signals of a two-channel system where the channels have transfer functions $\mathcal{W}_{1,m}(z^{-1})$ and $\mathcal{W}_{2,m}(z^{-1})$, respectively, and input signal $\theta_{i,1}(z^{-1})$. This model is illustrated in Figure 2(a). Comparing Figure 2(a) with Figure 1(b) we see that the two block diagrams are essentially the same. Note that each of the K pairs of transfer functions given by (56),(57) represents a distinct experiment in which the system transfer functions are the same, but the input signals $\theta_{i,1}(z^{-1})$ are different.

The "algorithmic fractals" framework is analogous to the original problem formulation. The main difference is that in the original problem, the input and output signals were assumed to be stochastic power signals whereas now they are finite length deterministic energy signals.

The solution proceeds in a similar fashion as in the original problem, and it involves an adaptive finite impulse response system as shown in Figure 2(b). The channel outputs are now obtained by partitioning the eigenvectors $\underline{q}_i$ for $i = 1, ..., K$. Once the orders of the adaptive channels in Figure 2(b) are proposed, linear equations in terms of the channel transfer function coefficients are obtained. Finally a similar eigenvector analysis is carried out for this new system of equations. If the orders are correctly chosen, the channel transfer functions will be

$$\tilde{\mathcal{W}}_1(z^{-1}) = \mathcal{W}_2(z^{-1}) \tag{58}$$

$$\tilde{\mathcal{W}}_2(z^{-1}) = \mathcal{W}_1(z^{-1}) \tag{59}$$

5. Experimental Results

In this section, we will present several experimental results both for the case where $\sigma_1 = \sigma_2 = 0$ and also for the case where $\sigma_1 \neq 0$ and $\sigma_2 \neq 0$. In all experiments, we will assume that the pole and zero polynomials of the channels are given by

$$\mathcal{N}_1(z^{-1}) = 1.0 + 1.3z^{-1} + 0.44z^{-2} - 2.178z^{-3} \tag{60}$$

$$\mathcal{N}_2(z^{-1}) = 1.0 - 1.1z^{-1} + 0.28z^{-2} + 1.64z^{-3} + 0.16z^{-4} \tag{61}$$

$$\mathcal{D}_1(z^{-1}) = 1.0 - 0.6z^{-1} + 0.21z^{-2} + 0.224z^{-3} - 0.078z^{-4} \tag{62}$$

$$\mathcal{D}_2(z^{-1}) = 1.0 + 0.1z^{-1} + 0.49z^{-2} - 0.223z^{-3} - 0.096z^{-4} - 0.1837z^{-5} \tag{63}$$

and their orders are, $N_1 = 3, N_2 = 4, D_1 = 4, D_2 = 5$.

The minimal orders, $W_{1,m}$ and $W_{2,m}$, of adaptive channels will be both 8, and the corresponding minimal root locations are shown in Figure 3(a) and (b), respectively.

5.1. Noise-free Case

Experiment 1:

Assume that $W_1 = W_2 = 8$. Then the matrix R_u will have a single zero eigenvalue with the eigenvector $\underline{q}_1$. The family of solutions for $\mathcal{W}_1(z^{-1})$ and $\mathcal{W}_2(z^{-1})$ for which $\mathcal{E}(\underline{w}) = 0$ will be given by (18) and (19). Note that the polynomials $\mathcal{W}_1(z^{-1})$ and $\mathcal{W}_2(z^{-1})$ will be the same as the equivalent polynomials $\mathcal{Q}_{1,1}(z^{-1})$ and $\mathcal{Q}_{1,2}(z^{-1})$ of the vectors $\underline{q}_{1,1}$ and $\underline{q}_{1,2}$ respectively, where $\underline{q}_{1,1}$ and $\underline{q}_{1,2}$ are the partitions of $\underline{q}_1$ as described by (12).

Obviously, $K_1 = K_2 = 0$ and the polynomials $\mathcal{Q}_{1,1}(z^{-1})$ and $\mathcal{Q}_{1,2}(z^{-1})$ will have no common roots.

Figures 4(a) and (b) show the roots of $\mathcal{Q}_{1,1}(z^{-1})$ and $\mathcal{Q}_{1,2}(z^{-1})$, respectively. They are exactly at the locations shown in Figures 3(a) and (b).

Figures 5(a) and (b) show the root locations obtained by the LMS algorithm. Although the iterations go up to 30000, convergence is far from being achieved even in the known order case and the absence of noise. The results concerning the LMS algorithm will not be given in the forthcoming experiments since they are all unsatisfactory.

Figures 6(a) and (b) show the root locations obtained by the Modular Multichannel RLS algorithm applied for 1000 iterations. Clearly, similar results have been obtained by the eigenvector-based method.

Experiment 2:

Assume that $W_1 = W_2 = 10$. The matrix R_u will have eigenvectors, $\underline{q}_i$, $i = 1, 2, 3$, corresponding to the 3 zero eigenvalues. The number of extraneous roots are $K_1 = K_2 = 2$.

In Figures 7, 8, and 9, the root locations of the polynomials $\mathcal{Q}_{i,1}(z^{-1})$ and $\mathcal{Q}_{i,2}(z^{-1})$ for $i = 1, 2, 3$, are shown. A careful observation reveals that the minimal roots of the channels appear at the true locations as shown in Figure 3. Furthermore, for each pair of vectors $\underline{q}_{i,1}$ and $\underline{q}_{i,2}$, $i = 1, 2, 3$, the extraneous roots appear at exactly the same locations. On the other hand the true roots appear at different locations.

The results of the modular RLS algorithm applied for 1000 iterations is shown in Figure 10.. Since the modular RLS solution satisfies $\mathcal{E}(\underline{w}) = 0$, the corresponding equivalent polynomials can be factorized as in (38) and (39). Therefore the modular RLS solution has

2 ($= K_1 = K_2$) pairs of roots occuring at exactly the same locations.

Experiment 3:

Assume that $W_1 = W_2 = 14$. Thus the matrix R_u will have 7 eigenvectors $\underline{q}_i$, $i = 1,...,7$ corresponding to the zero eigenvalues. The number of extraneous roots are $K_1 = K_2 = 6$. Figures 11-17 show the root locations corresponding to each of the eigenvectors, $\underline{q}_i$, $i = 1,...,7$.

Figure 18 shows the results obtained by the modular RLS algorithm. The minimal roots appear at different locations and the 6 extraneous roots appear at exactly the same locations.

Obviously, for the noiseless case, the performances of the eigenvector based algorithm and the modular multichannel RLS algorithm are similar in terms of correctly determining the orders and roots of the unknown channel transfer functions.

5.2. Noisy Case

We repeated the three experiments described in the previous section by including the presence of additive, uniformly distributed, white noise with $\sigma_1 = \sigma_2 = 1$. This corresponds to SNR $\approx$ 10dB at both channel outputs. Since the noise variances have been chosen to be the same for both channels, noise balancing has not been used in the following experiments.

Experiment 4:

The adaptive channel orders are $W_1 = W_2 = 8$, which implies that $K_1 = K_2 = 0$. Therefore the matrix R_r defined in (48) will have a single zero eigenvalue. The corresponding eigenvector will approximately be equal to the eigenvector of R_u corresponding to its minimum eigenvalue.

In Figure 19, the roots obtained by the eigenvector of R_u corresponding to its minimum eigenvalue are illustrated. Although some of the roots appear to be very close to the true ones, there is a significant shift in the locations of some others.

In Figure 20, the modular multichannel RLS results are presented. Although the algorithm has been applied for 10000 iterations, the convergence is not satisfactory.

Experiment 5:

The adaptive channel orders are as in experiment 2. Figures 21-23 show the roots of the eigenvectors of R_u corresponding to the 3 minimum eigenvalues. Note that some of the roots are very close to their true locations. Also some of the extraneous roots may be easily determined since they appear approximately at the same locations for both channels and for

each of the three eigenvectors. However, it seems difficult to determine the exact orders.

In Figure 24, the modular multichannel RLS results are shown. The results are far from being satisfactory. The eigenvector-based method seems to give a better insight to the true orders and root locations of the channels.

Experiment 6:

In this experiment, the adaptive channel orders are chosen as in experiment 3. Figures 25-31 show the roots obtained by the eigenvectors of R_u corresponding to the 7 minimum eigenvalues.

In Figure 32, the modular multichannel RLS results are shown. Although in the presence of noise, both the eigenvector decomposition and the modular multichannel RLS seem to perform badly, it is clear that the eigenvector decomposition gives a better idea about the true root locations and true orders.

6. Conclusions

In this paper, results have been summarized which lead to the development of a new algorithm for the deconvolution of unknown signals observed through two or more unknown channels.

It has been observed through experimental results that some of the well known methods in the literature (LMS and modular multichannel RLS) perform quite unsatisfactorily in the presence of noise.

The eigenvector analysis of the sample correlation matrix R_u seems to be very promising for more accurately determining the roots and orders of the channels through which the unknown signal is observed. The cost of enhanced accuracy will probably be a significant increase in the computational requirements compared to many of the other algorithms.

Appendix A

Without loss of generality, assume that $K_1 = \min\{K_1, K_2\}$ and define $\Delta K = K_2 - K_1$. Let

$$W_1' = N_2 + D_1 \tag{A.1}$$

$$W_2' = N_1 + D_2 + \Delta K \tag{A.2}$$

and

$$A_{u'} = [\ A_{u_1'}\ \ A_{u_2'}\ ] \tag{A.3}$$

where

$$A_{u_1'} = \begin{bmatrix} \underline{u}_1'(T-K) \\ \vdots \\ \underline{u}_1'(1) \end{bmatrix} \quad \text{and} \quad A_{u_2'} = \begin{bmatrix} \underline{u}_2'(T-K) \\ \vdots \\ \underline{u}_2'(1) \end{bmatrix} \tag{A.4}$$

and the regressors, $\underline{u}_1'(t)$ and $\underline{u}_2'(t)$ are defined by

$$\underline{u}_1'(t) = [\ u_1(t),\ u_1(t-1),\ \ldots,\ u_1(t-W_1+K)\ ] \tag{A.5}$$

$$\underline{u}_2'(t) = [\ u_2(t),\ u_2(t-1),\ \ldots,\ u_2(t-W_1+K)\ ] \quad . \tag{A.6}$$

From the discussion leading to (21) and (22), we have

$$\dim(\aleph(A_{u'})) = 1 \tag{A.7}$$

where $\aleph(.)$ denotes the null space of a matrix, and dim(.) denotes the dimension of a vector space.

Let

$$\underline{u}_{1,t} = [\ u_1(t),\ u_1(t-1),\ \ldots,\ u_1(1)\ ]^T \tag{A.8}$$

$$\underline{u}_{2,t} = [\ u_2(t),\ u_2(t-1),\ \ldots,\ u_2(1)\ ]^T \tag{A.9}$$

and define

$$A_{u'}^{(m,n)} = [\ \underline{u}_{1,T-K+m},\ \cdots,\ \underline{u}_{1,T-K+1} \mid A_{u_1'} \mid \underline{u}_{2,T-K+n},\ \cdots,\ \underline{u}_{2,T-K+1} \mid A_{u_2'}\ ] \quad . \tag{A.10}$$

With this definition, we have,

$$A_{u'}^{(0,0)} = A_{u'} \qquad \text{and} \qquad A_{u'}^{(K,K)} = A_u \tag{A.11}$$

where A_u is given by (30).

Consider $A_{u'}^{(1,0)}$ given as

$$A_{u'}^{(1,0)} = [\, \underline{u}'_{1,T-K+1} \mid A_{u'_1} \mid A_{u'_2} \,] \quad . \tag{A.12}$$

Note that, in each row of $A_{u'}^{(1,0)}$, the first entry belongs to a strictly more recent time instant than the other entries of the same row. Since we can control this entry arbitrarily by the input $x(t)$ at the same time instant without affecting the other entries of the same row, it is always possible to make the first column of $A_{u'}^{(1,0)}$, that is, $\underline{u}'_{1,T-K+1}$, linearly independent from the remaining columns by properly controlling $u_1(t)$ through sufficiently many number of time instants. Therefore, we have,

$$\dim(\aleph(A_{u'}^{(1,0)})) = \dim(\aleph(A_{u'})) = 1 \quad . \tag{A.13}$$

Now consider $A_{u'}^{(2,0)}$, that is,

$$A_{u'}^{(2,0)} = [\, \underline{u}'_{1,T-K+2},\ \underline{u}'_{1,T-K+1} \mid A_{u'_1} \mid A_{u'_2} \,] \quad . \tag{A.14}$$

Following a similar argument, it can be shown that it is always possible to make the first column of $A_{u'}^{(2,0)}$ linearly independent from the other columns. Therefore, we have

$$\dim(\aleph(A_{u'}^{(2,0)})) = \dim(\aleph(A_{u'}^{(1,0)})) = 1 \quad . \tag{A.15}$$

Extending the above discussion further, we find that

$$\dim(\aleph(A_{u'}^{(K,0)})) = \dim(\aleph(A_{u'}^{(1,0)})) = 1 \quad . \tag{A.16}$$

Now consider $A_{u'}^{(K,1)}$ giben by

$$A_{u'}^{(K,1)} = [\, \underline{u}'_{1,T},\ \ldots,\ \underline{u}'_{1,T-K+1} \mid A_{u'_1} \mid \underline{u}'_{2,T-K+1} \mid A_{u'_2} \,] \quad . \tag{A.17}$$

Using (18)-(20), it is trivial to show that the column $\underline{u}'_{2,T-K+1}$ can be expressed as a linear combination of the remaining columns. Therefore

$$\dim(\aleph(A_{u'}^{(K,1)})) = 1 + \dim(\aleph(A_{u'}^{(K,0)})) = 2 \quad . \tag{A.18}$$

Similarly,

$$\dim(\aleph(A_{u'}^{(K,2)})) = 1 + \dim(\aleph(A_{u'}^{(K,1)})) = 3 \quad . \tag{A.19}$$

Finally, we obtain

$$\dim(\aleph(A_{u'}^{(K,K)})) = K + 1 \quad . \tag{A.20}$$

Using the fact that $A_{u'}^{(K,K)} = A_u$ and remembering that the matrices A_u and R_u have the same null spaces, we have

$$\dim(\aleph(R_u)) = K + 1 \quad . \tag{A.21}$$

Appendix B

From Lemma 2, we conclude that the K extraneous roots of $\mathcal{W}_1(z^{-1})$ and $\mathcal{W}_2(z^{-1})$ can be chosen in an arbitrary manner. Also, it can be shown that these K arbitrary roots, together with the arbitrary constant α appearing in (34) and (35), imply an exactly $(K+1)$-dimensional subspace $\mathcal{S}_1$ for $\underline{w}$ such that for each $\underline{w} \in \mathcal{S}_1$, we have $\mathcal{E}(\underline{w}) = 0$. Furthermore, there is a one to one correspondence with the set of K extraneous roots and the vectors in $\mathcal{S}_1$.

From Lemma 1, we know that the dimension of null space of R_u (or equivalently, A_u) is exactly $(K+1)$. Therefore this space must be $\mathcal{S}_1$ and thus Corollary 2.

References

[1] R. P. Gooch, "Adaptive pole-zero filtering: The equation-error approach," Ph.D. dissertation, Stanford University, Stanford, CA, June 1983.

[2] B. Widrow and S. D. Stearns, *Adaptive Signal Processing.* Englewood Cliffs, NJ, Prentice-Hall, 1985.

[3] B. Widrow, J. M. McCool, M. G. Larimore, and C. R. Johnson, JR., "Stationary and nonstationary learning characteristics of the LMS adaptive filter," *Proc. IEEE*, vol. 64, no. 8, pp.1151-1162, Aug. 1976.

[4] T. A. C. M. Claasen and W. F. G. Mecklenbrauker, "Comparison of the convergence of two algorithms for Adaptive FIR digital filters," *IEEE Trans. Circuits and Systems*, vol. CAS-28, no. 6, pp. 510-518, June 1981.

[5] J. M. Cioffi and T. Kailath, "Fast, recursive least squares transversal filters for adaptive filtering," *IEEE Trans. Acoust., Speech, Signal Processing*, vol. ASSP-32, no. 2, pp. 304-337, Apr. 1984.

[6] D. T. M. Slock and T. Kailath, "Numerically stable fast transversal filters for recursive least squares adaptive filtering," *IEEE Trans. Signal Processing*, vol. 39, no. 1, pp. 92-114, Jan. 1991.

[7] D. T. M. Slock, L. Chisci, H. Lev-Ari, and T. Kailath, "Modular and numerically stable fast transversal filters for multichannel and multiexperiment RLS," *IEEE Trans. Signal Processing*, vol. 40, no. 4, pp. 784-802, Apr. 1992.

[8] S. Haykin, *Adaptive Filter Theory.* Englewood Cliffs, NJ: Prentice Hall, 1991.

[9] M. G. Larimore, J. R. Treichler, and C. R. Johnson, JR., "SHARF: An algorithm for adapting IIR digital filters," *IEEE Trans. Acoust., Speech, Signal Processing*, vol. ASSP-28, no. 4, pp. 428-440, Aug. 1980.

[10] C. R. Johnson, JR., M. G. Larimore, J. R. Treichler, and B. D. O. Anderson, "SHARF convergence properties," *IEEE Trans. Circuits and Systems*, vol. CAS-28, no. 6, pp. 499-510, June 1981.

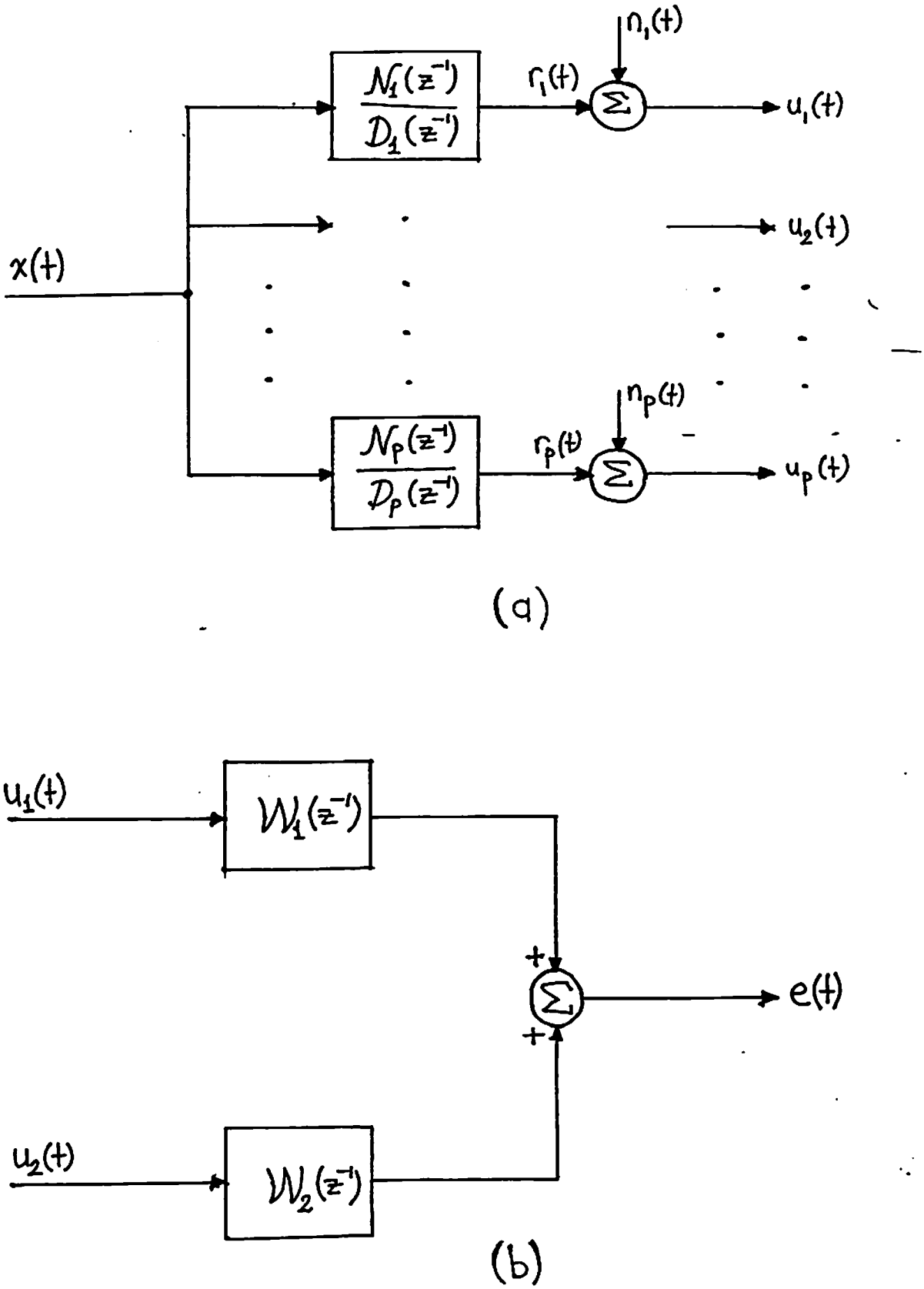

Figure 1: (a) The unknown multichannel system model. (b) the two channel adaptive system model.

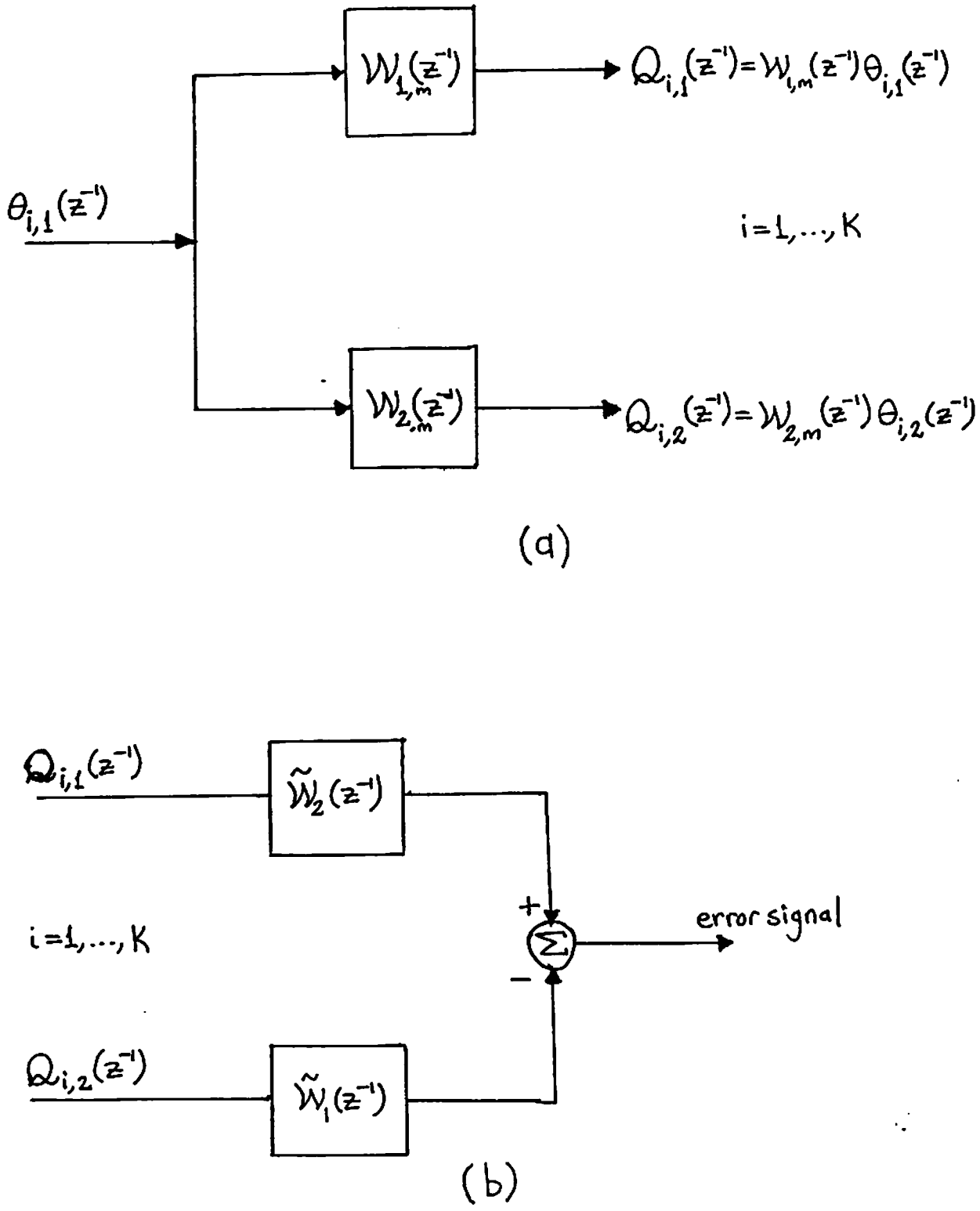

Figure 2: Modeling of the Algorithmic Fractals approach as a two channel blind deconvolution problem.

Figure 3: Desired root locations for (a) adaptive channel-1, and (b) adaptive channel-2.

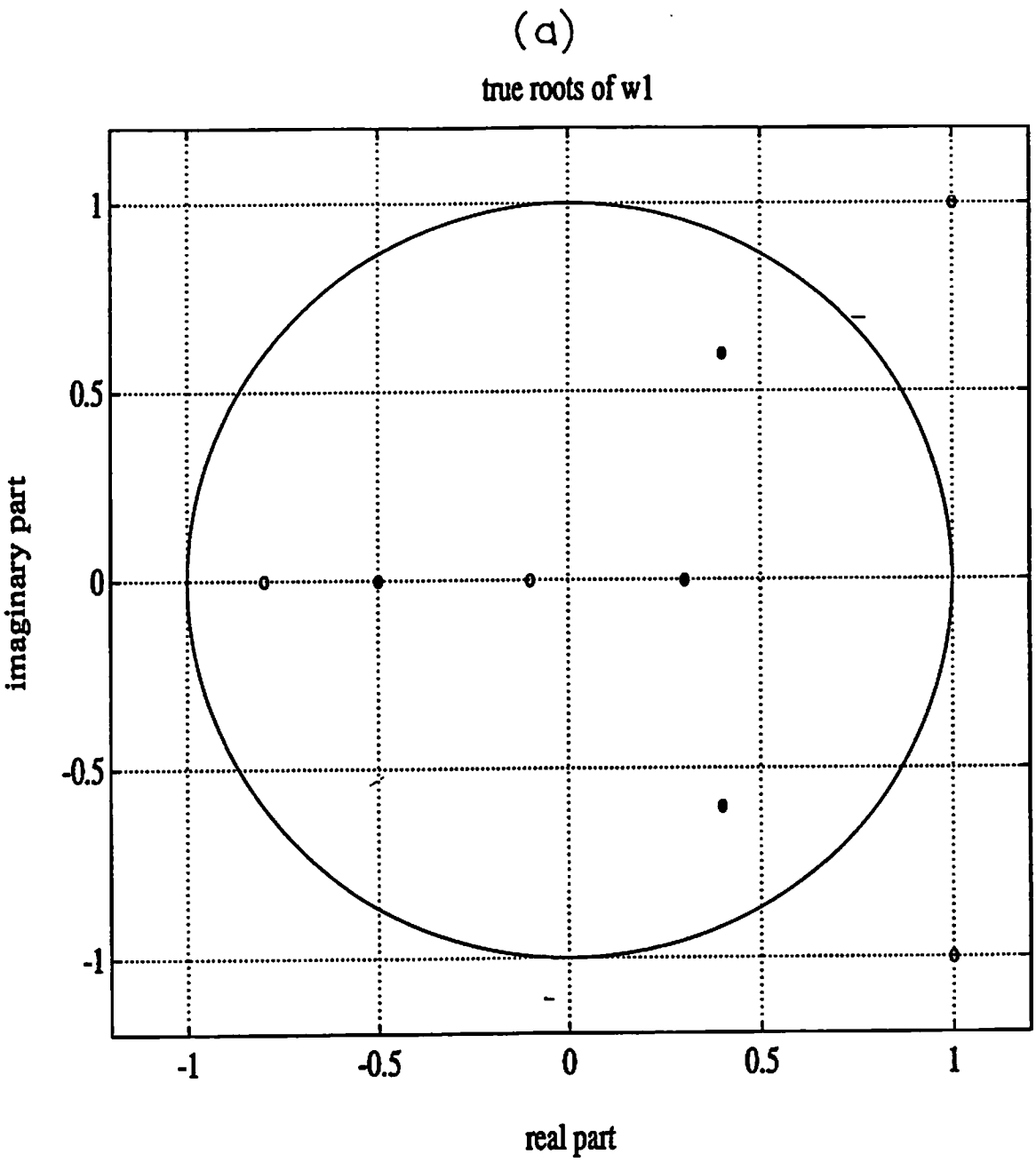

Figure 3: (Cont'd)

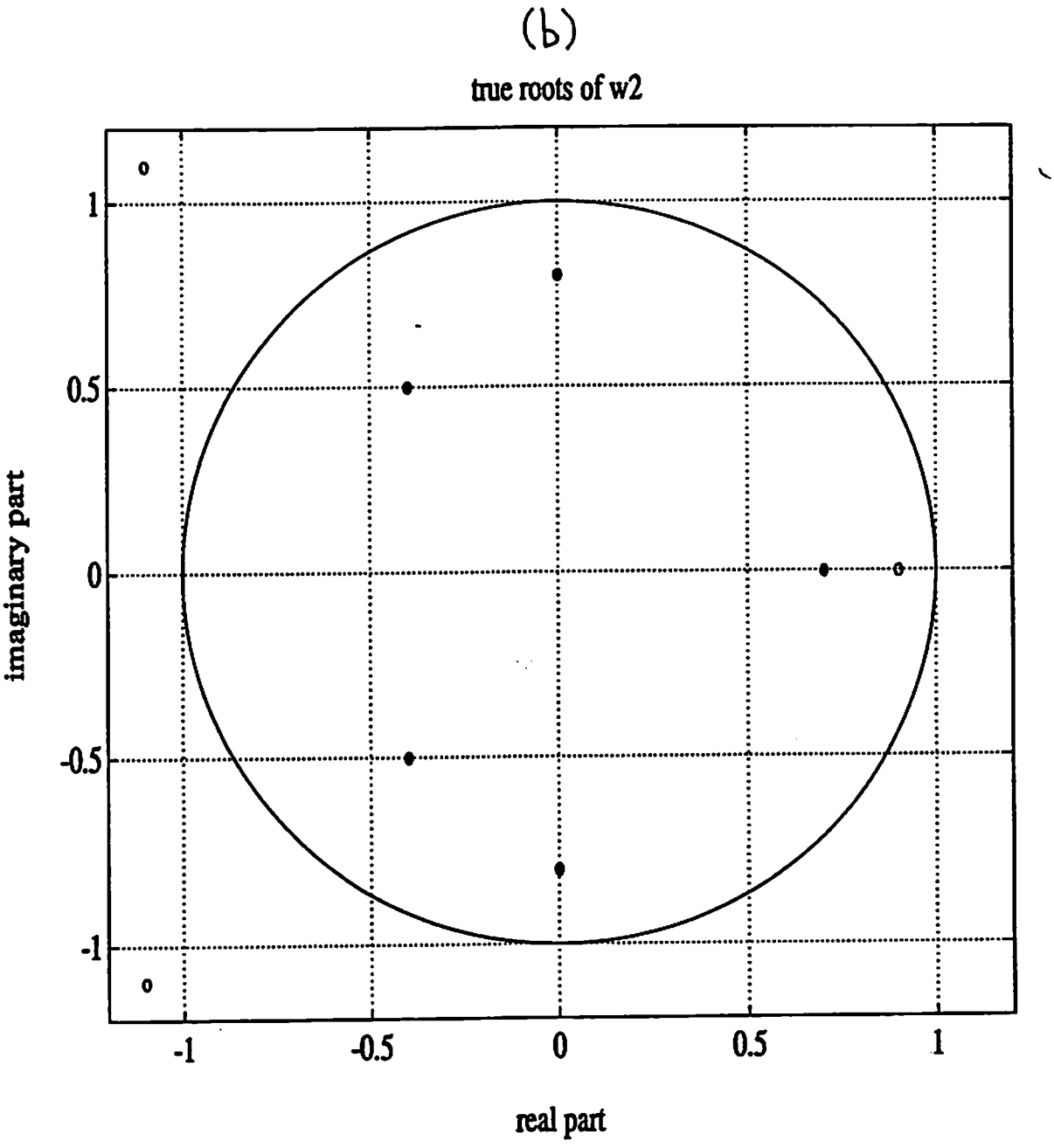

Figure 4: Adaptive channel root locations obtained by EVAM for the noiseless case. (a) channel-1, (b) channel-2.

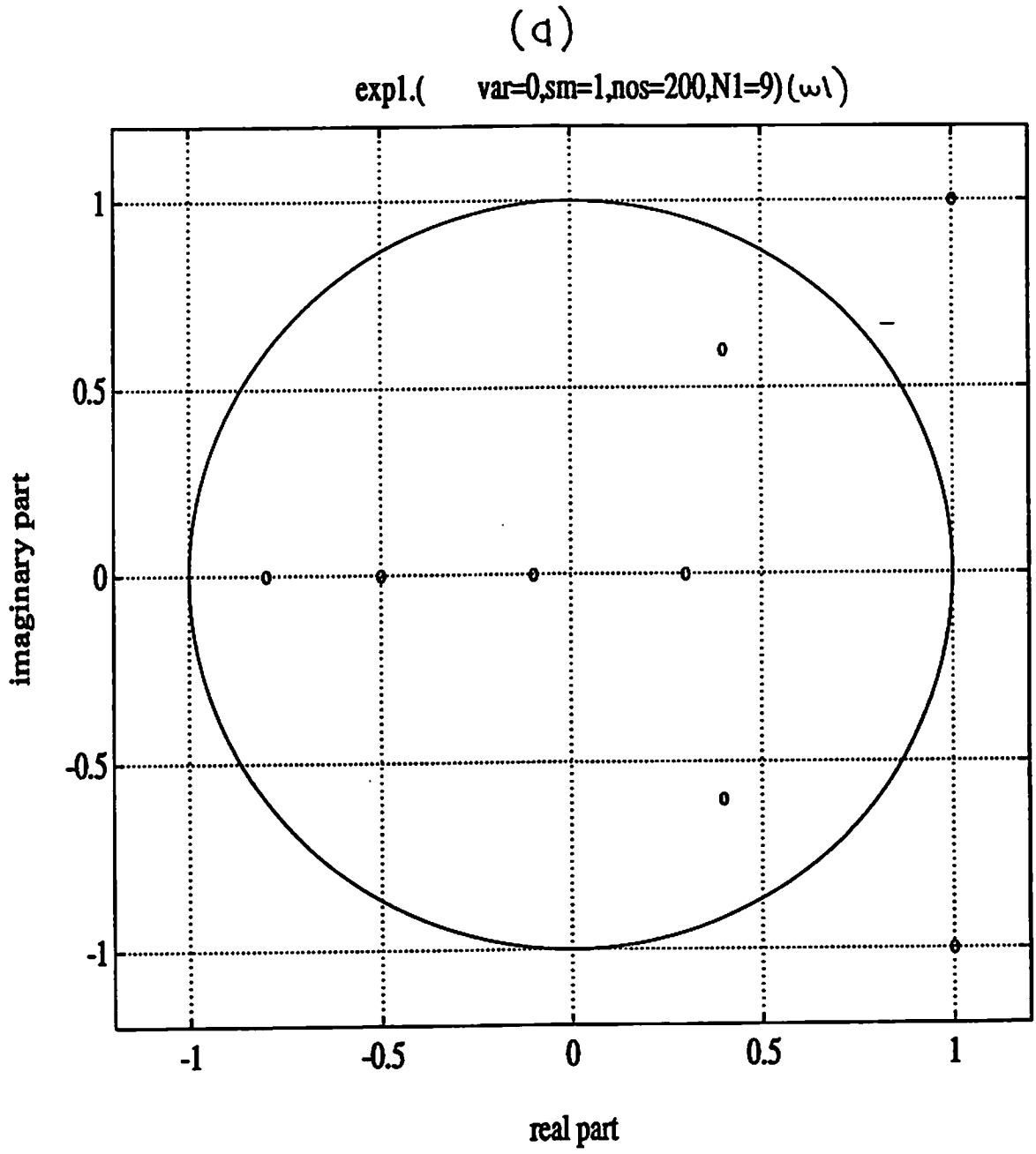

Figure 4: (Cont'd)

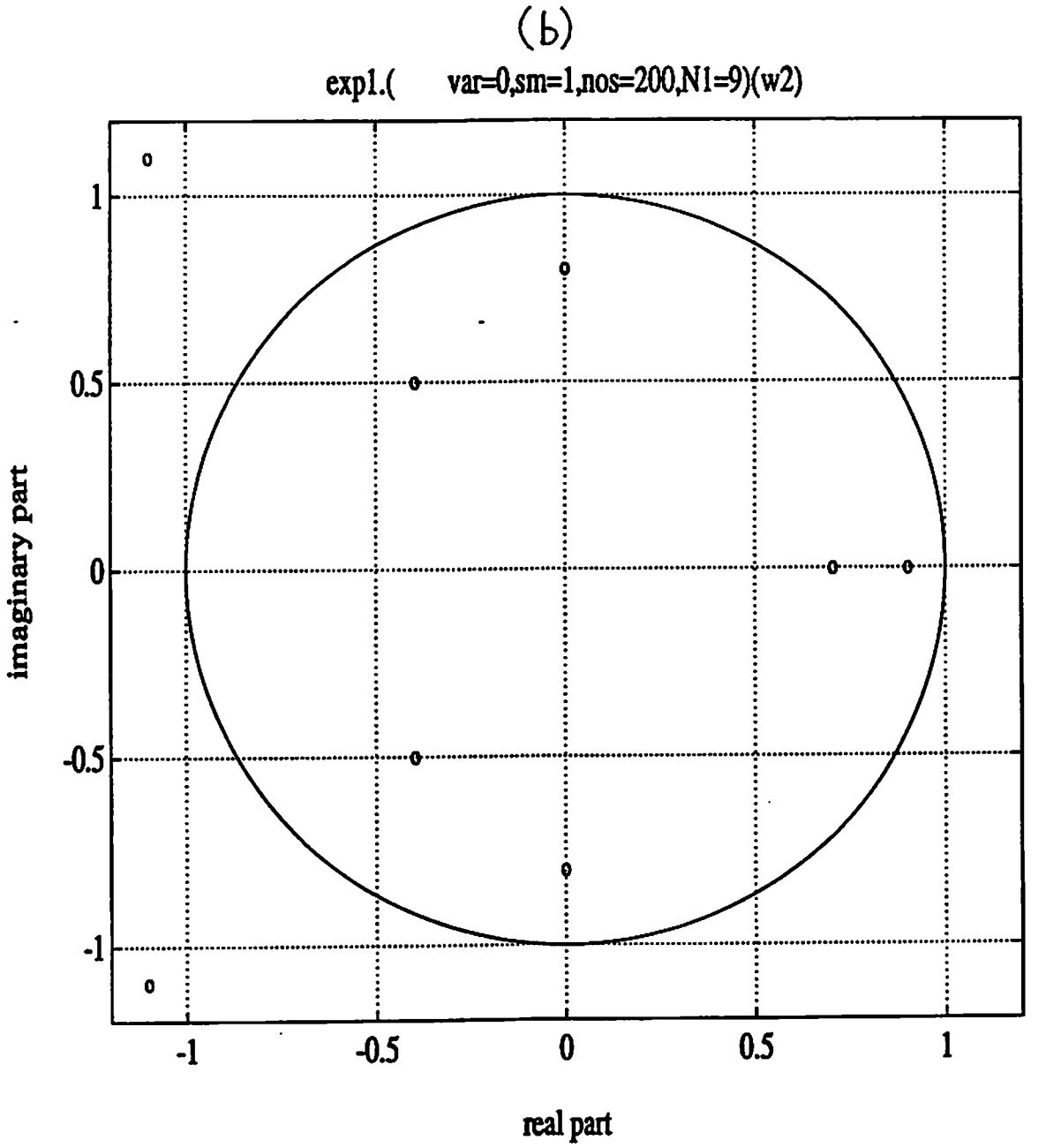

Figure 5: Adaptive channel root locations obtained by LMS algorithm for the noiseless case. (a) channel-1, (b) channel-2.

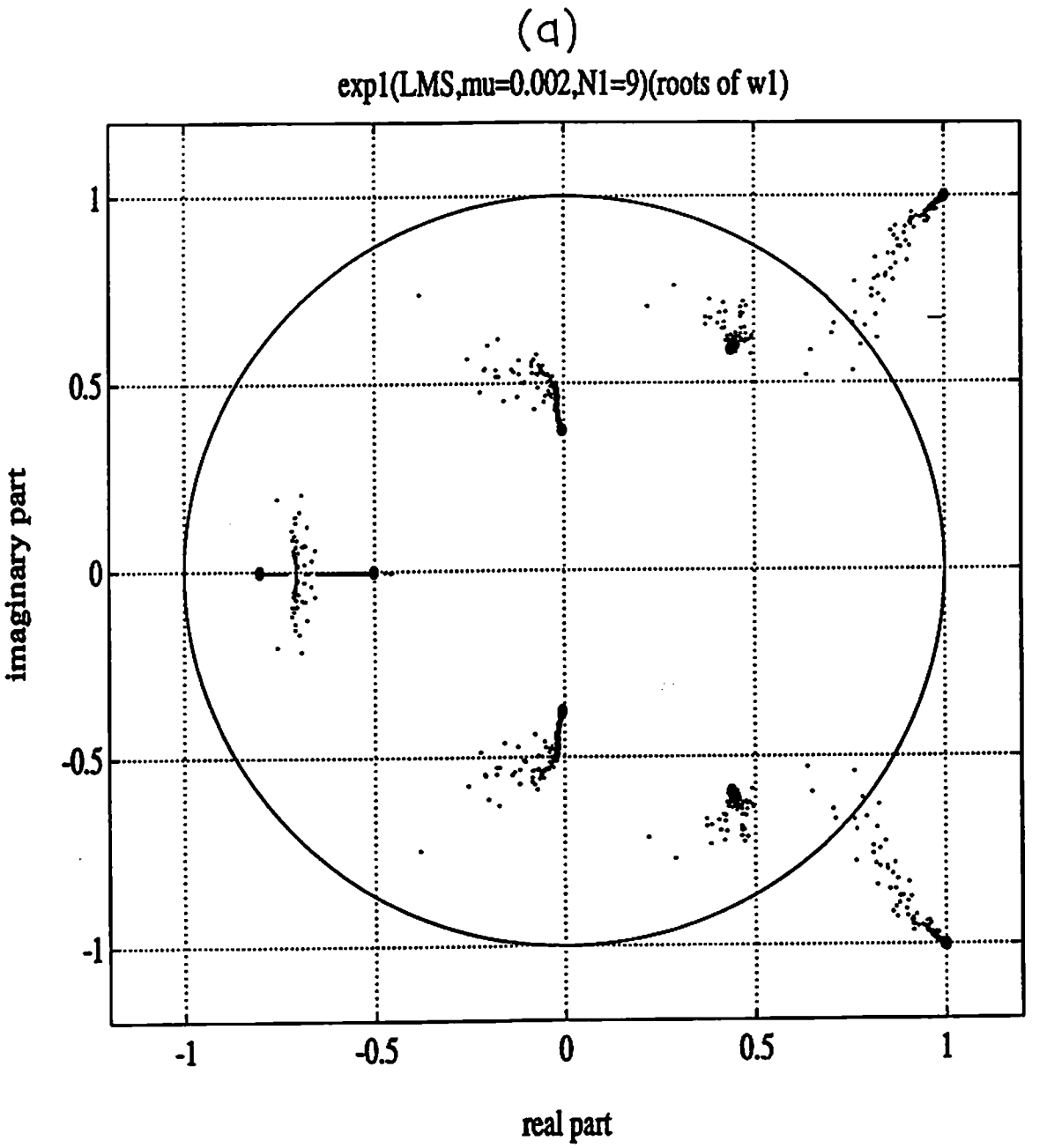

Figure 5: (Cont'd)

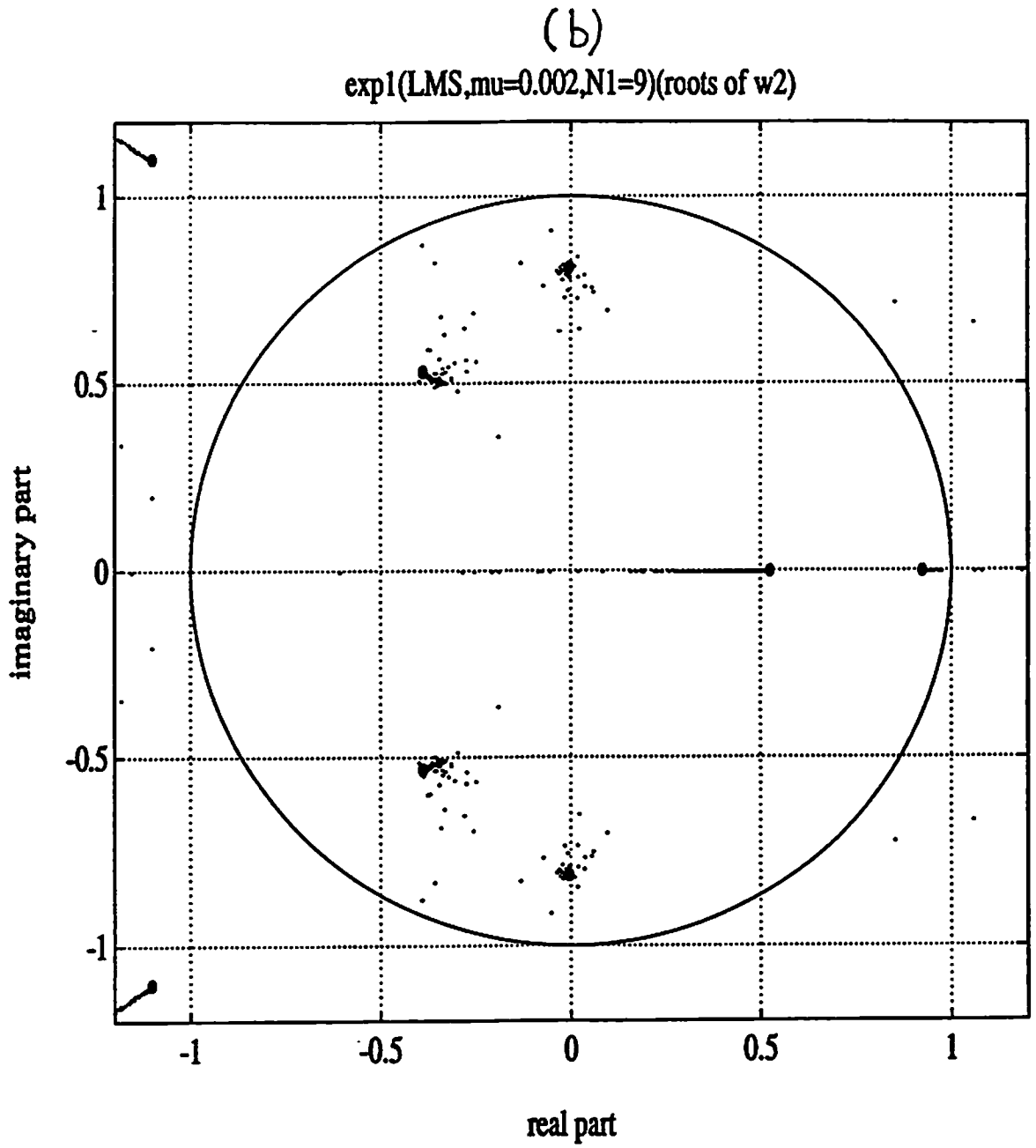

Figure 6: Adaptive channel root locations obtained by Modular RLS algorithm for the noiseless case. (a) channel-1, (b) channel-2.

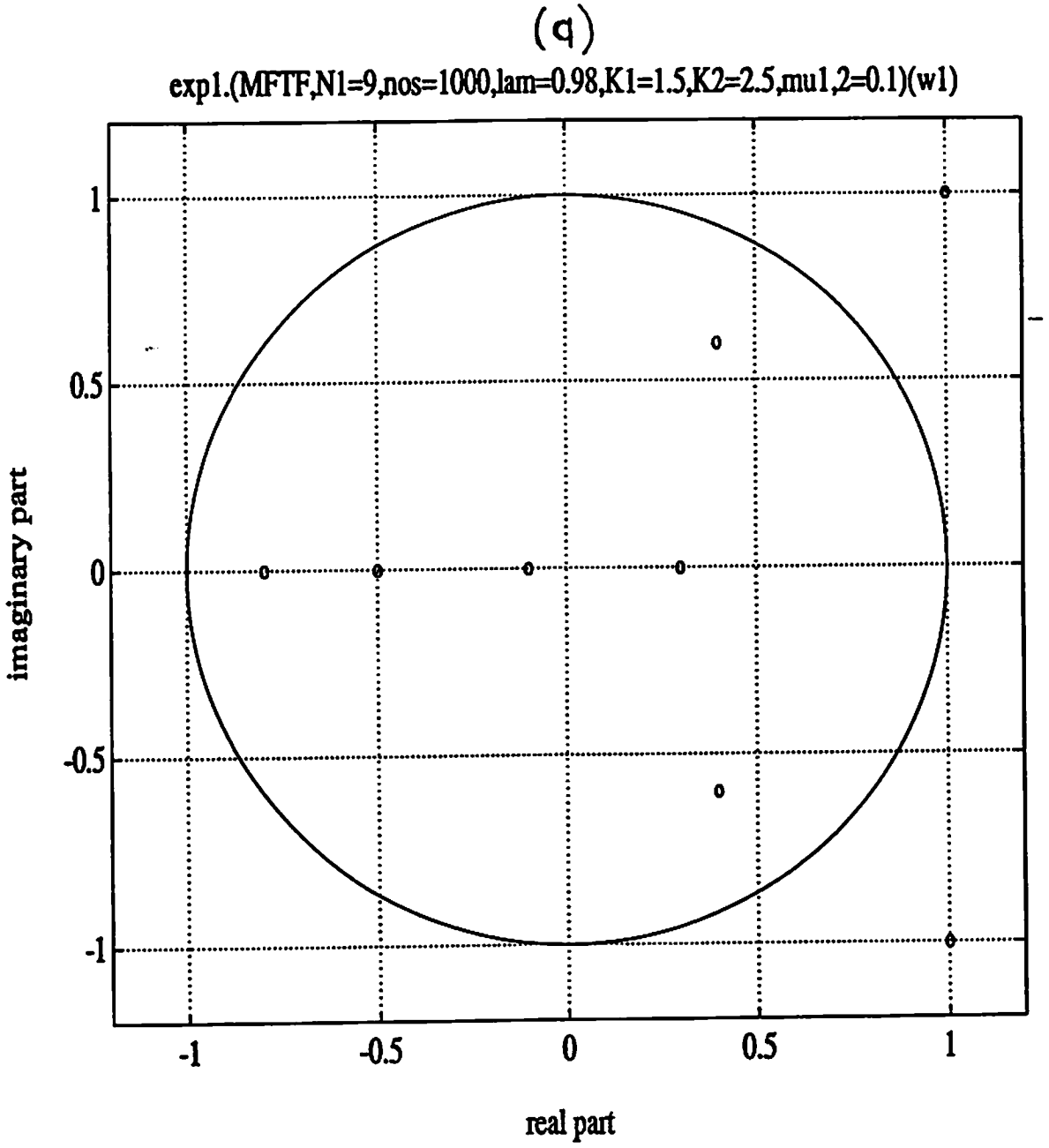

Figure 6: (Cont'd)

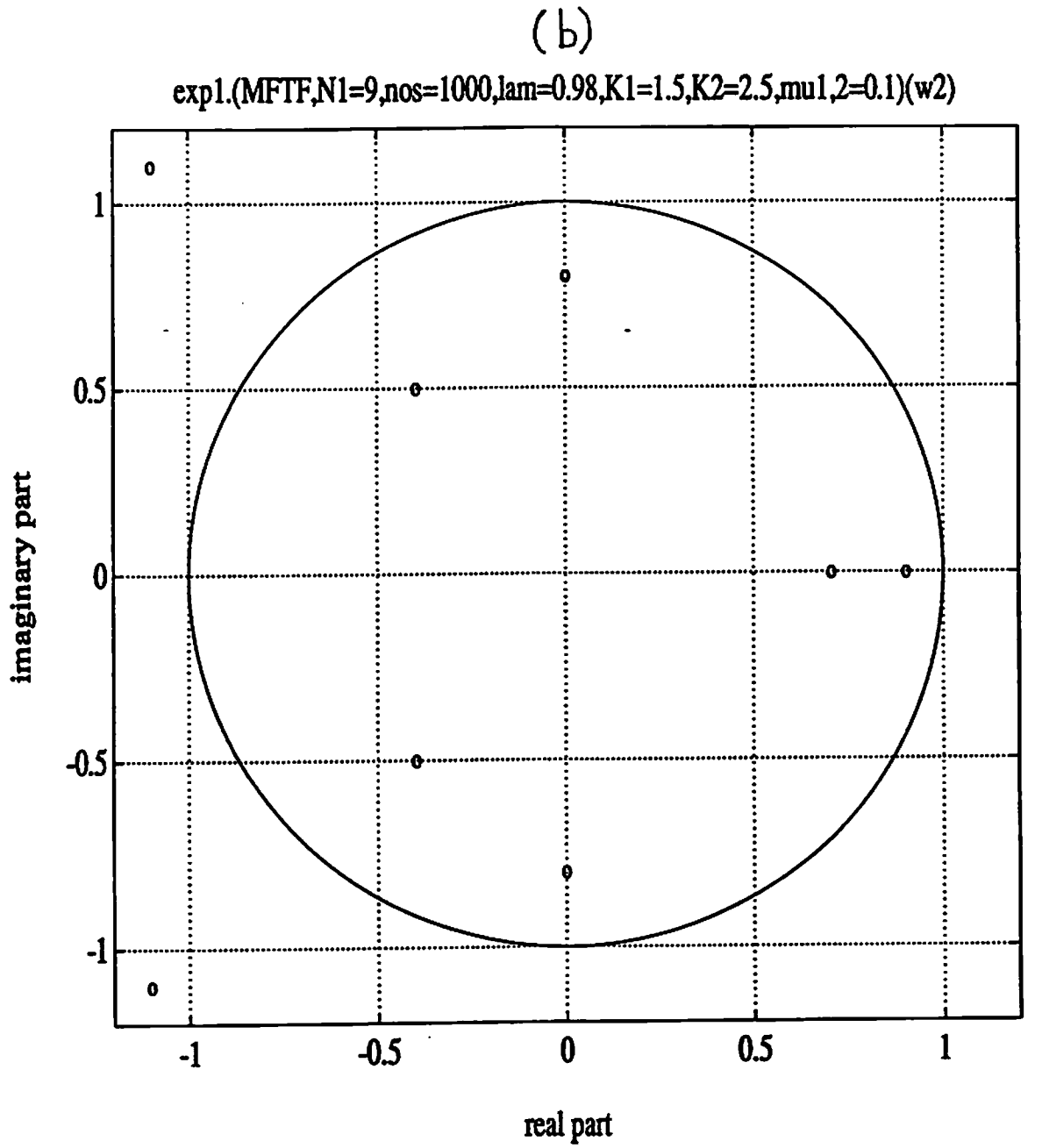

Figure 7: Adaptive channel root locations obtained by EVAM (using $\underline{q}_1$) for the noiseless case. (a) channel-1, (b) channel-2.

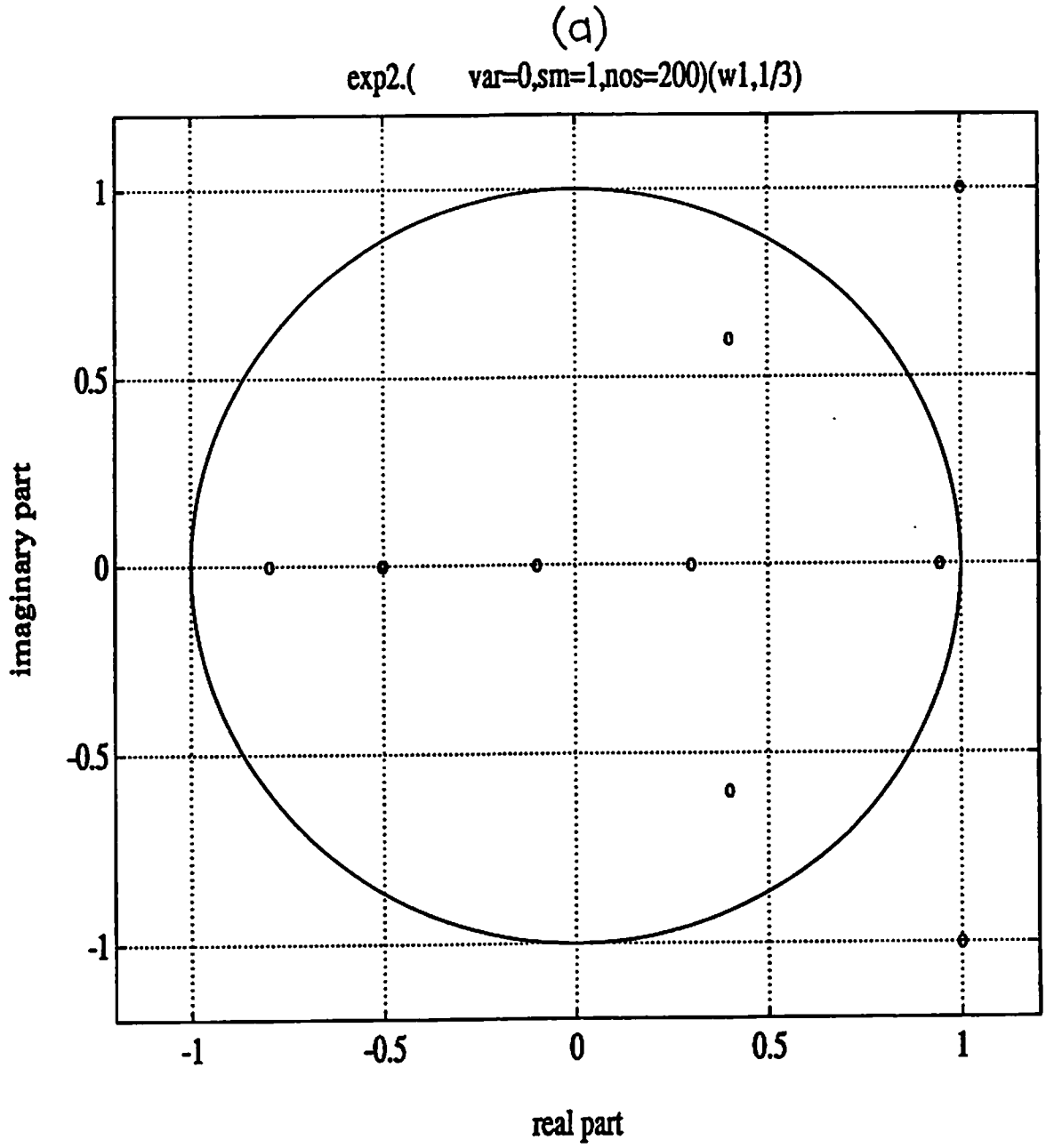

Figure 7: (Cont'd)

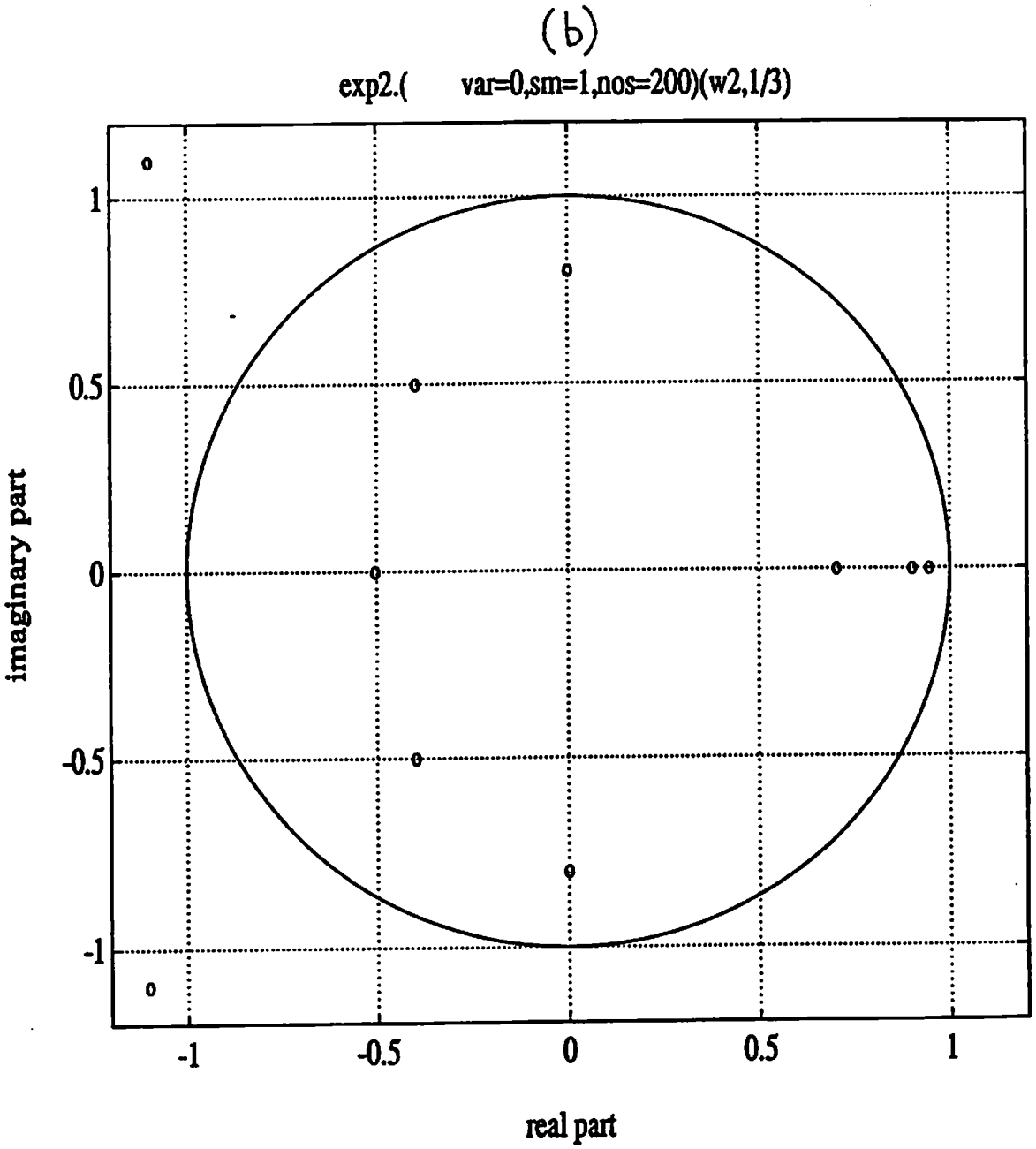

Figure 8: Adaptive channel root locations obtained by EVAM (using q_2) for the noiseless case. (a) channel-1, (b) channel-2.

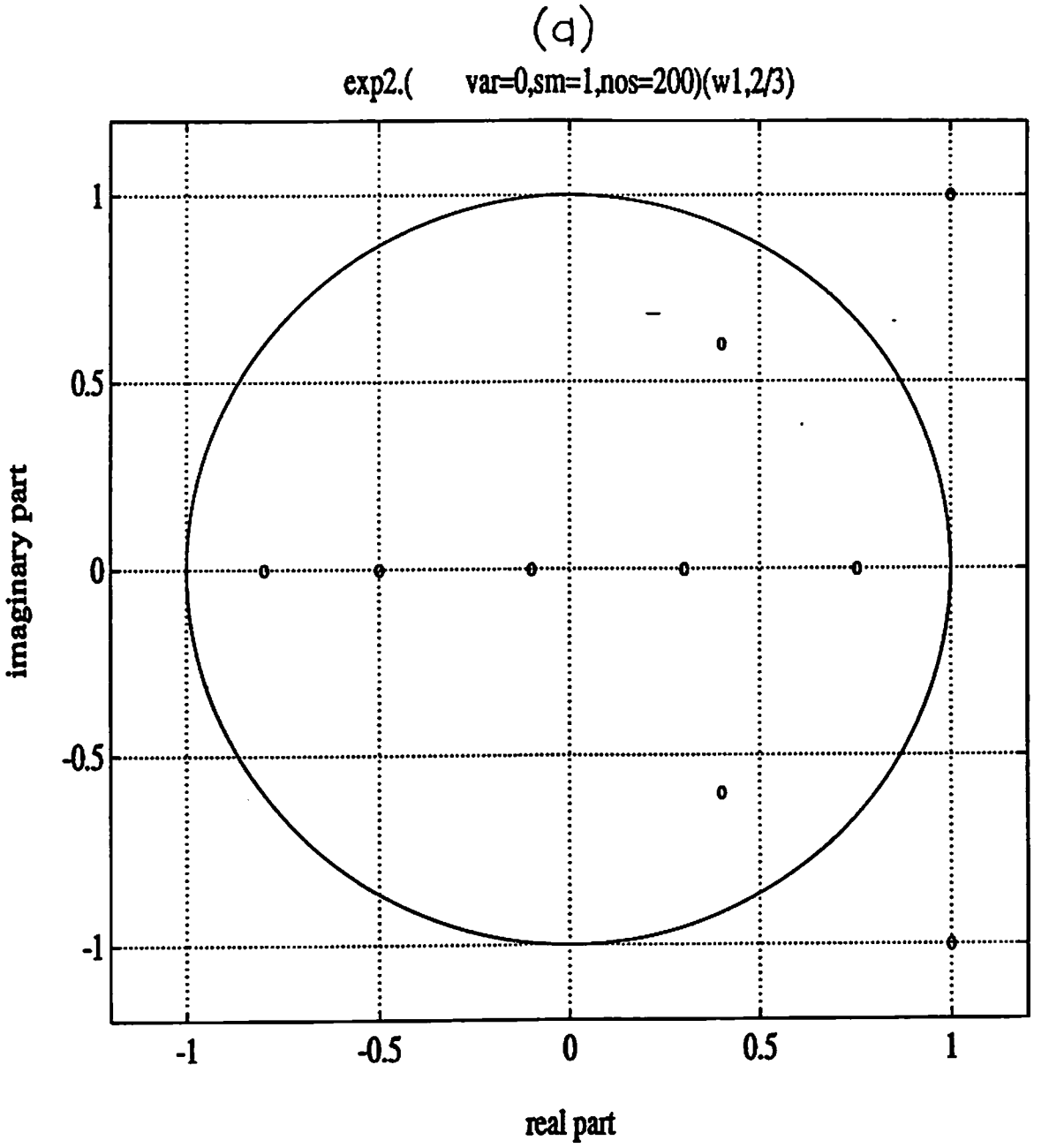

Figure 8: (Cont'd)

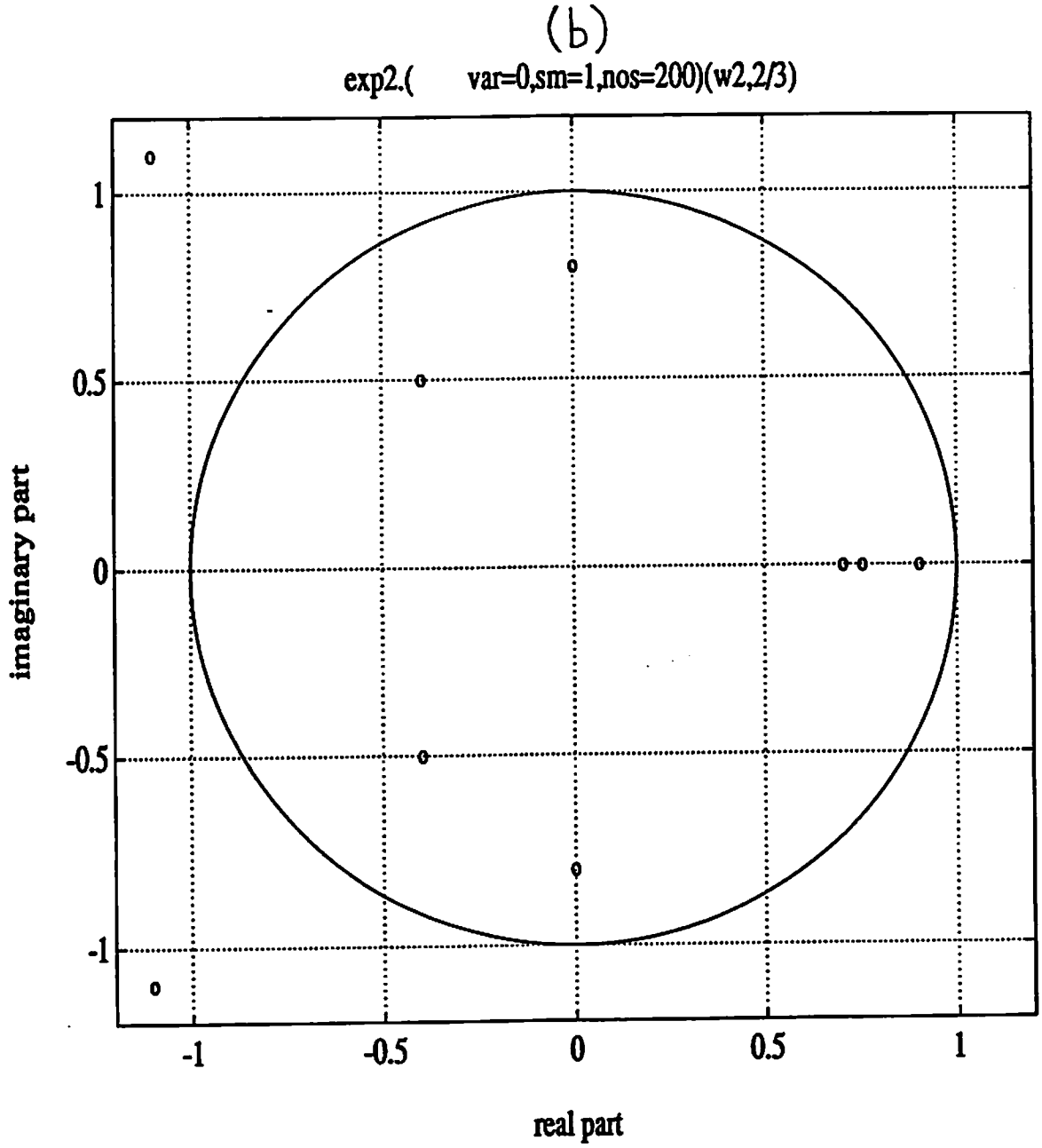

Figure 9: Adaptive channel root locations obtained by EVAM (using q_3) for the noiseless case. (a) channel-1, (b) channel-2.

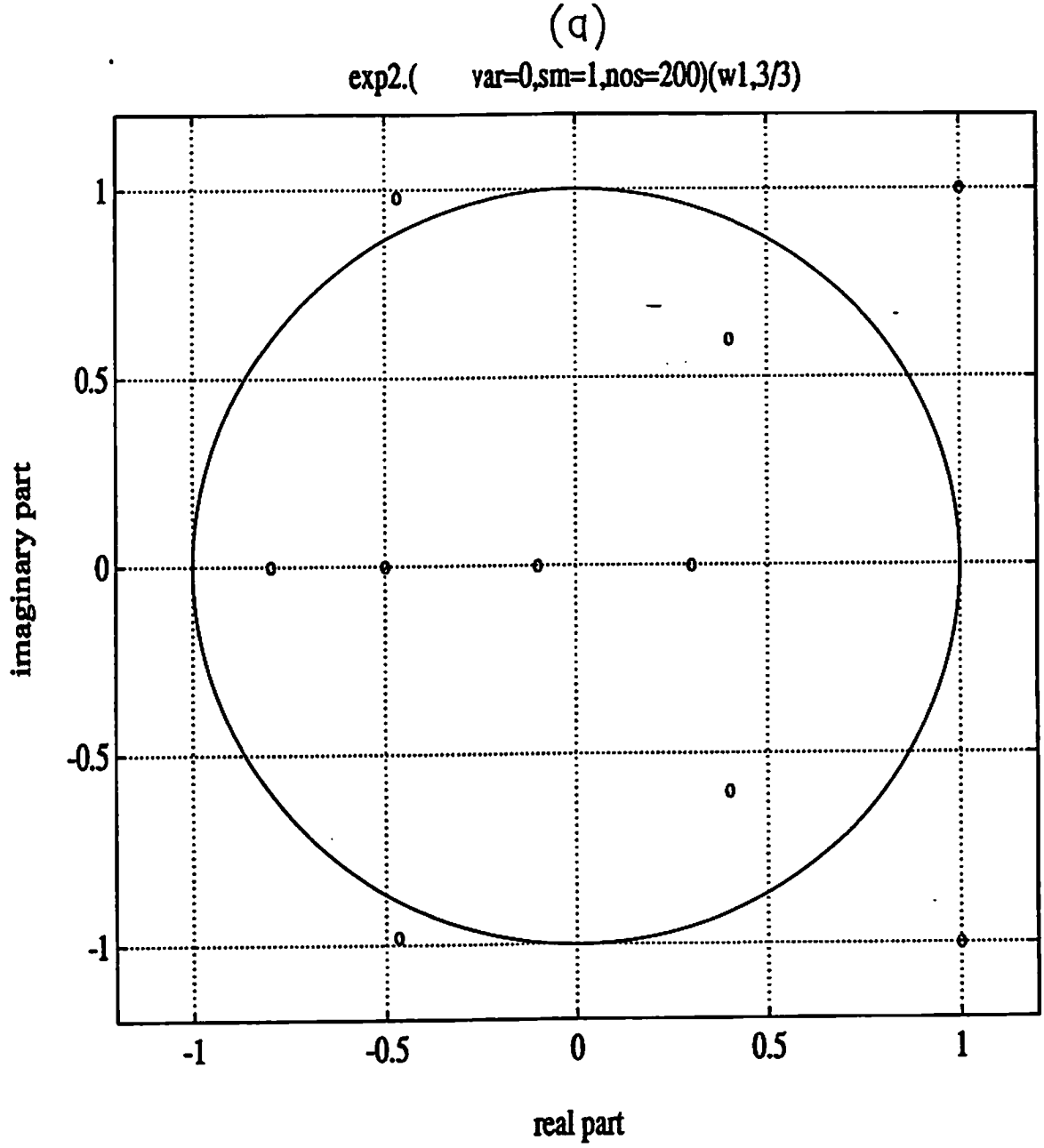

Figure 9: (Cont'd)

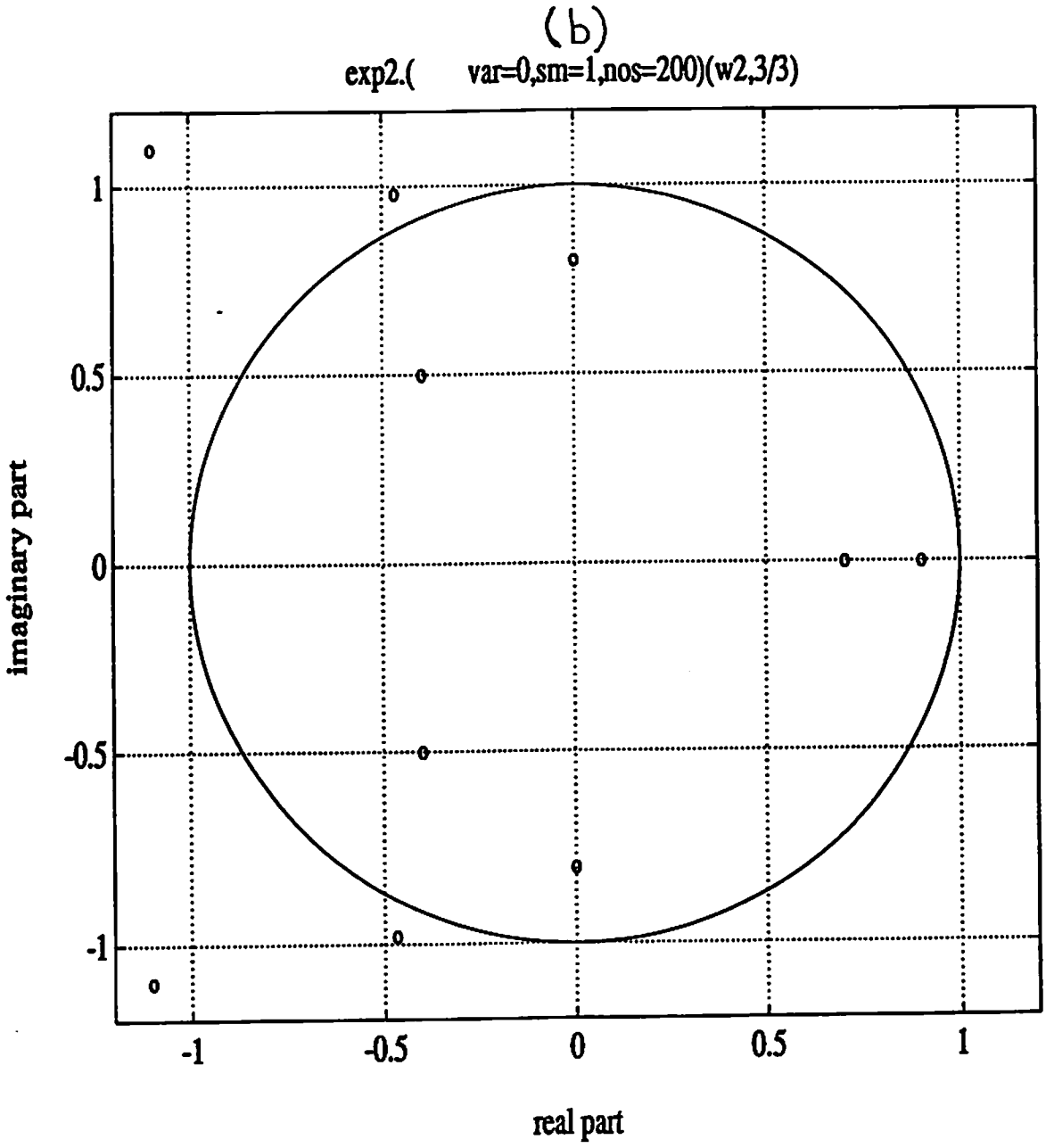

Figure 10: Adaptive channel root locations obtained by Modular RLS algorithm for the noiseless case. (a) channel-1, (b) channel-2.

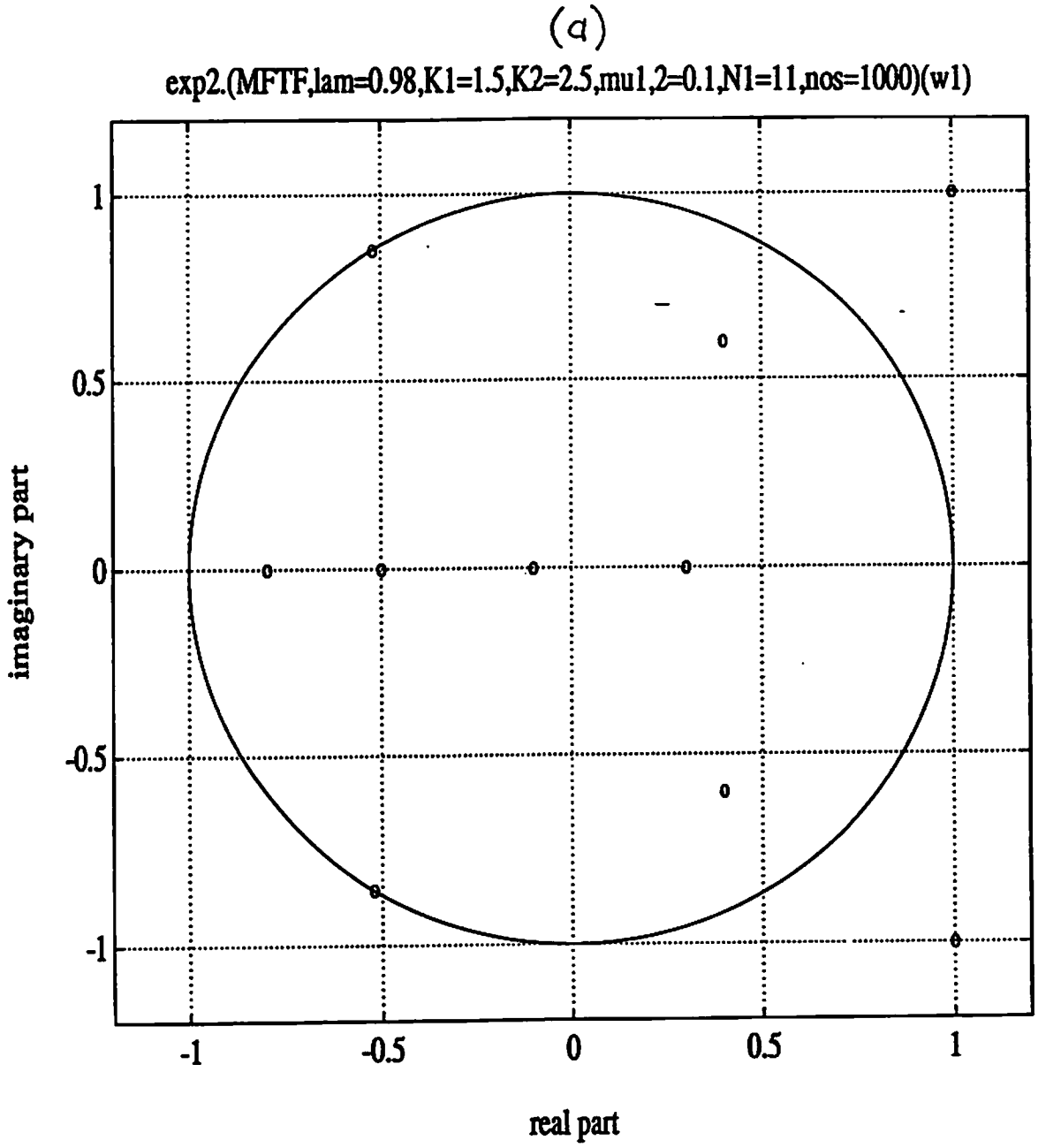

Figure 10: (Cont'd)

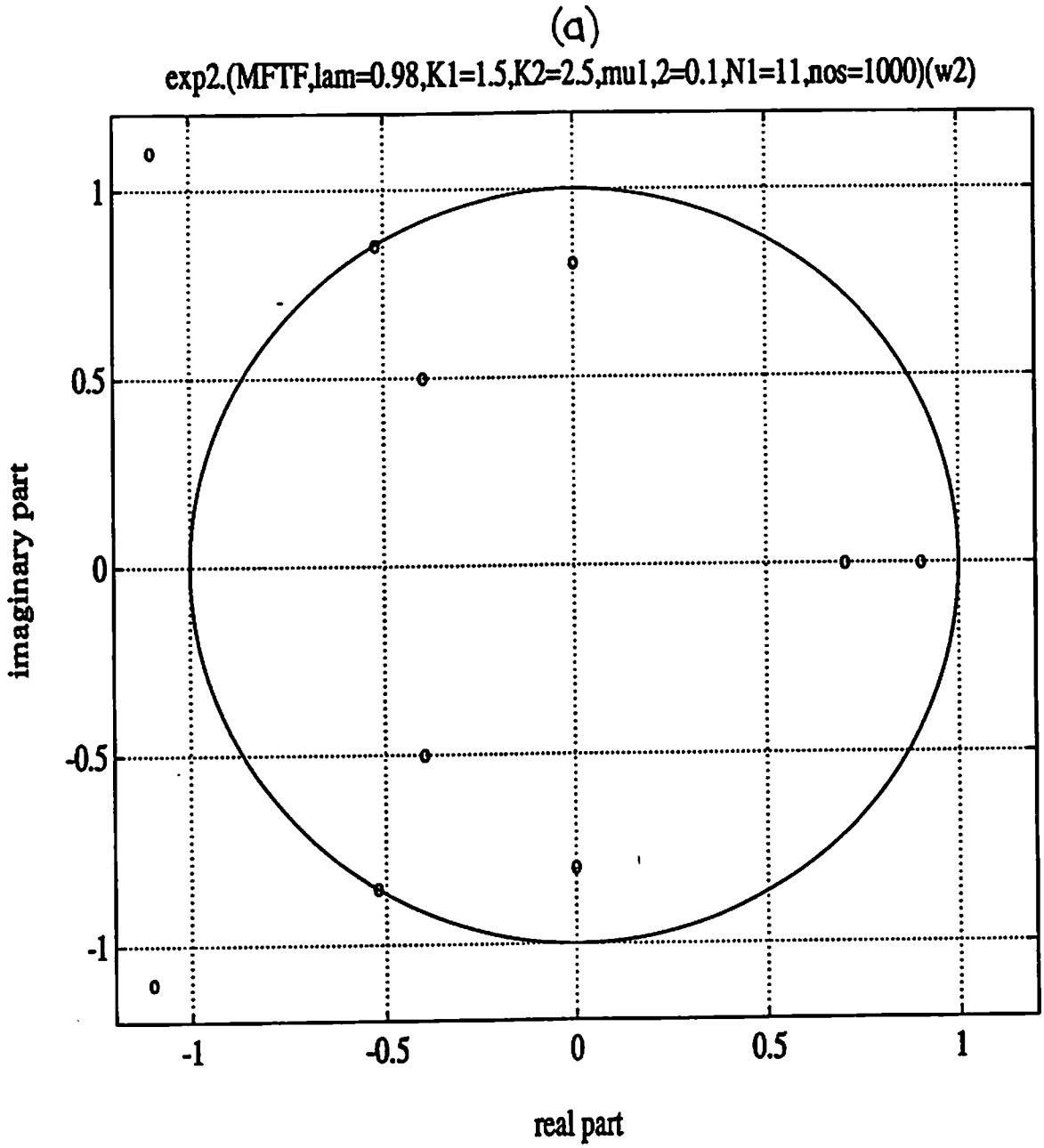

Figure 11: Adaptive channel root locations obtained by EVAM (using q_1) for the noiseless case. (a) channel-1, (b) channel-2.

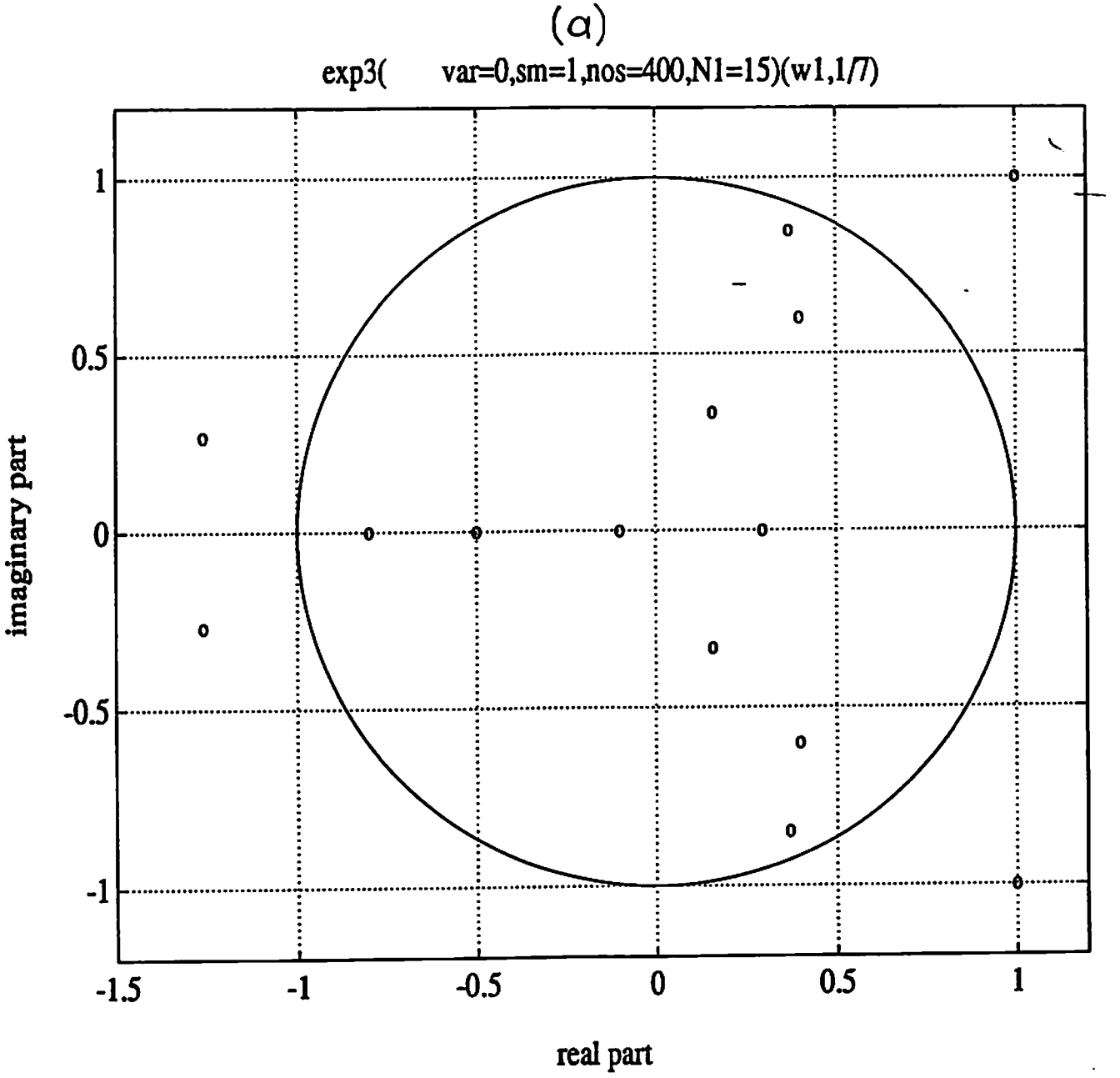

Figure 11: (Cont'd)

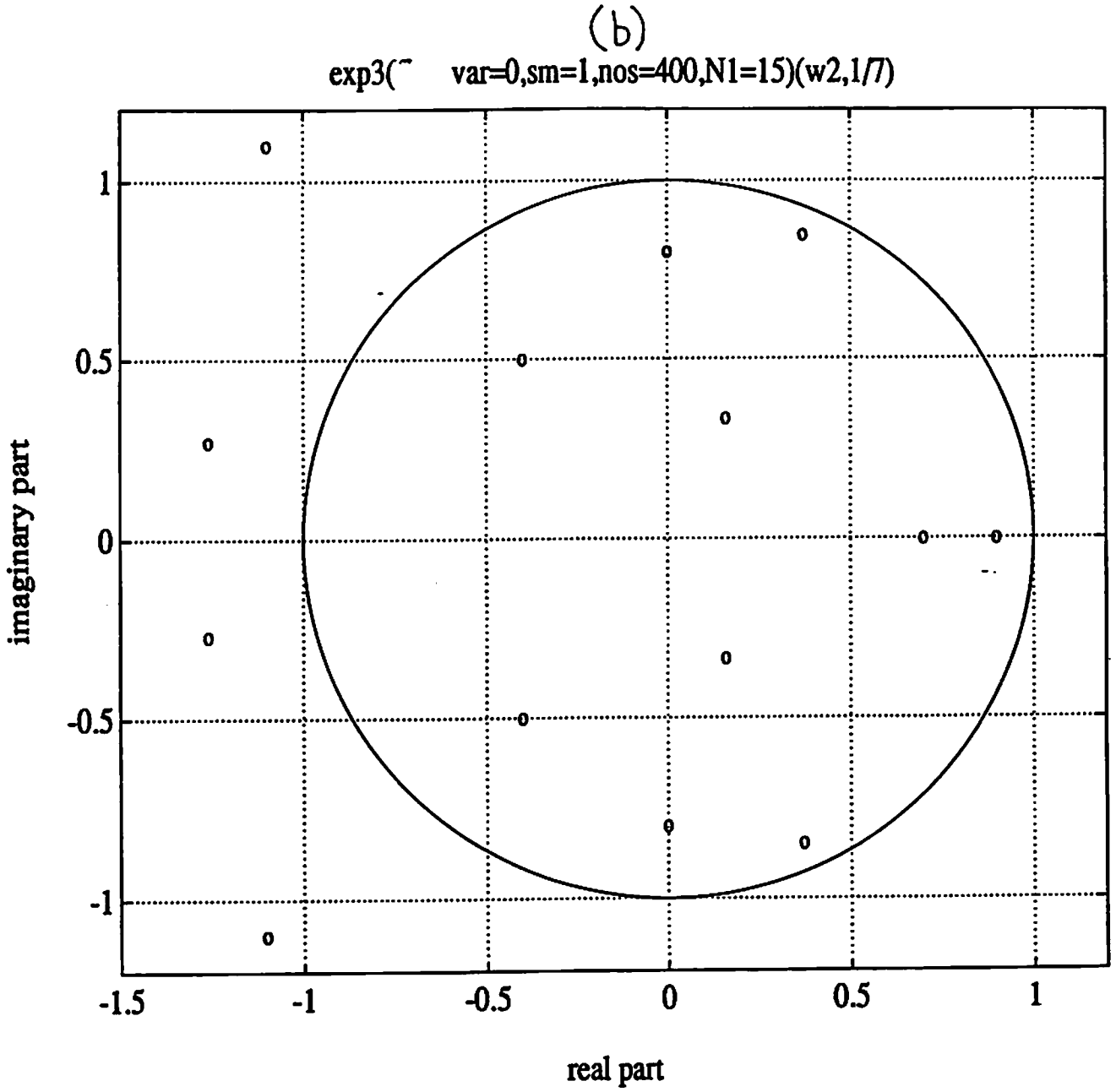

Figure 12: Adaptive channel root locations obtained by EVAM (using $\underline{q}_2$) for the noiseless case. (a) channel-1, (b) channel-2.

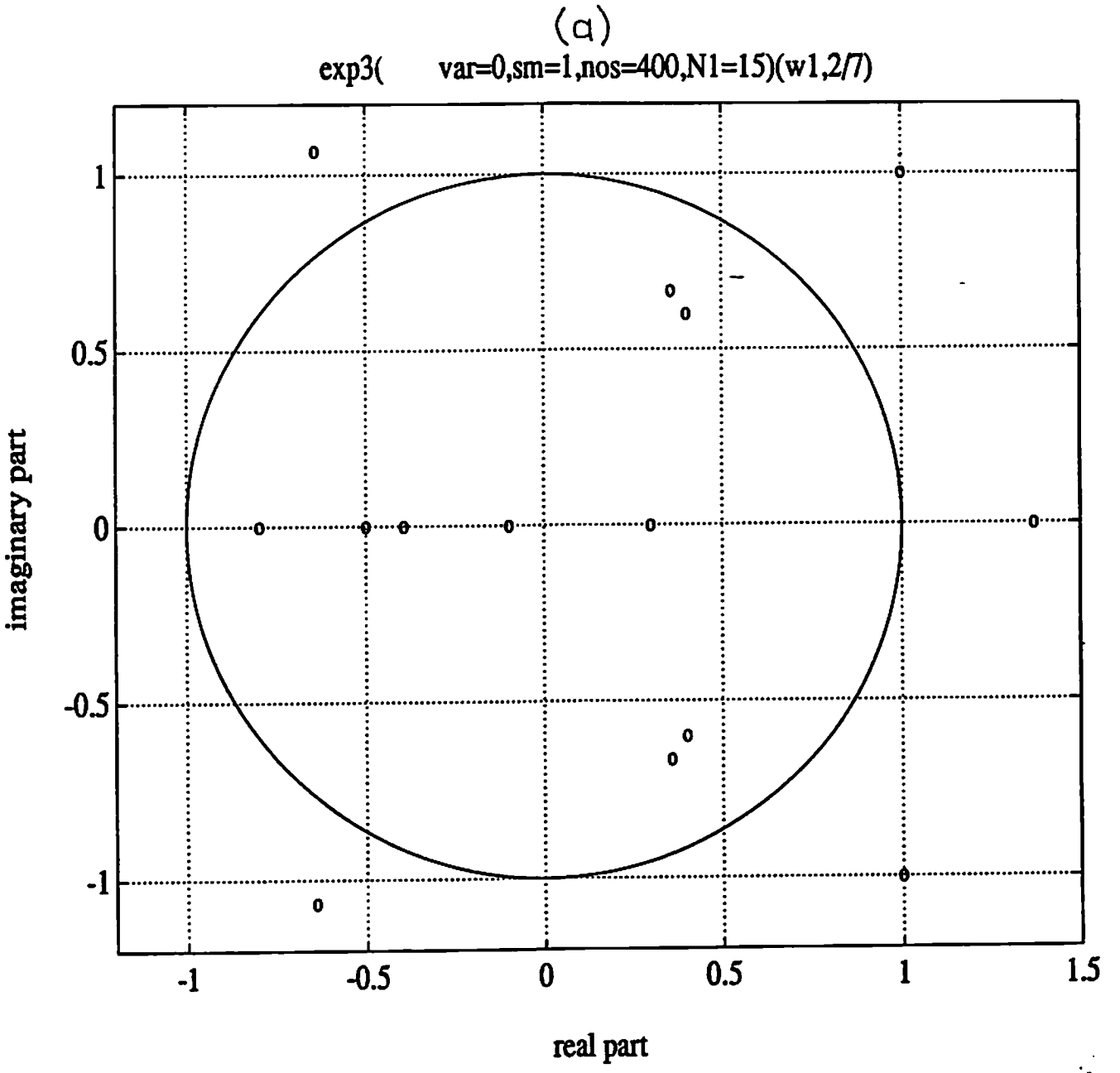

Figure 12: (Cont'd)

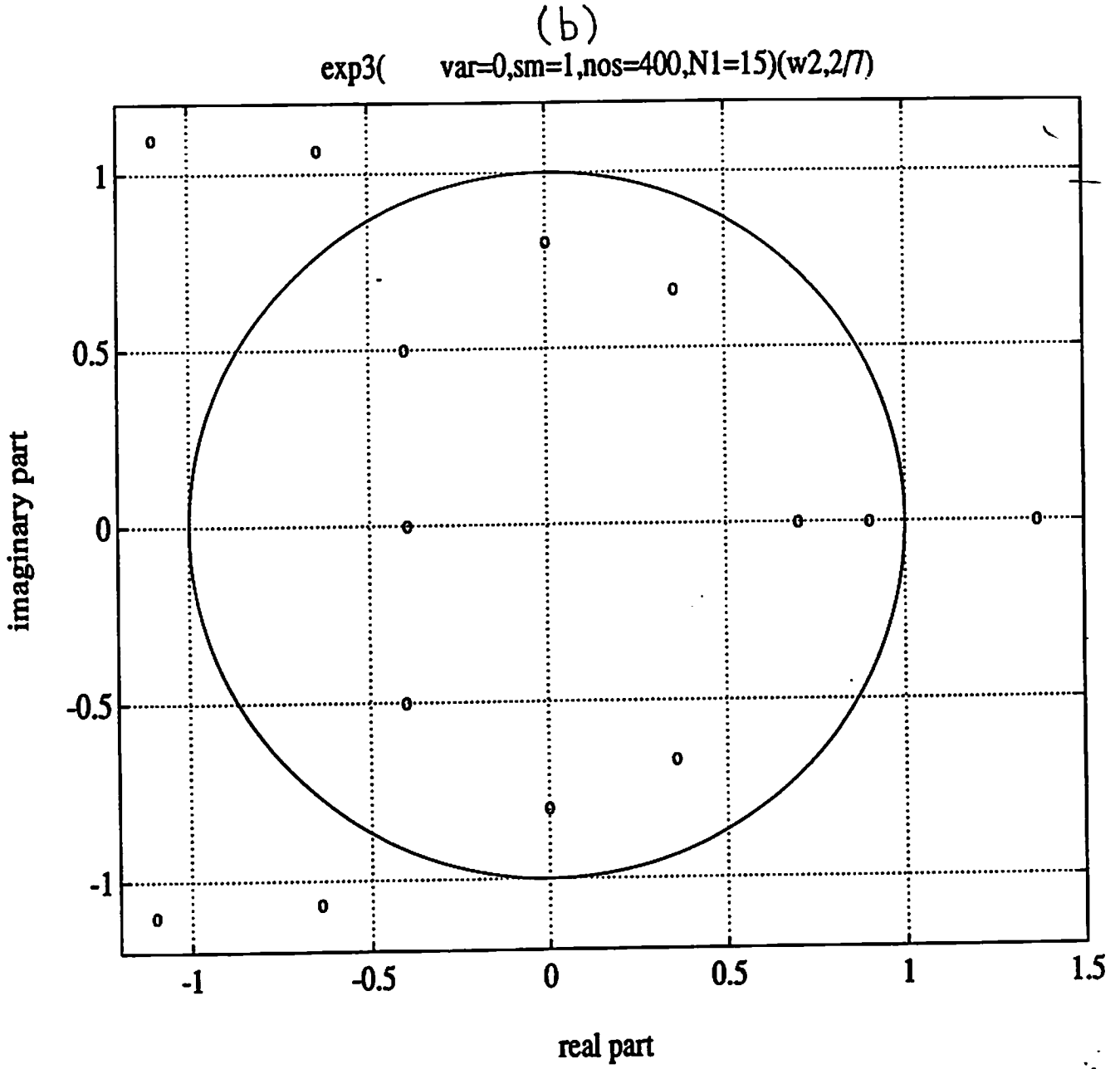

Figure 13: Adaptive channel root locations obtained by EVAM (using q_3) for the noiseless case. (a) channel-1, (b) channel-2.

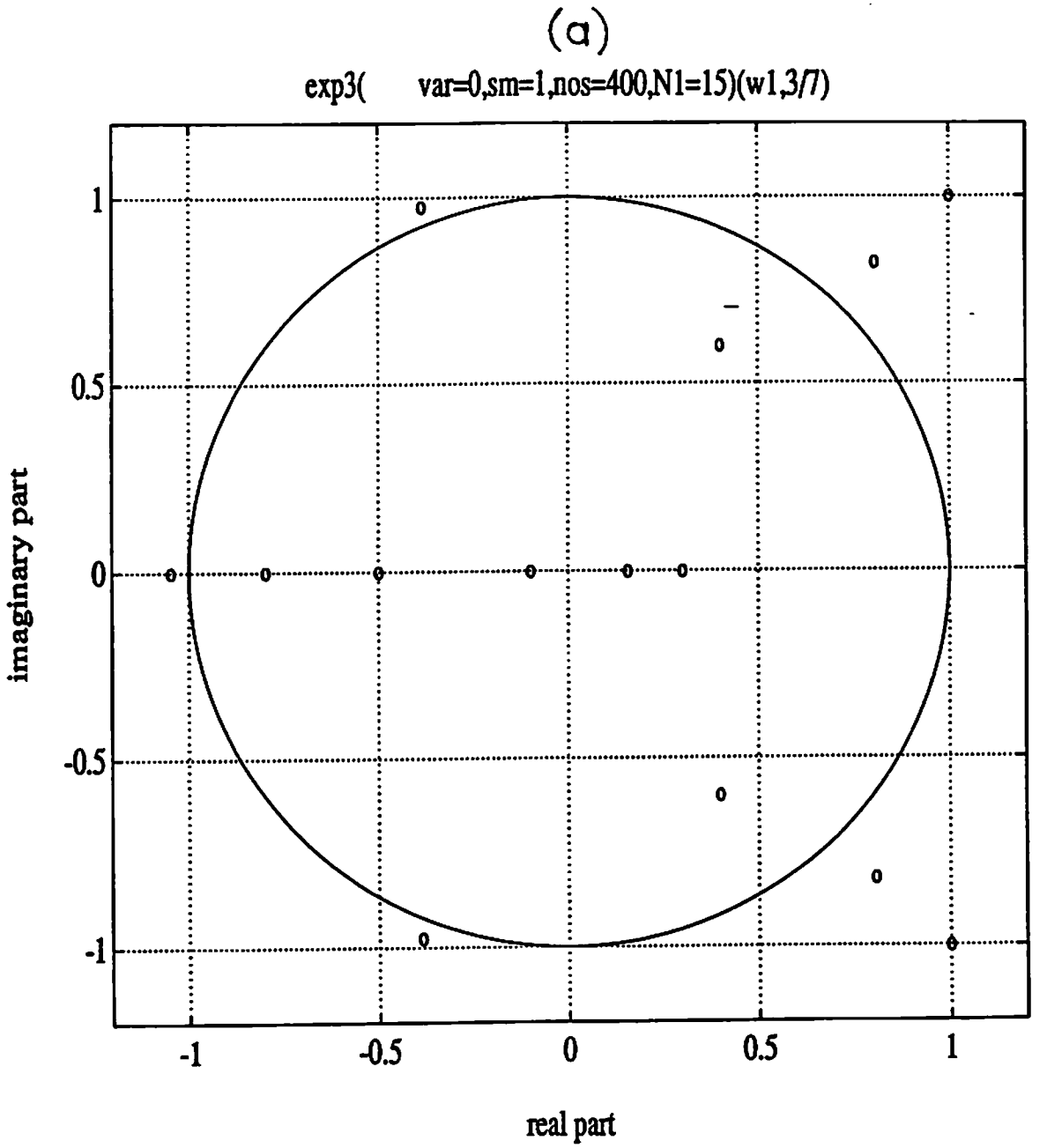

Figure 13: (Cont'd)

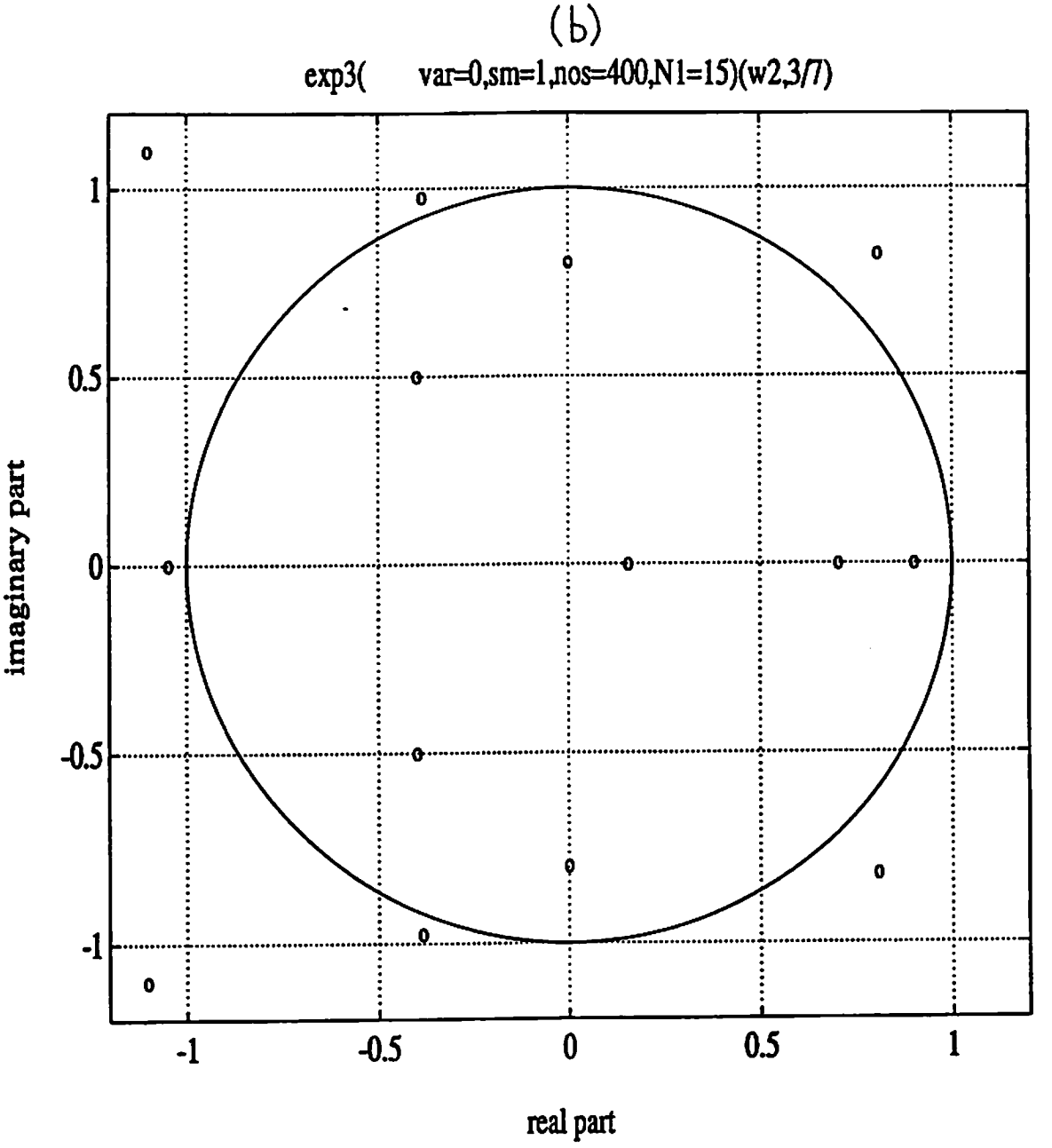

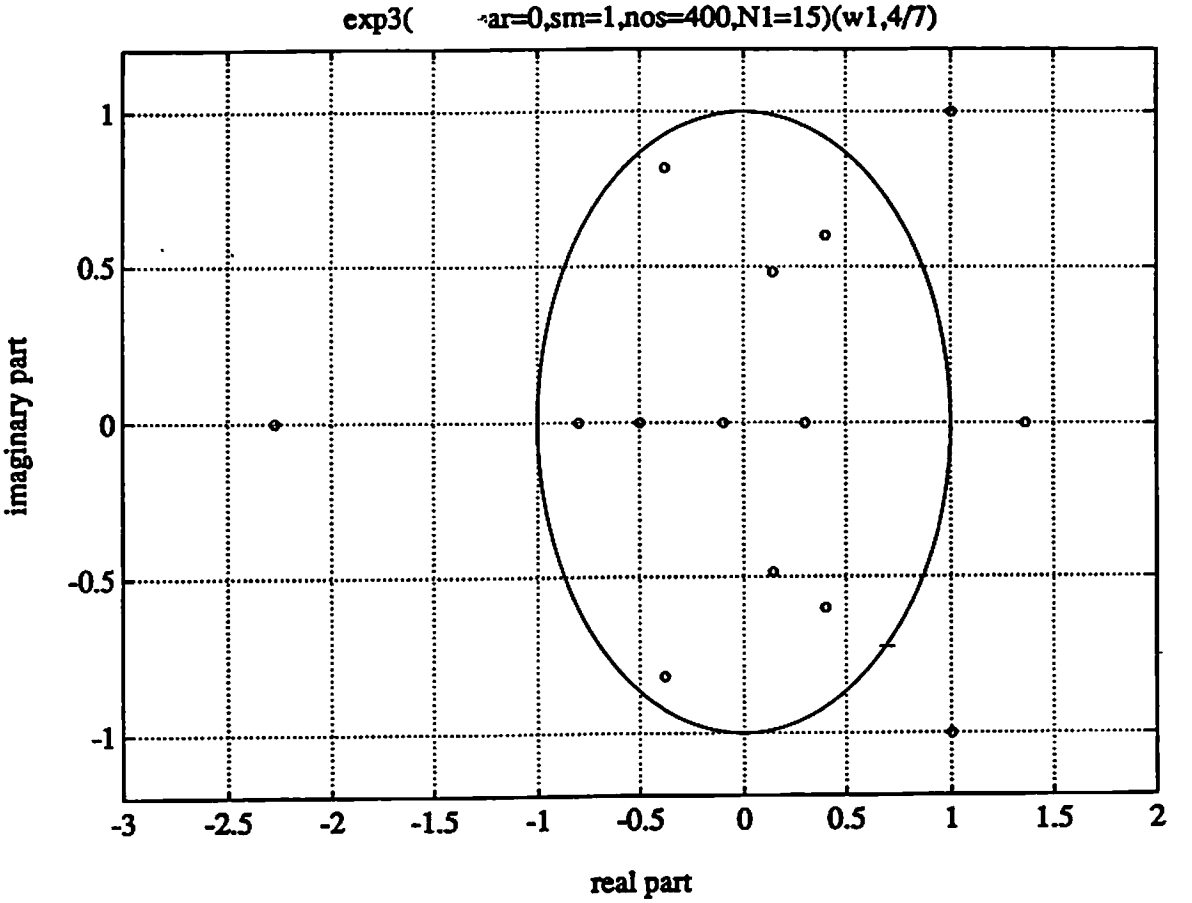

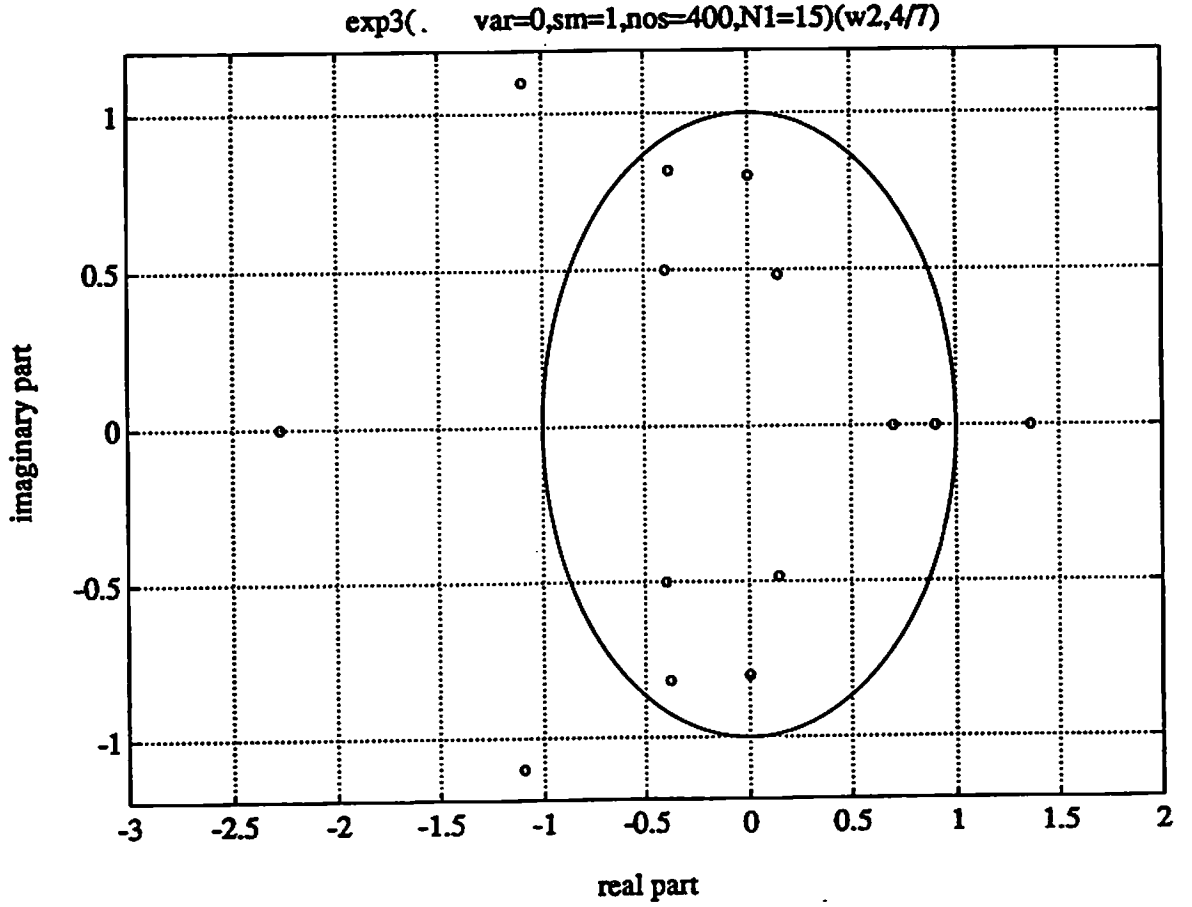

Figure 14: Adaptive channel root locations obtained by EVAM (using q_4) for the noiseless case. (a) channel-1, (b) channel-2.

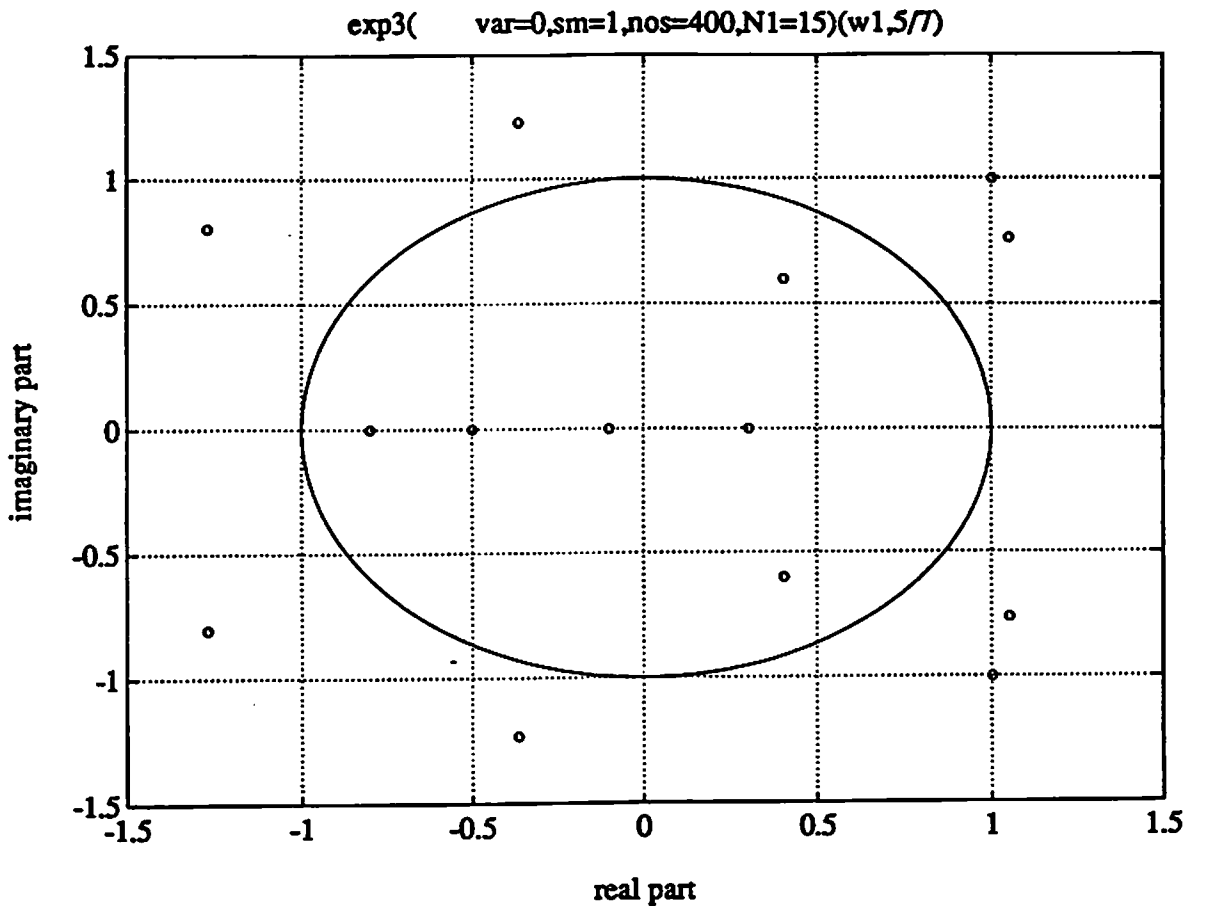

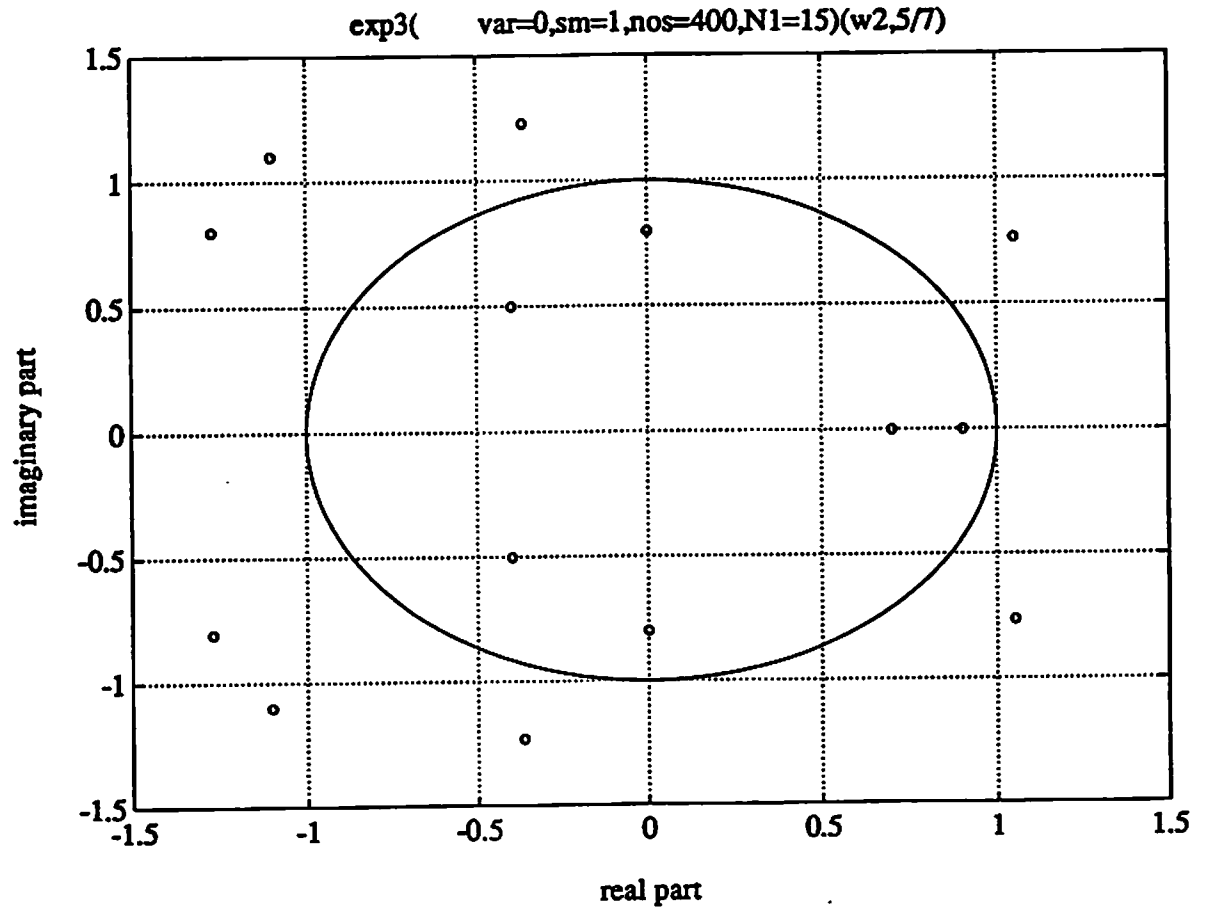

Figure 15: Adaptive channel root locations obtained by EVAM (using $\underline{q}_5$) for the noiseless case. (a) channel-1, (b) channel-2.

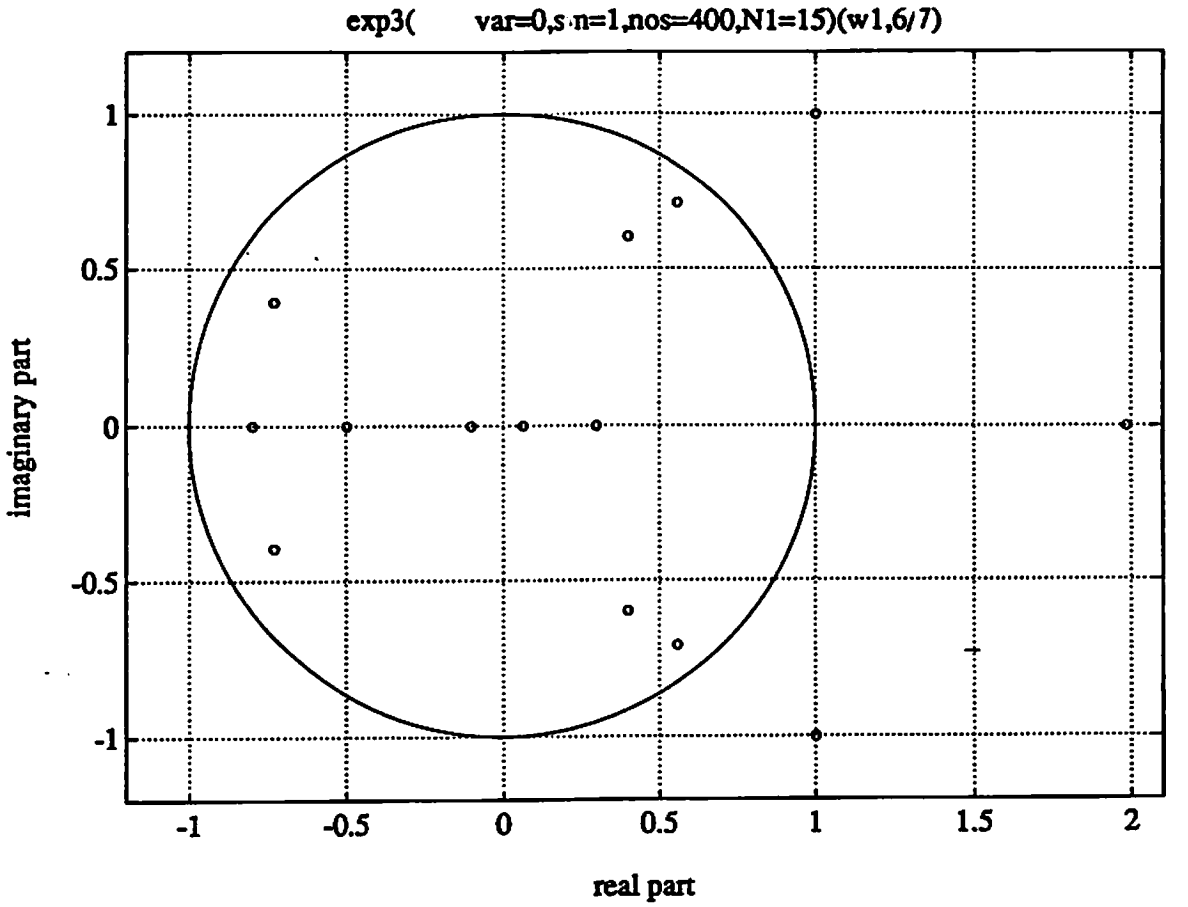

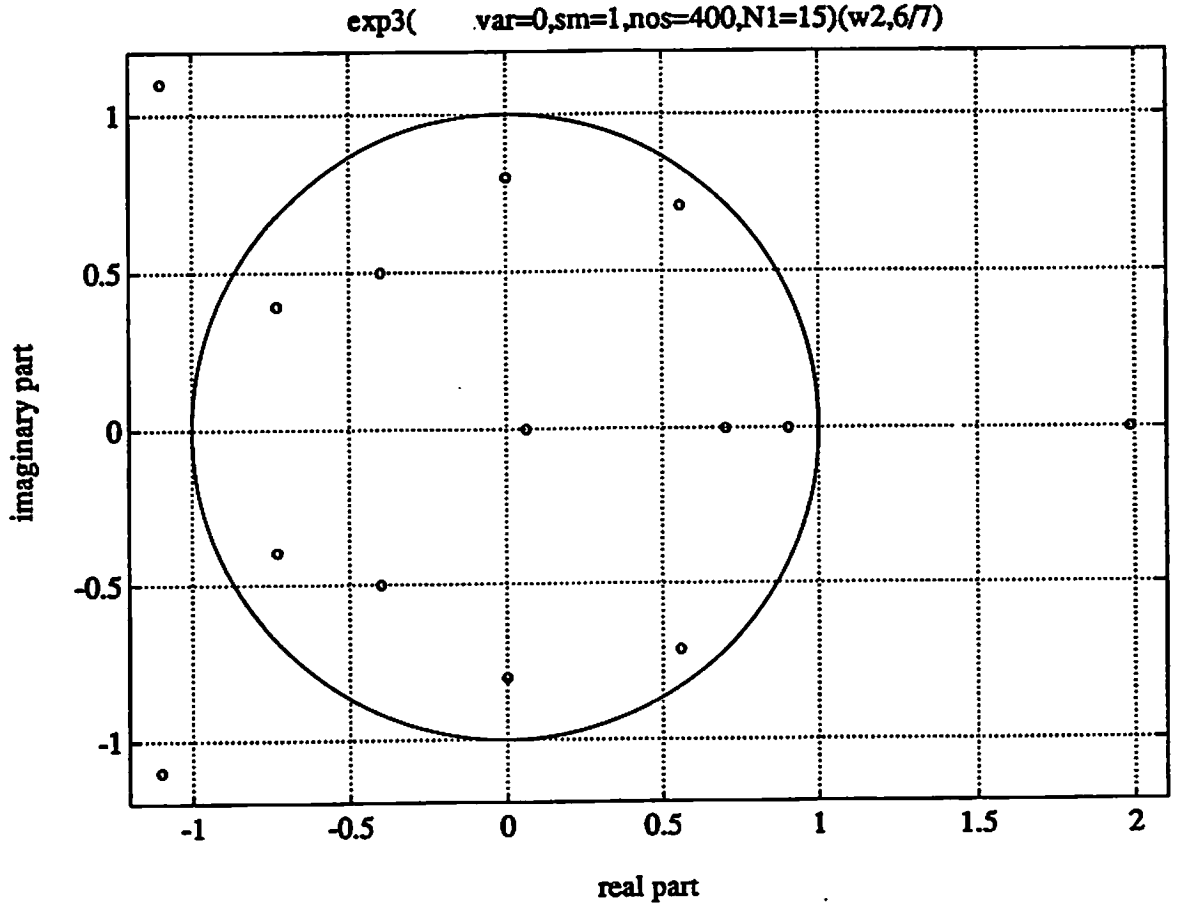

Figure 16: Adaptive channel root locations obtained by EVAM (using $\underline{q}_6$) for the noiseless case. (a) channel-1, (b) channel-2.

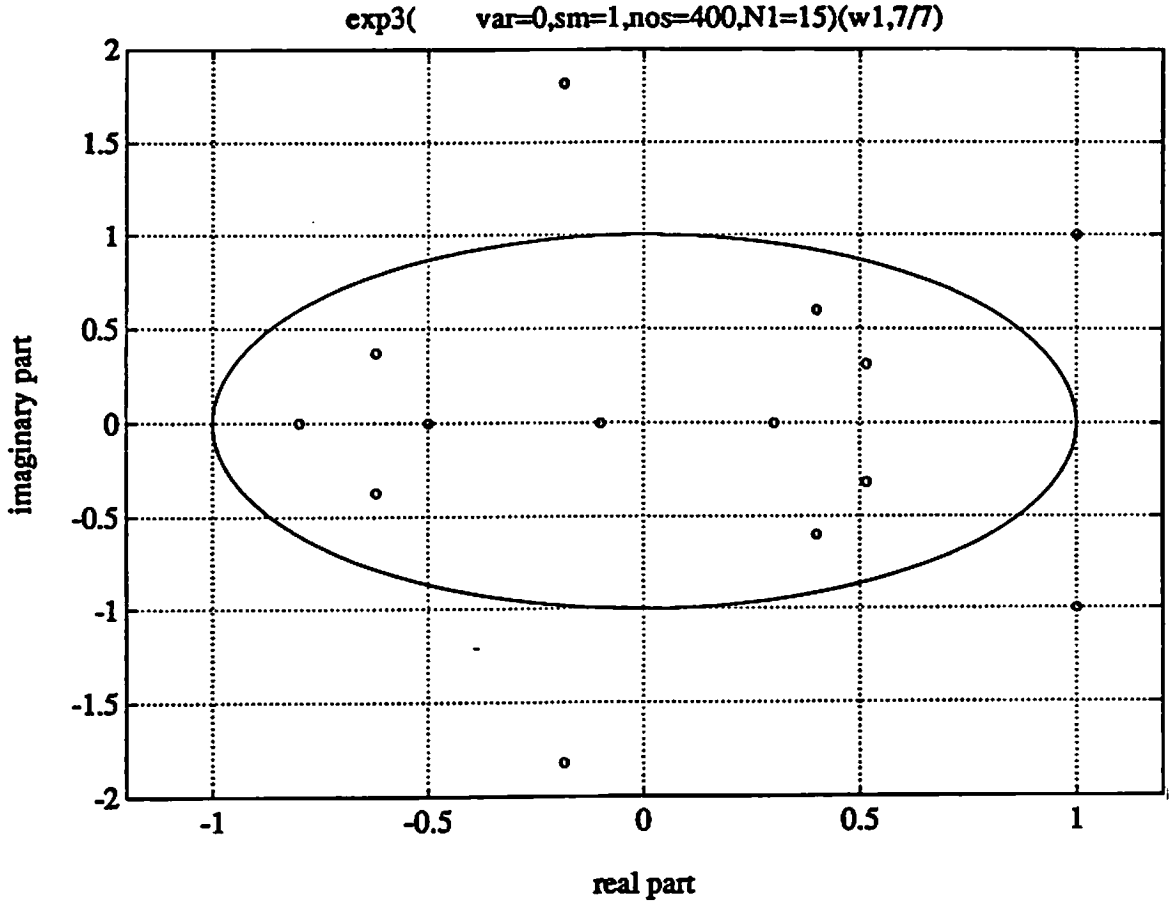

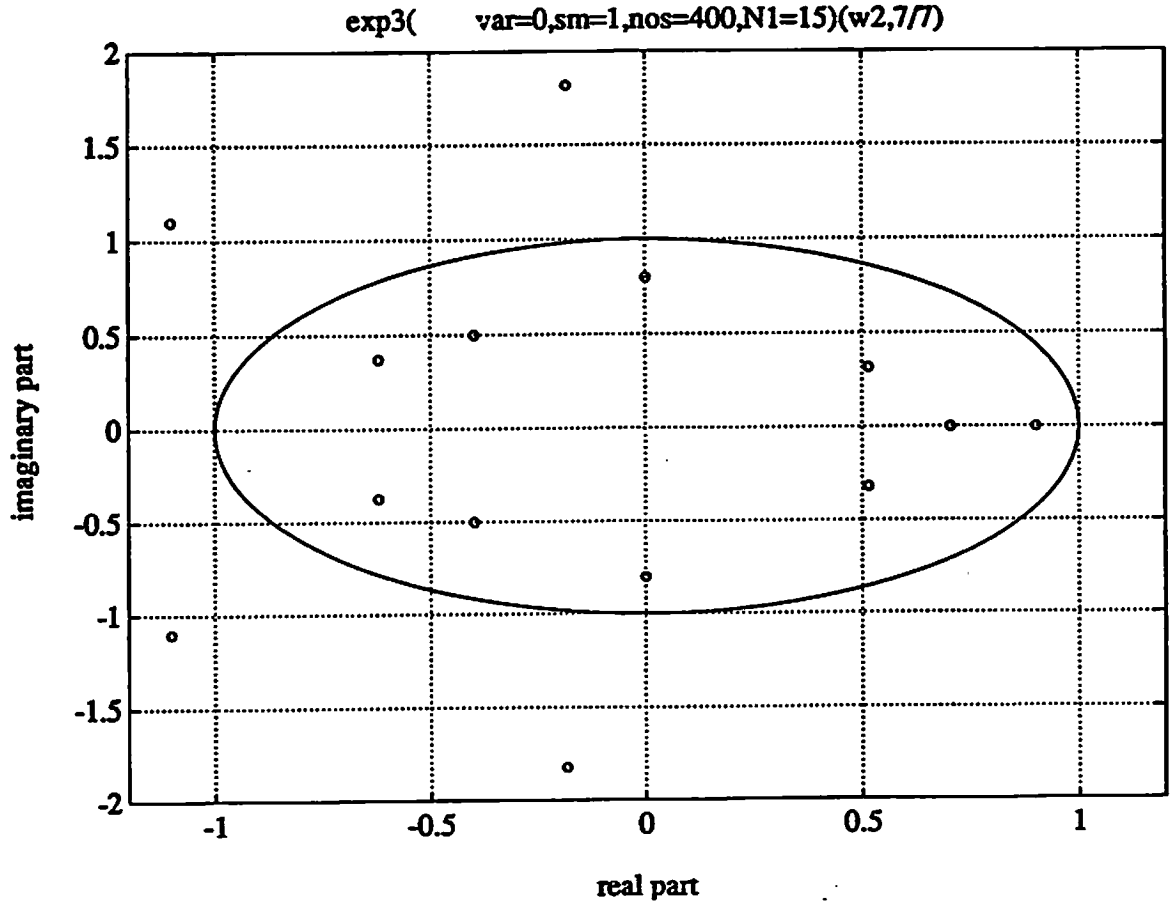

Figure 17: Adaptive channel root locations obtained by EVAM (using $\underline{q}_7$) for the noiseless case. (a) channel-1, (b) channel-2.

Figure 18: Adaptive channel root locatio ıs obtained by Modular RLS algorithm for the noiseless case. (a) channel-1, (b) channel-2.

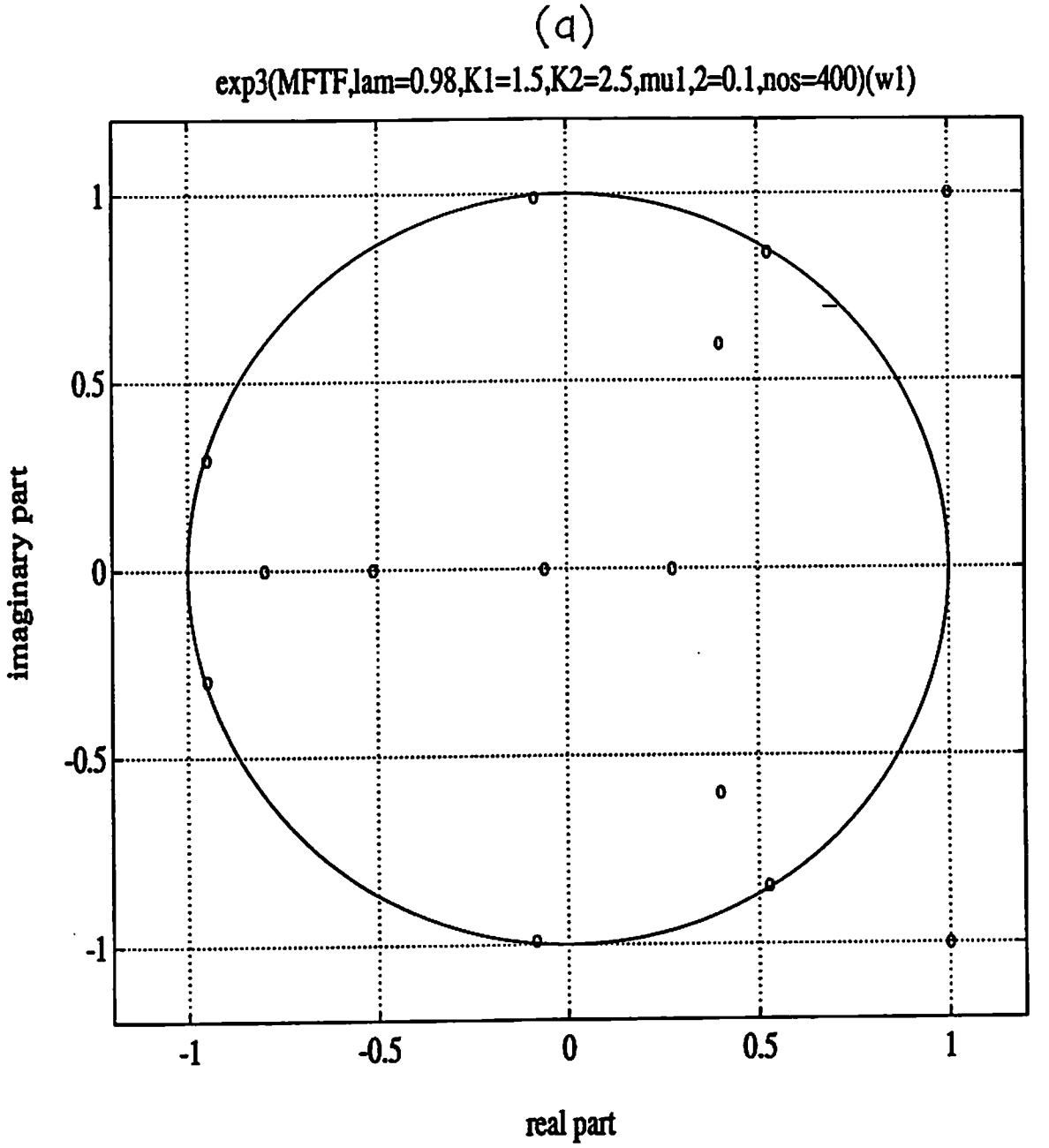

Figure 18: (Cont-d)

(b)

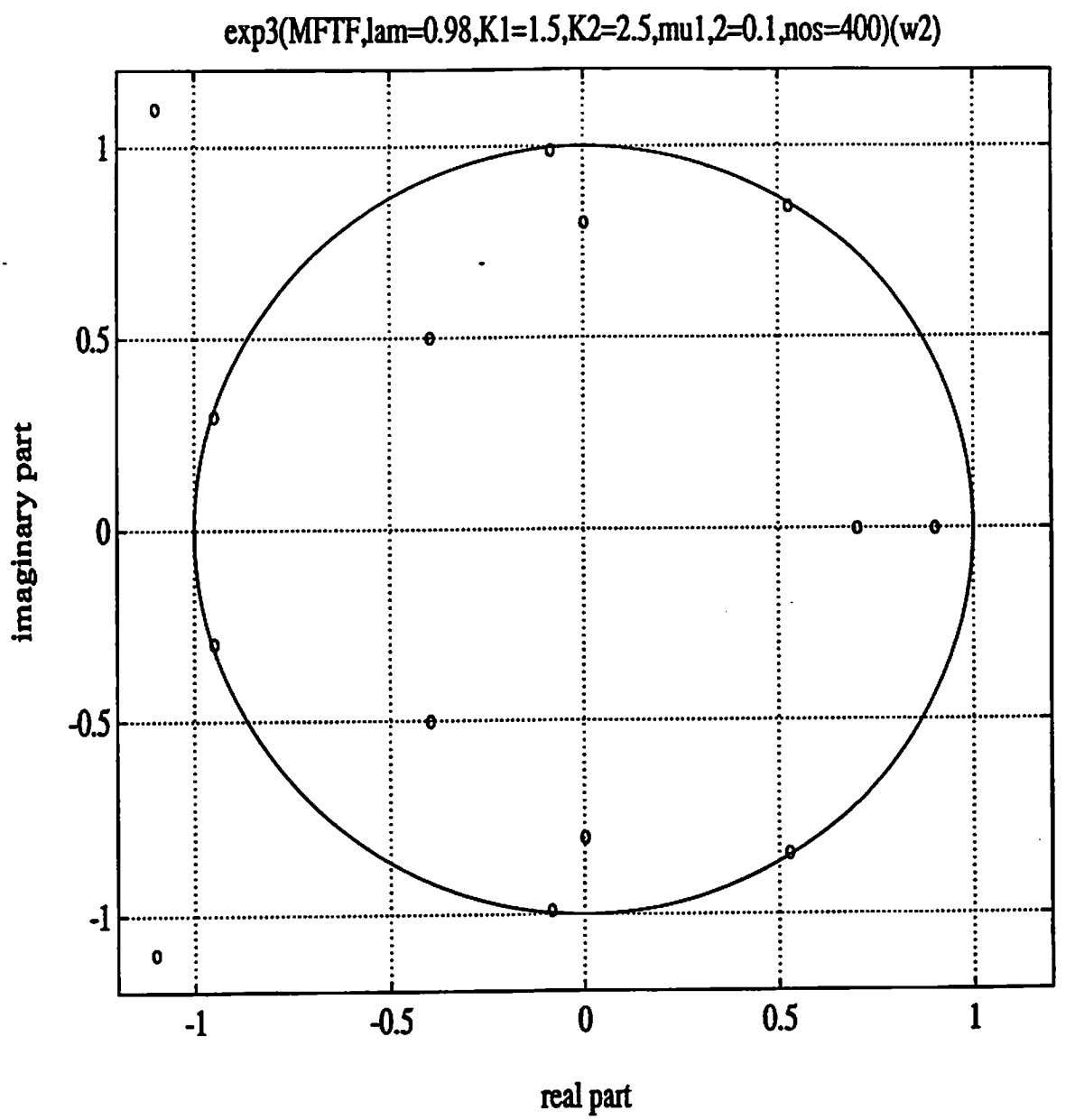

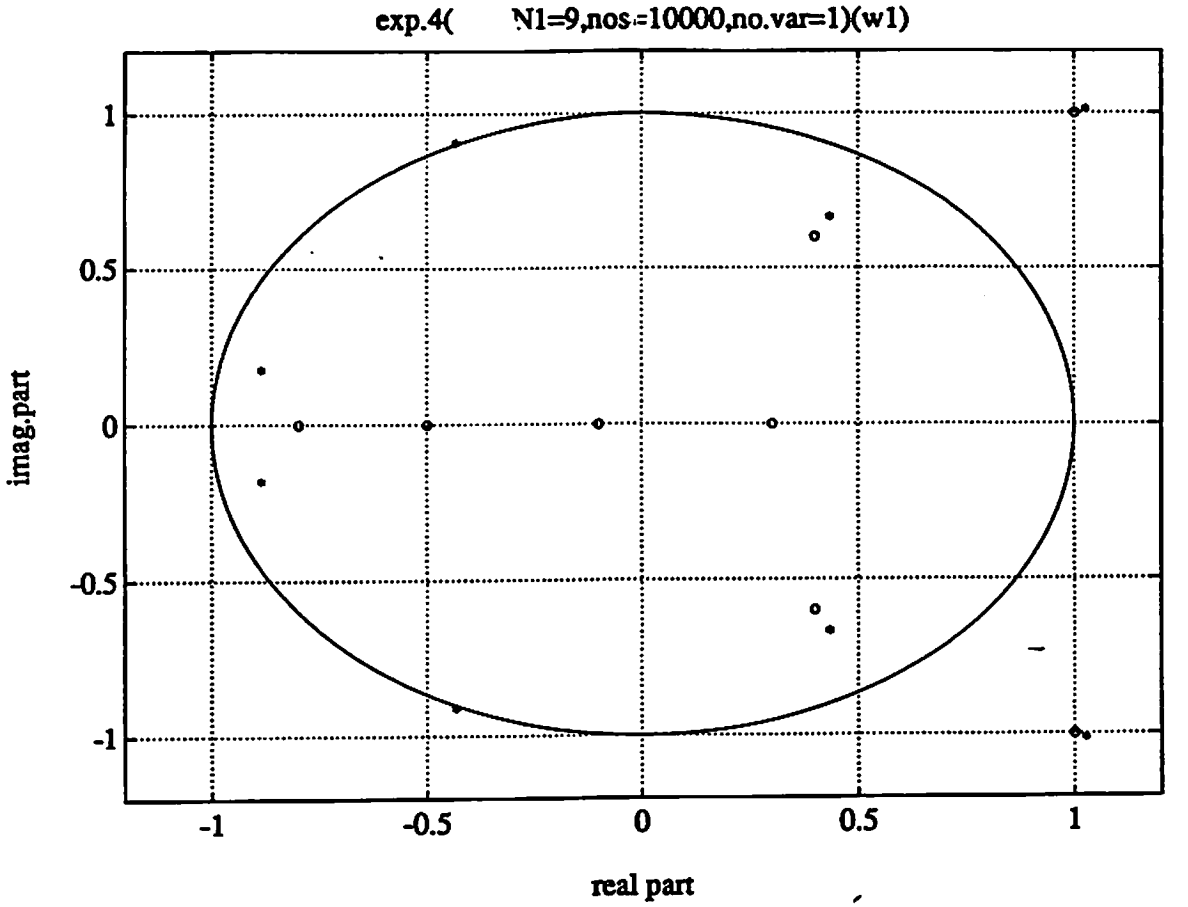

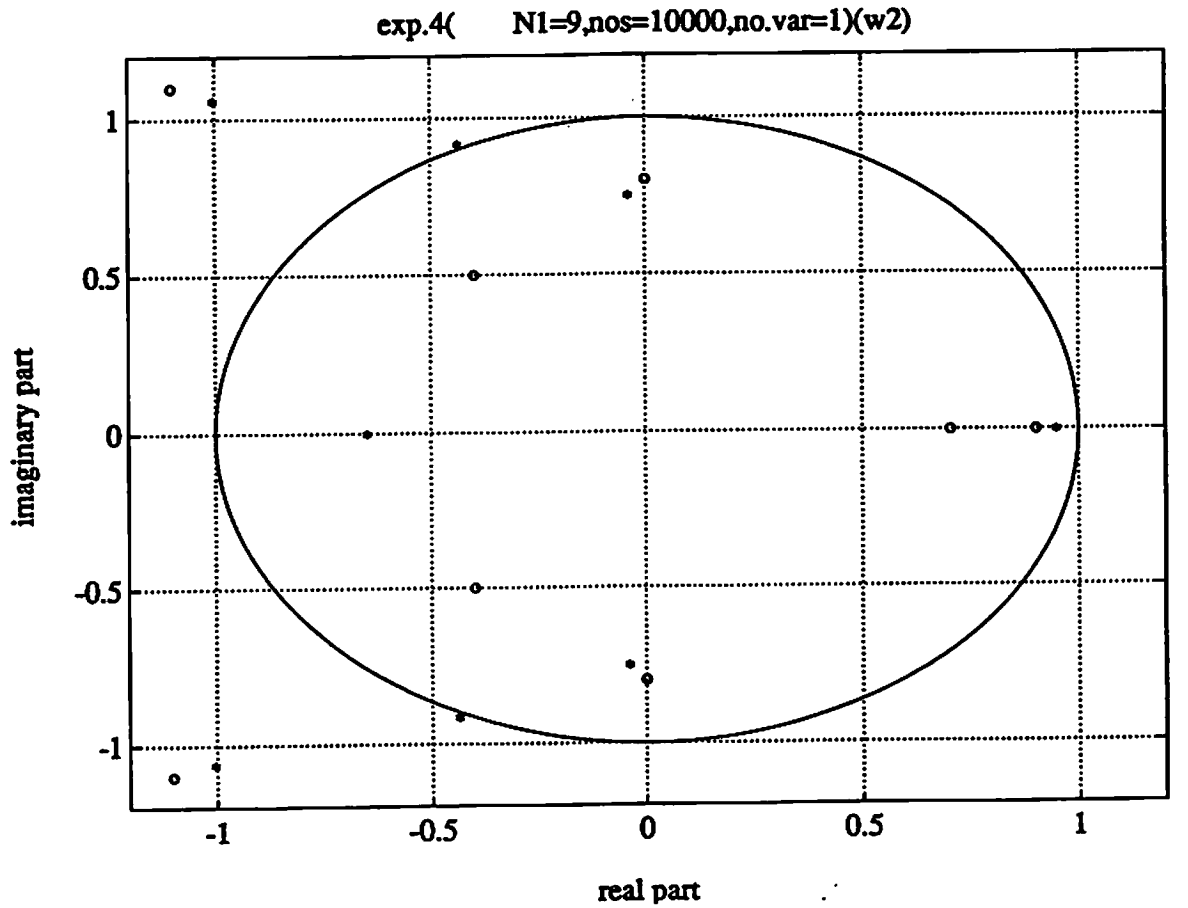

Figure 19: Adaptive channel root locations obtained by EVAM for SNR $\approx$ 10dB. (a) channel-1, (b) channel-2.

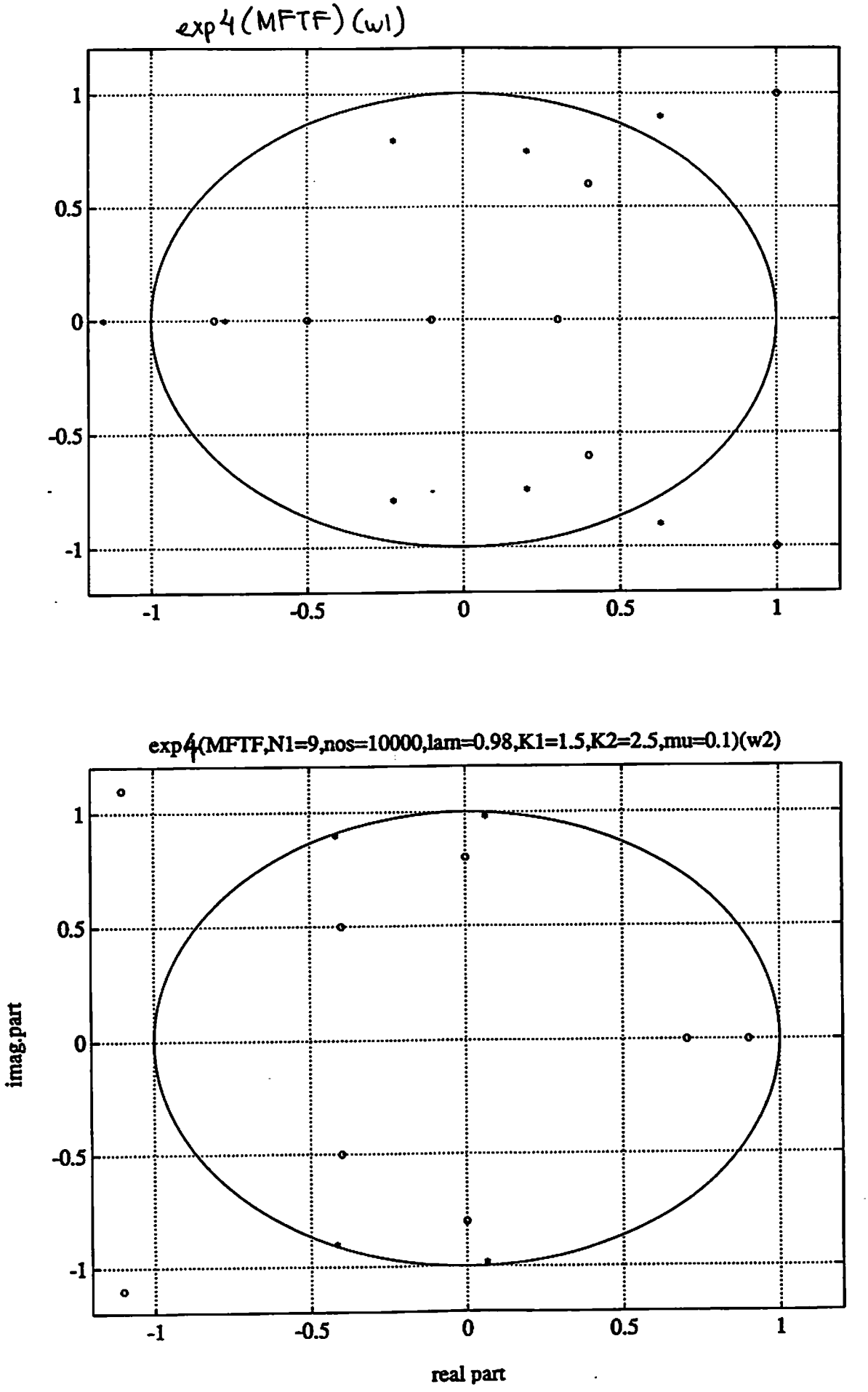

Figure 20: Adaptive channel root locations obtained by Modular RLS algorithm for SNR $\approx$ 10dB. (a) channel-1, (b) channel-2.

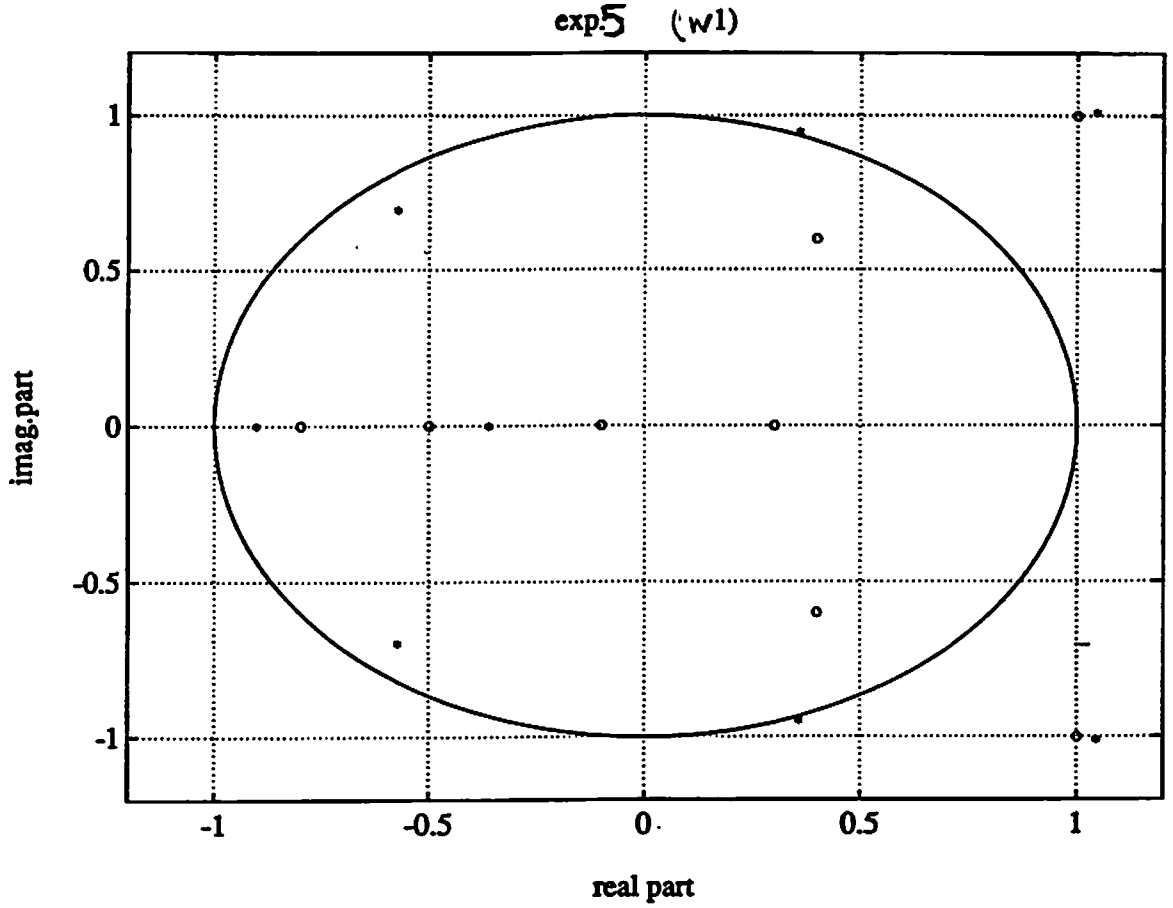

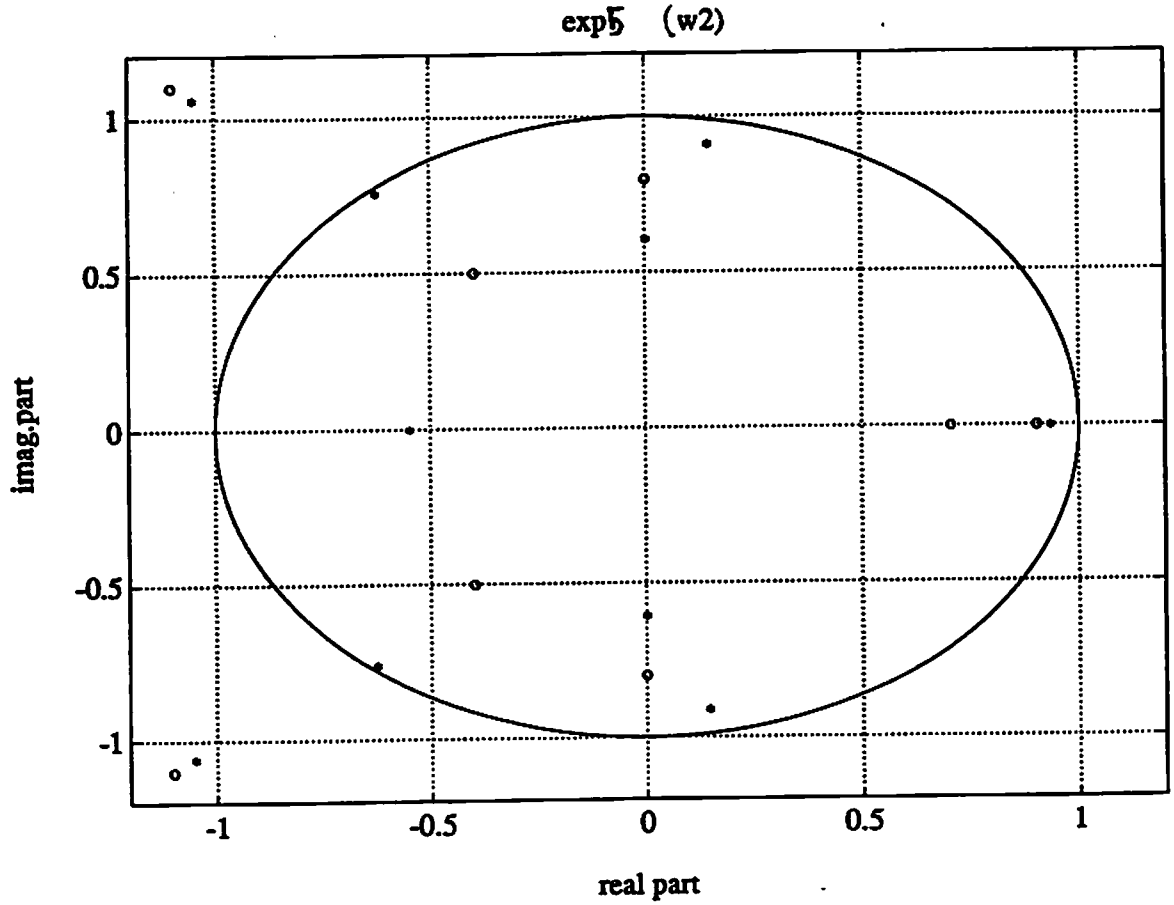

Figure 21: Adaptive channel root locations obtained by EVAM (using q_1) for SNR $\approx$ 10dB. (a) channel-1, (b) channel-2.

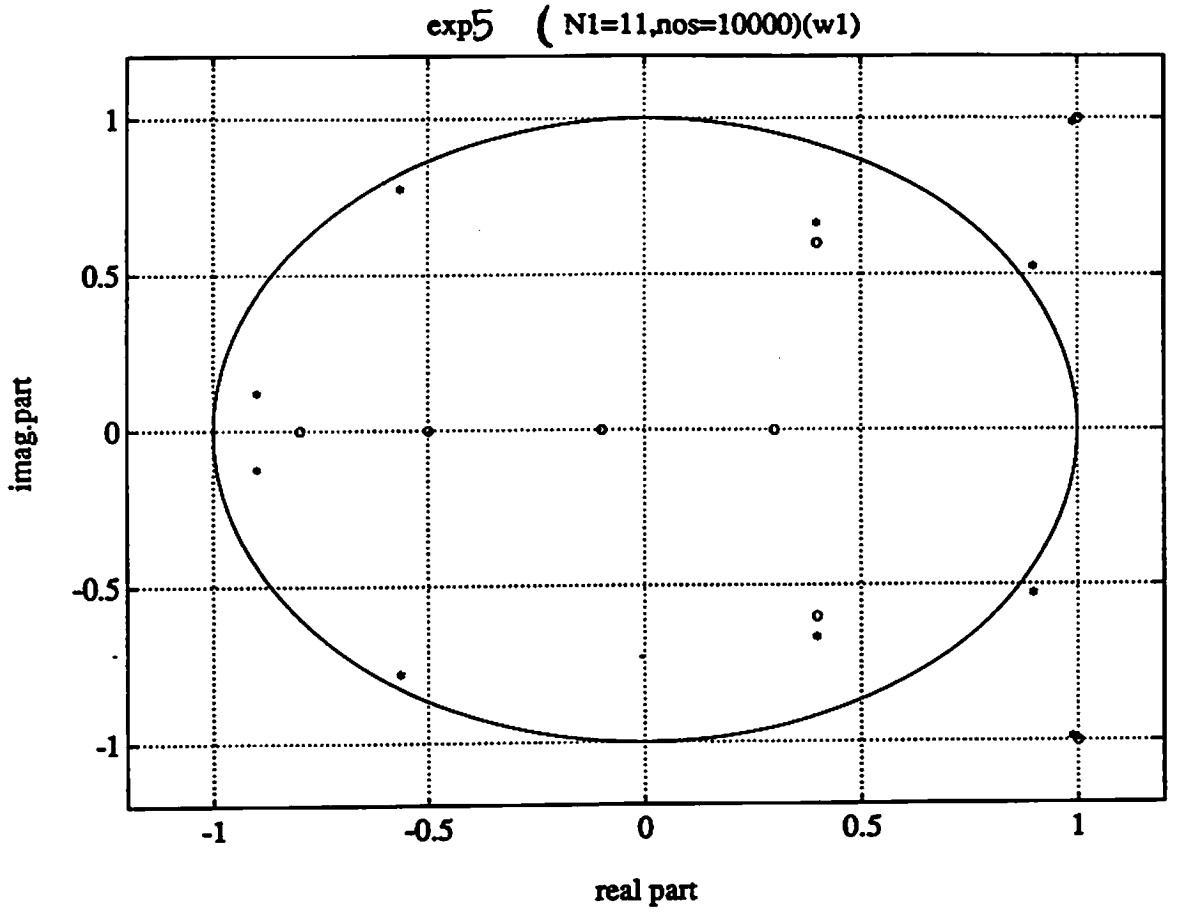

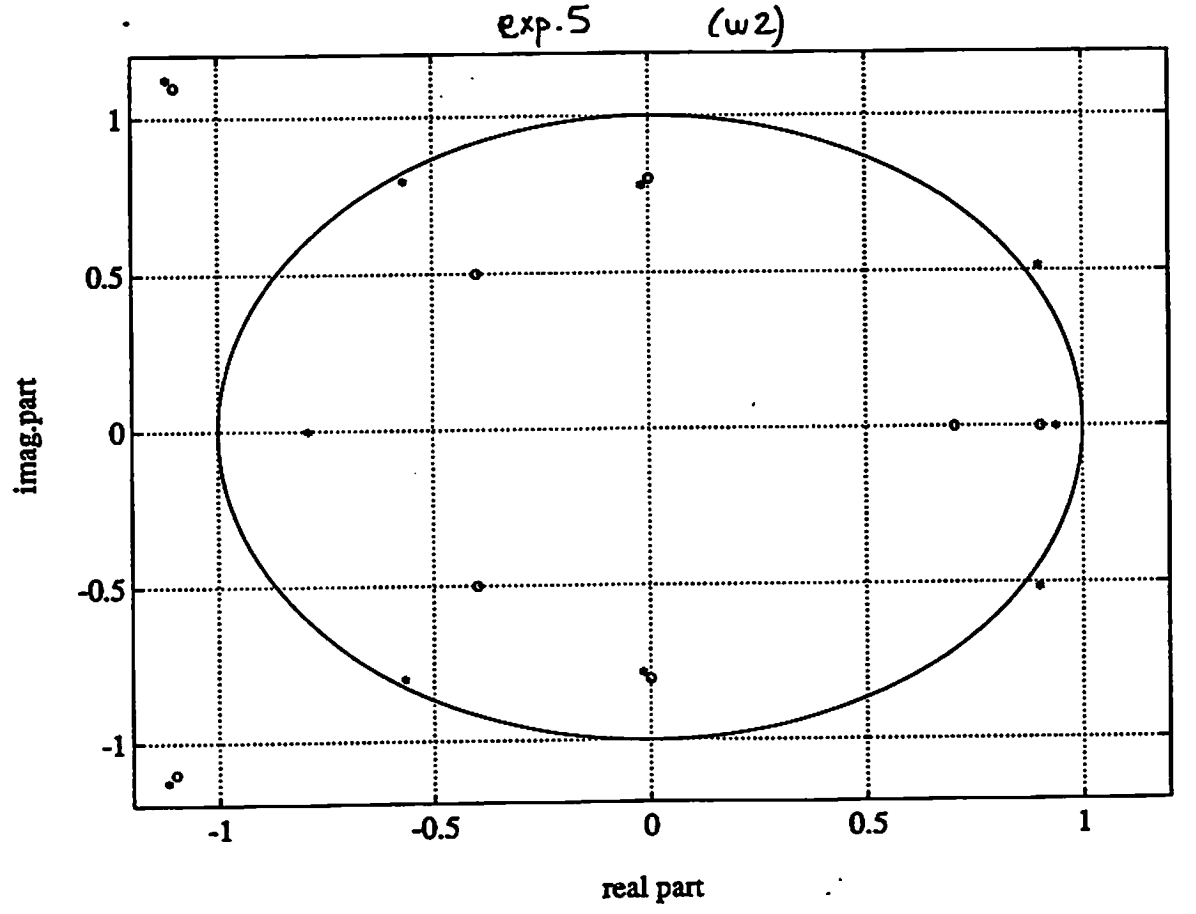

Figure 22: Adaptive channel root locations obtained by EVAM (using q_2) for SNR $\approx$ 10dB. (a) channel-1, (b) channel-2.

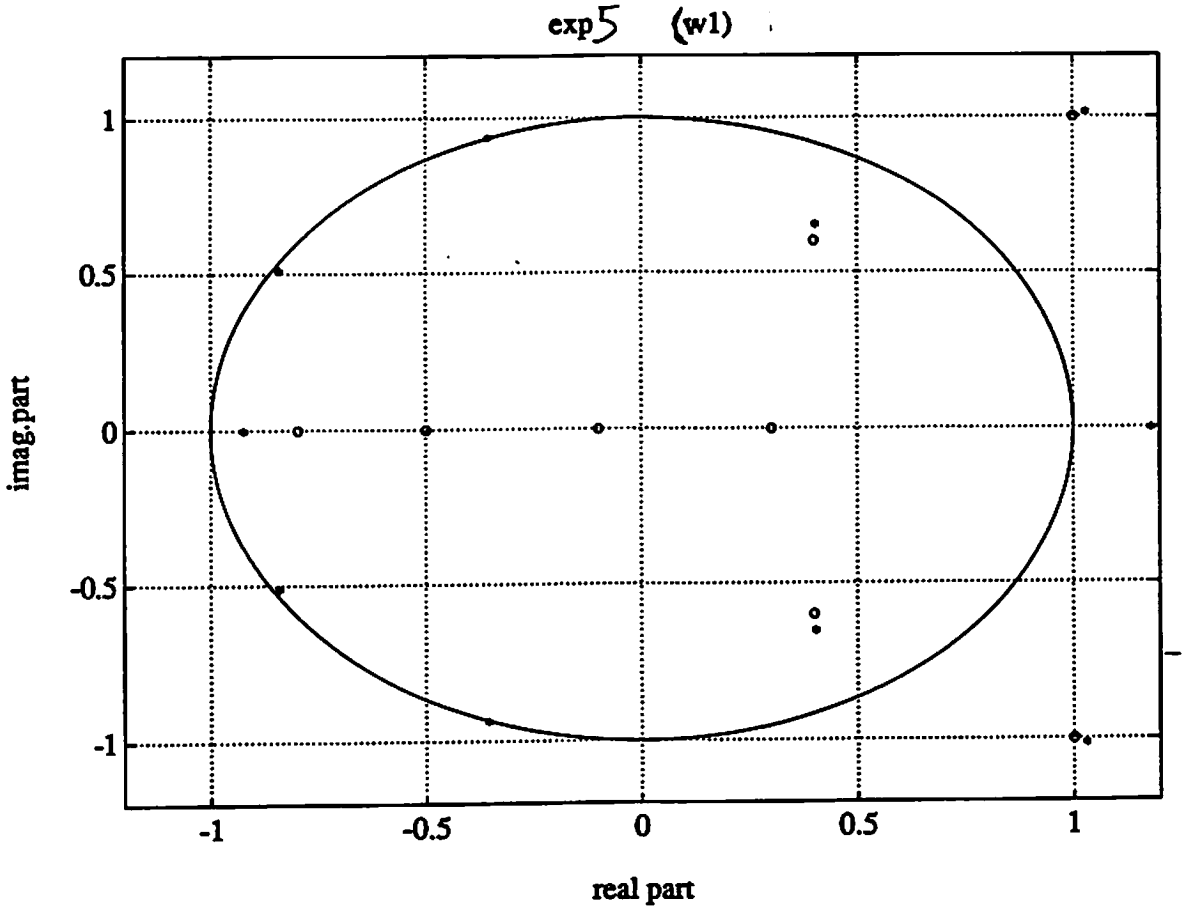

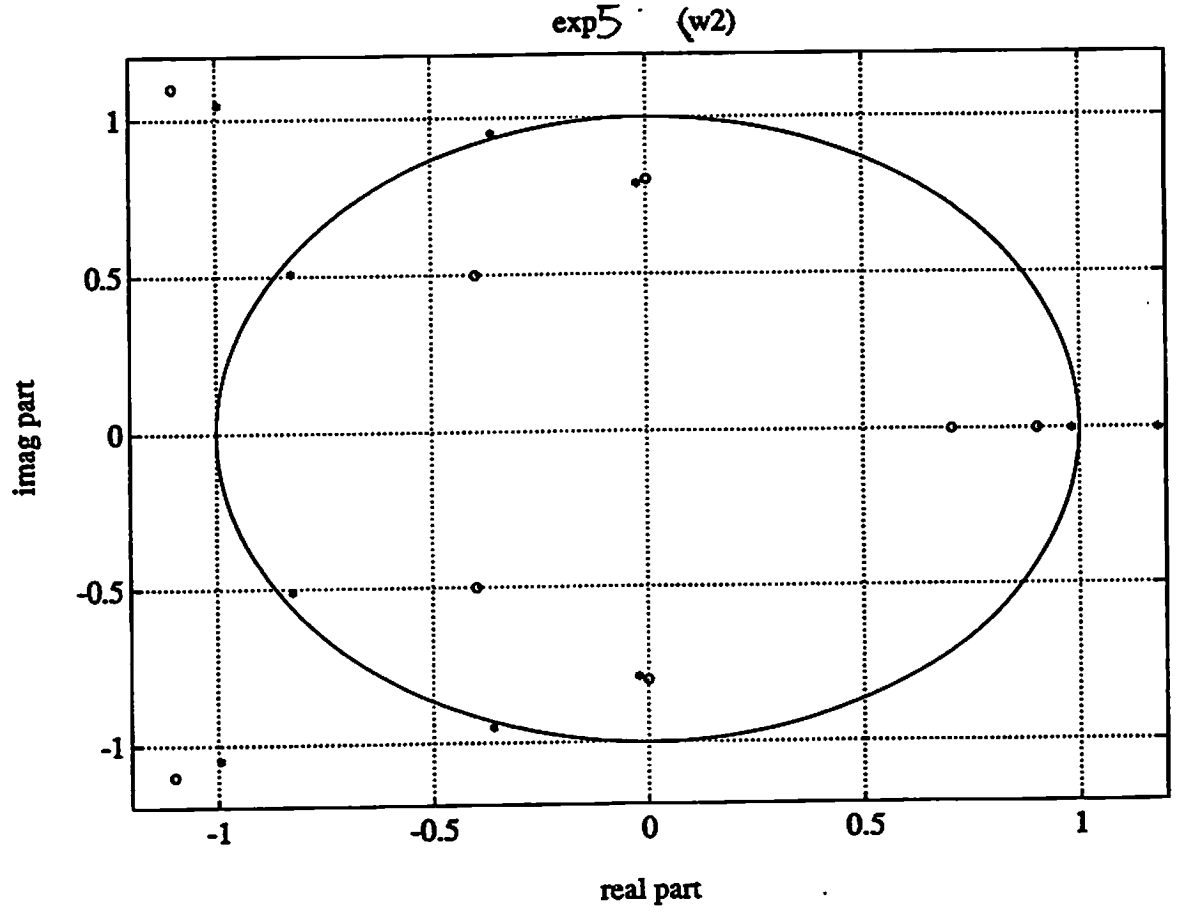

Figure 23: Adaptive channel root locations obtained by EVAM (using $\underline{q}_3$) for SNR $\approx$ 10dB. (a) channel-1, (b) channel-2.

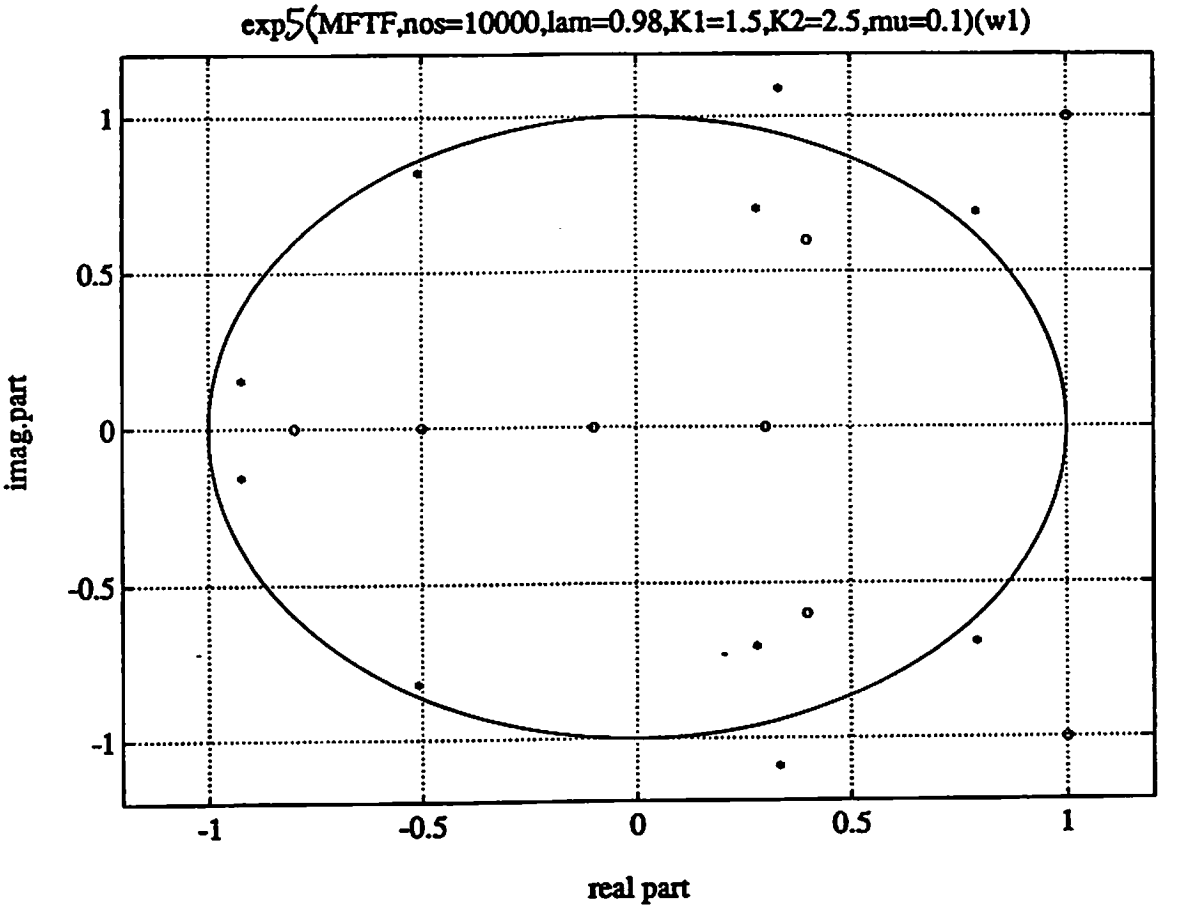

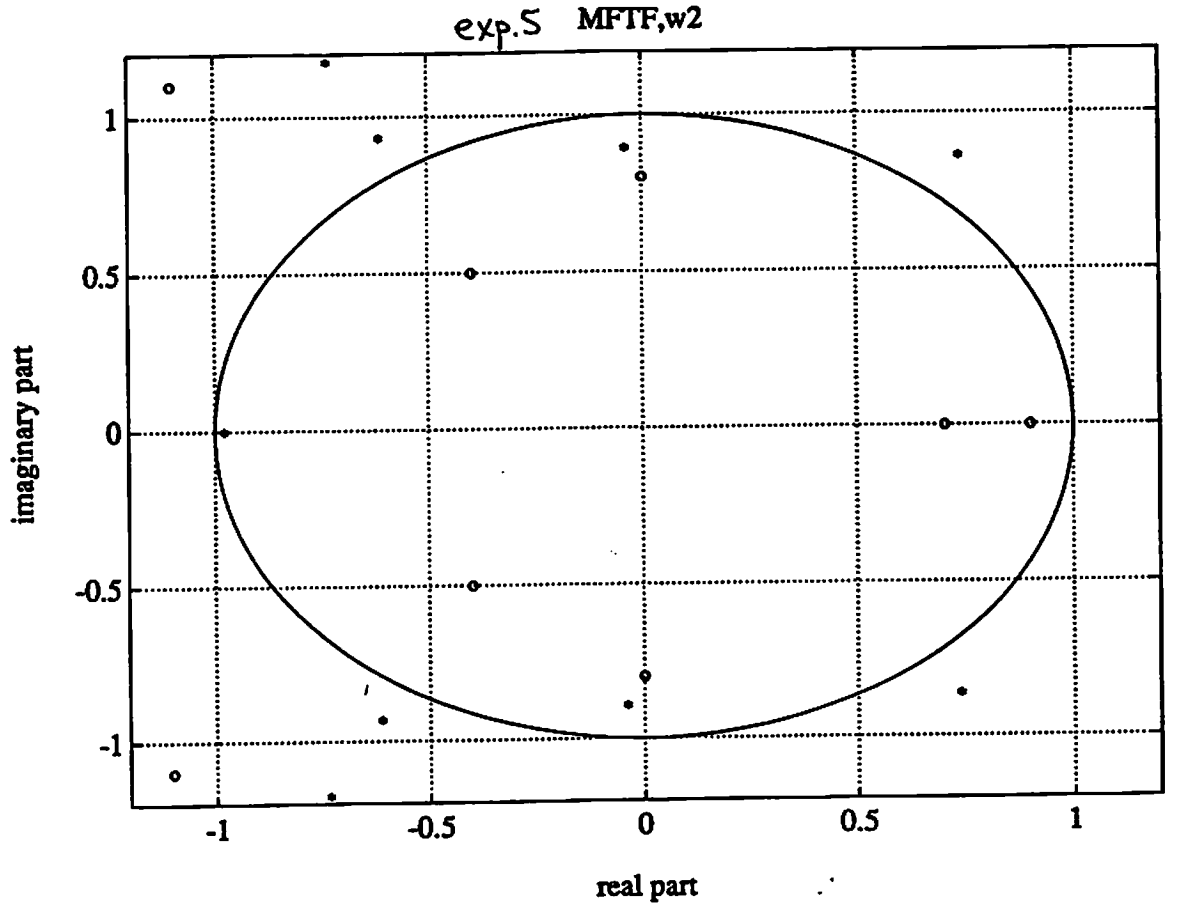

Figure 24: Adaptive channel root locations obtained by Modular RLS algorithm for SNR $\approx$ 10dB. (a) channel-1, (b) channel-2.

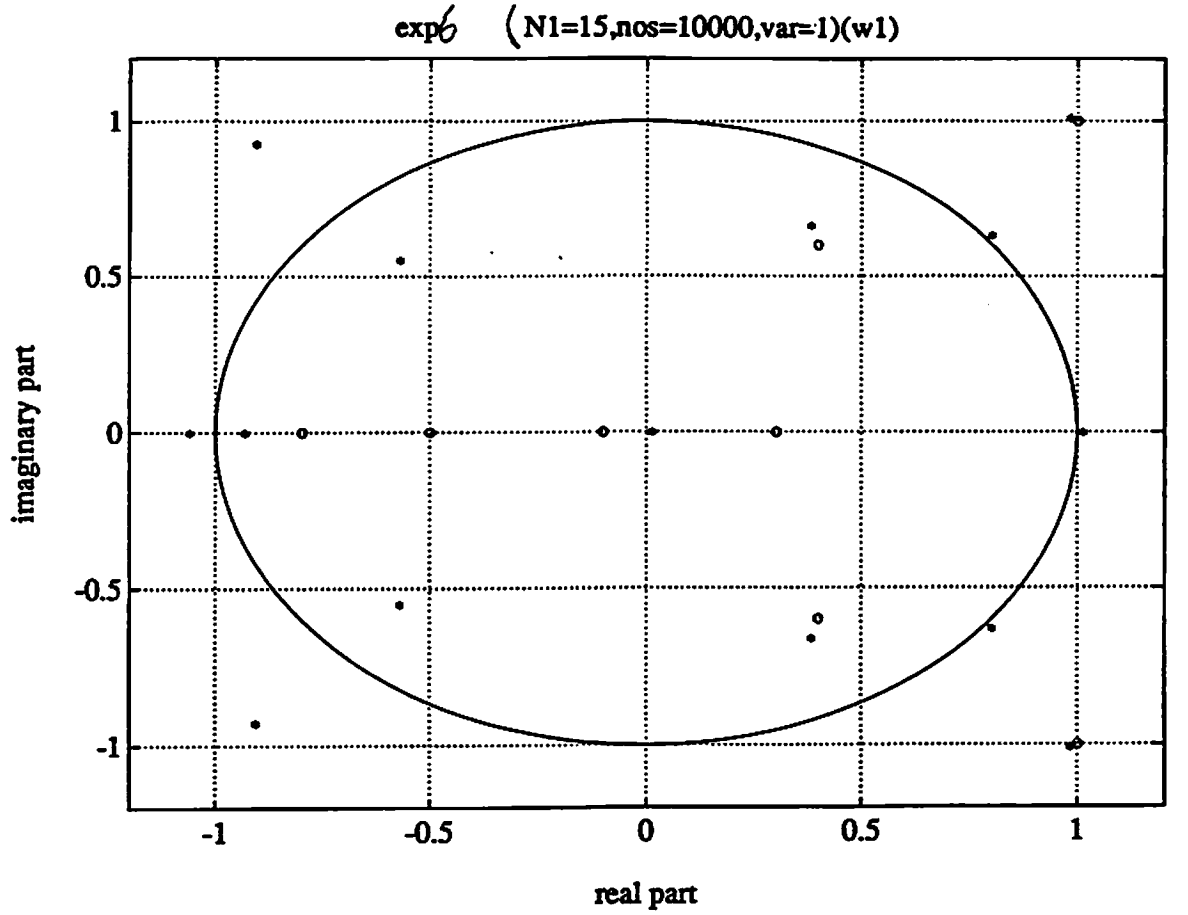

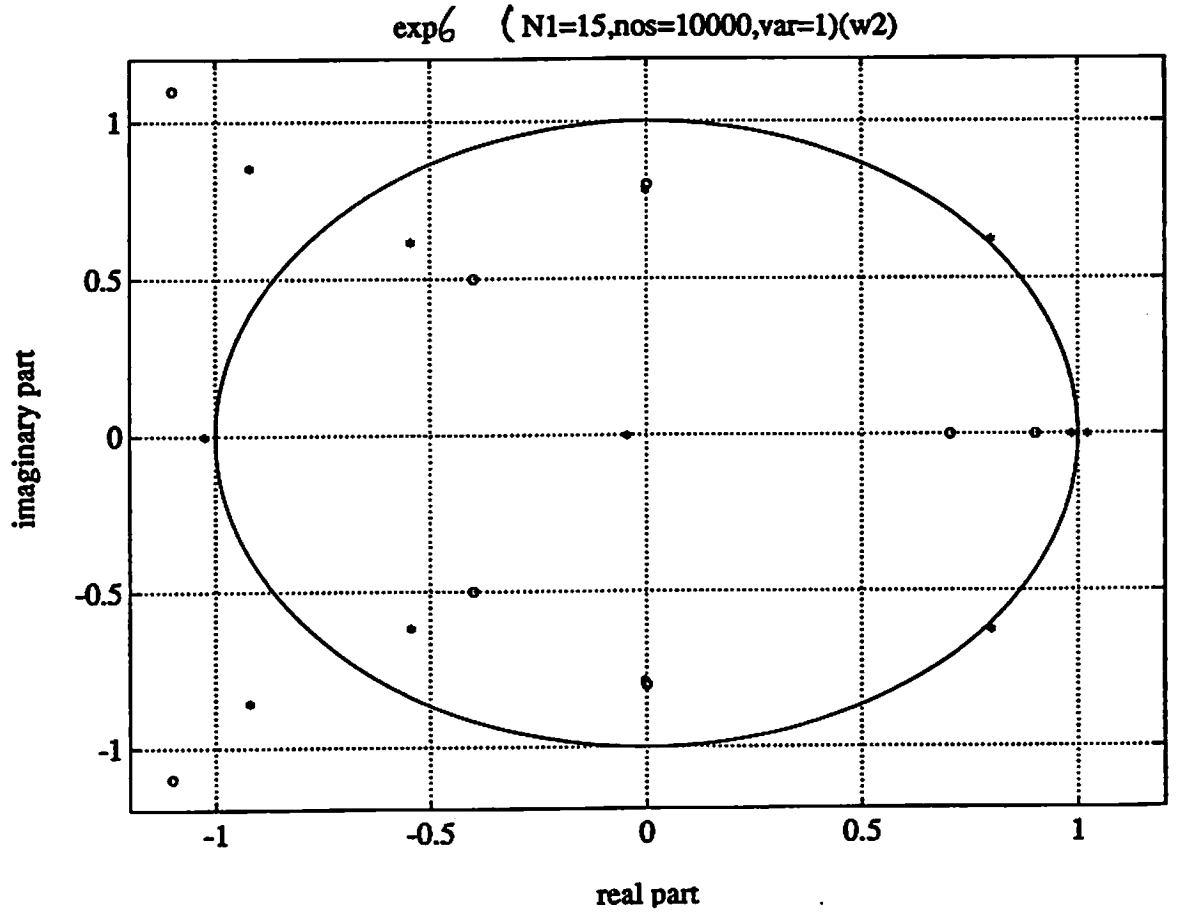

Figure 25: Adaptive channel root locations obtained by EVAM (using q_1) for SNR $\approx$ 10dB. (a) channel-1, (b) channel-2.

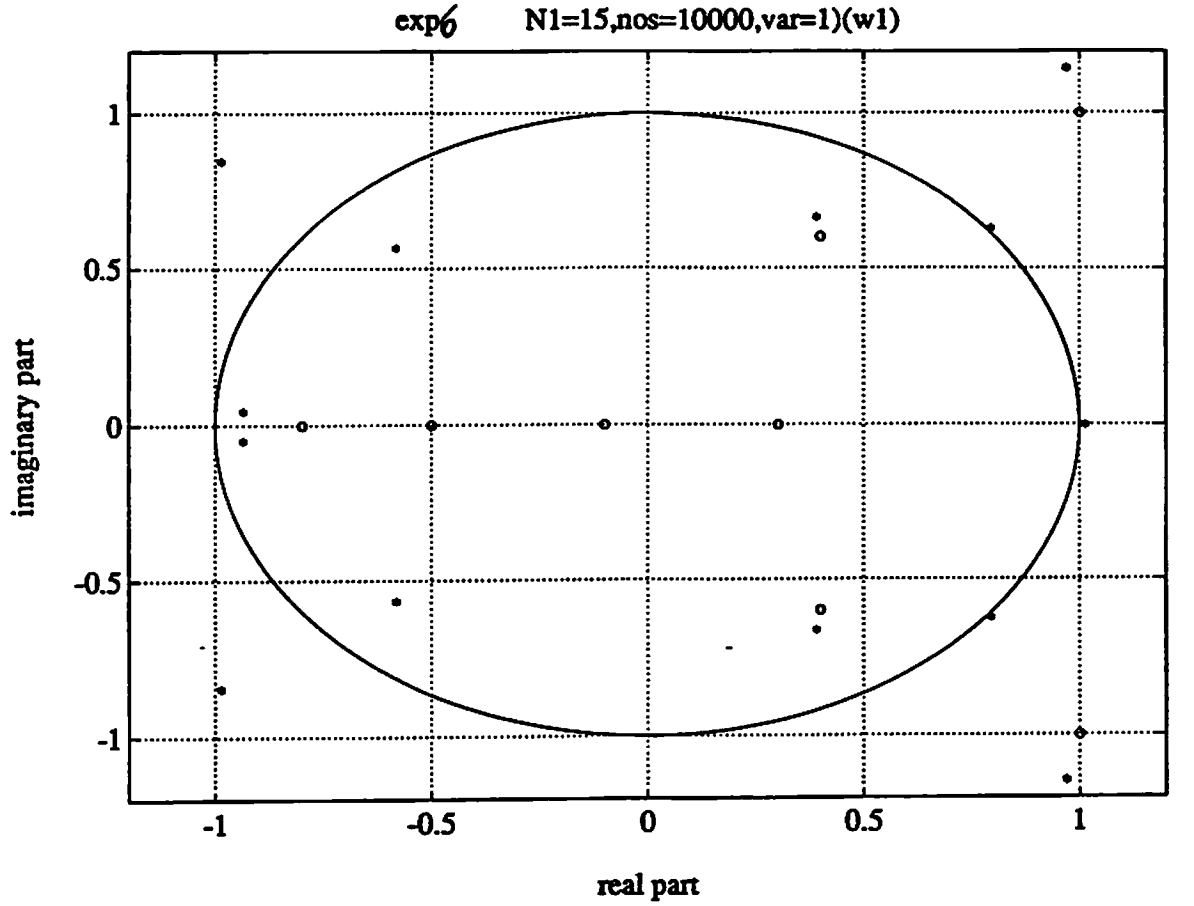

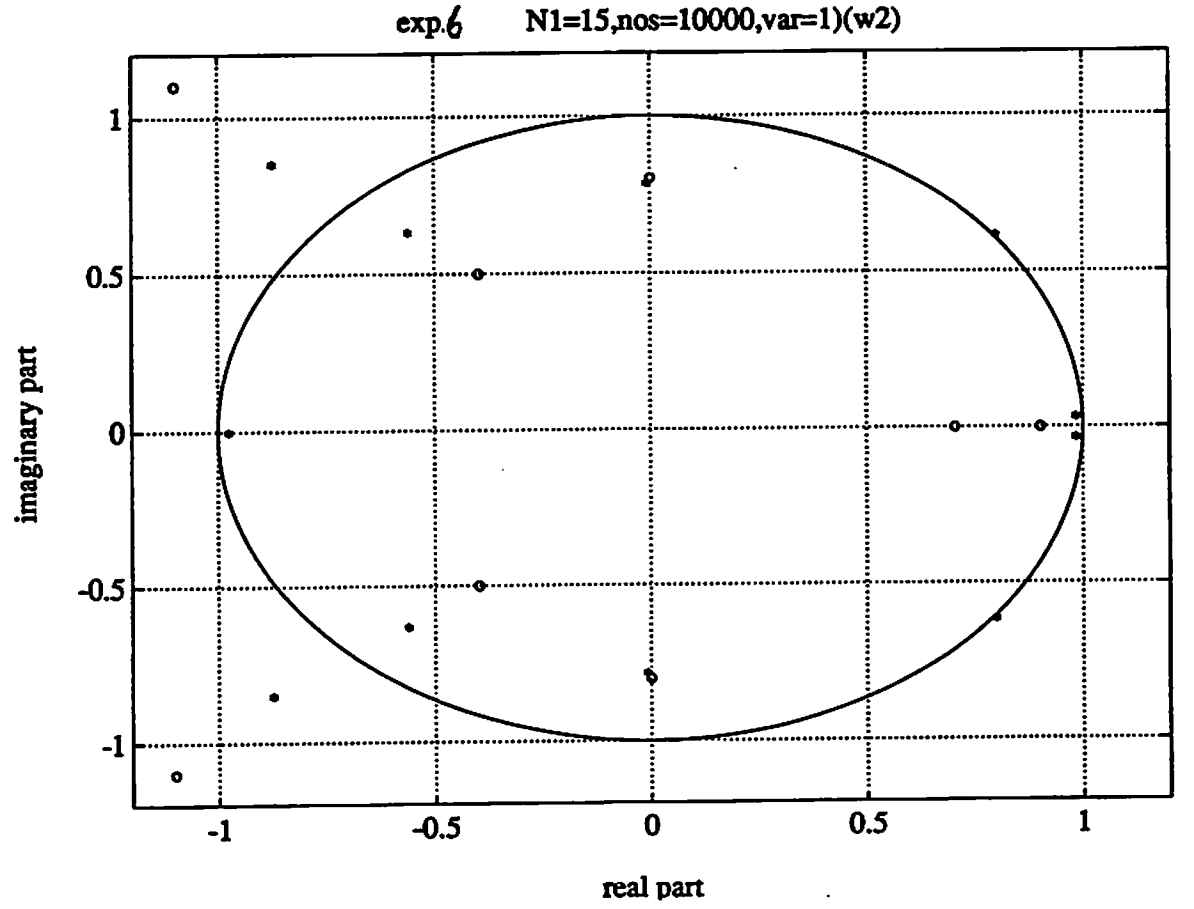

Figure 26: Adaptive channel root locations obtained by EVAM (using $\underline{q}_2$) for SNR $\approx$ 10dB. (a) channel-1, (b) channel-2.

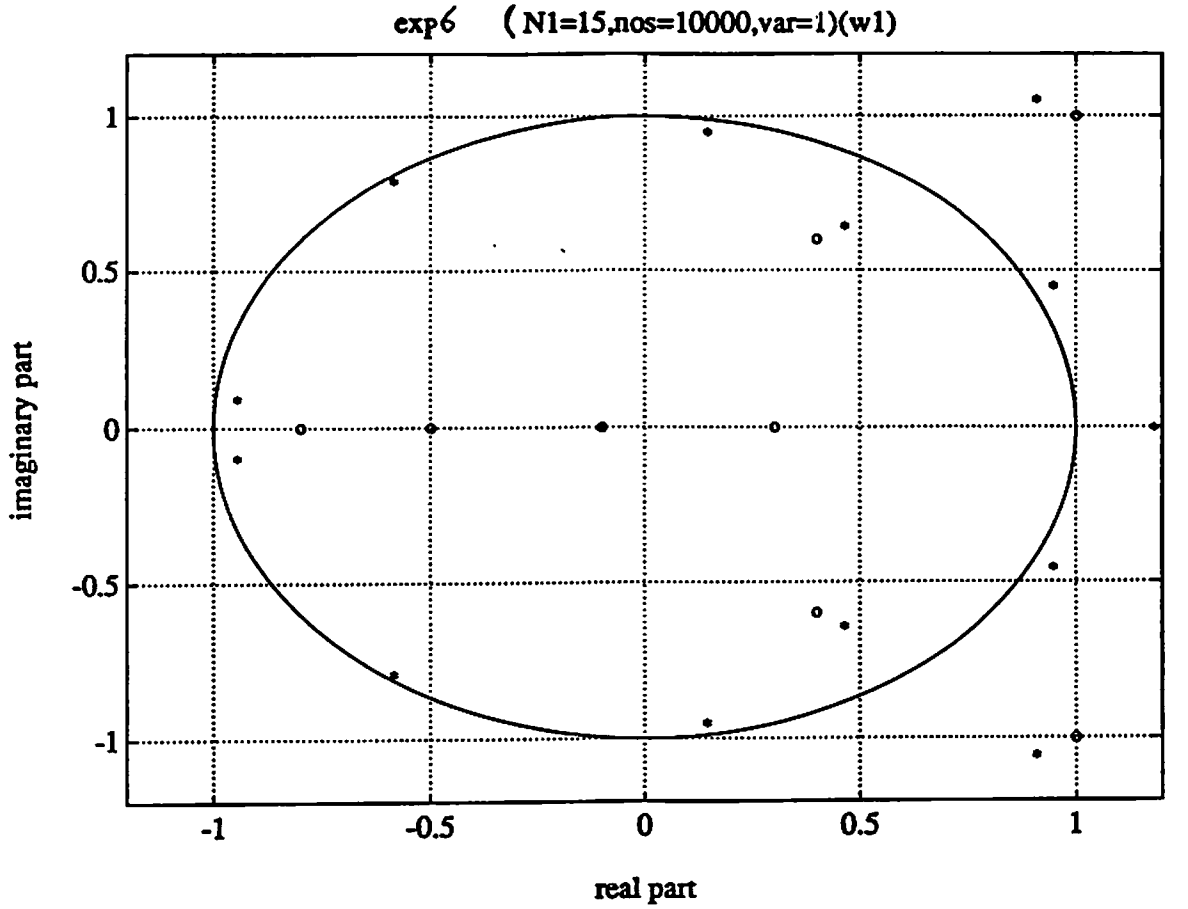

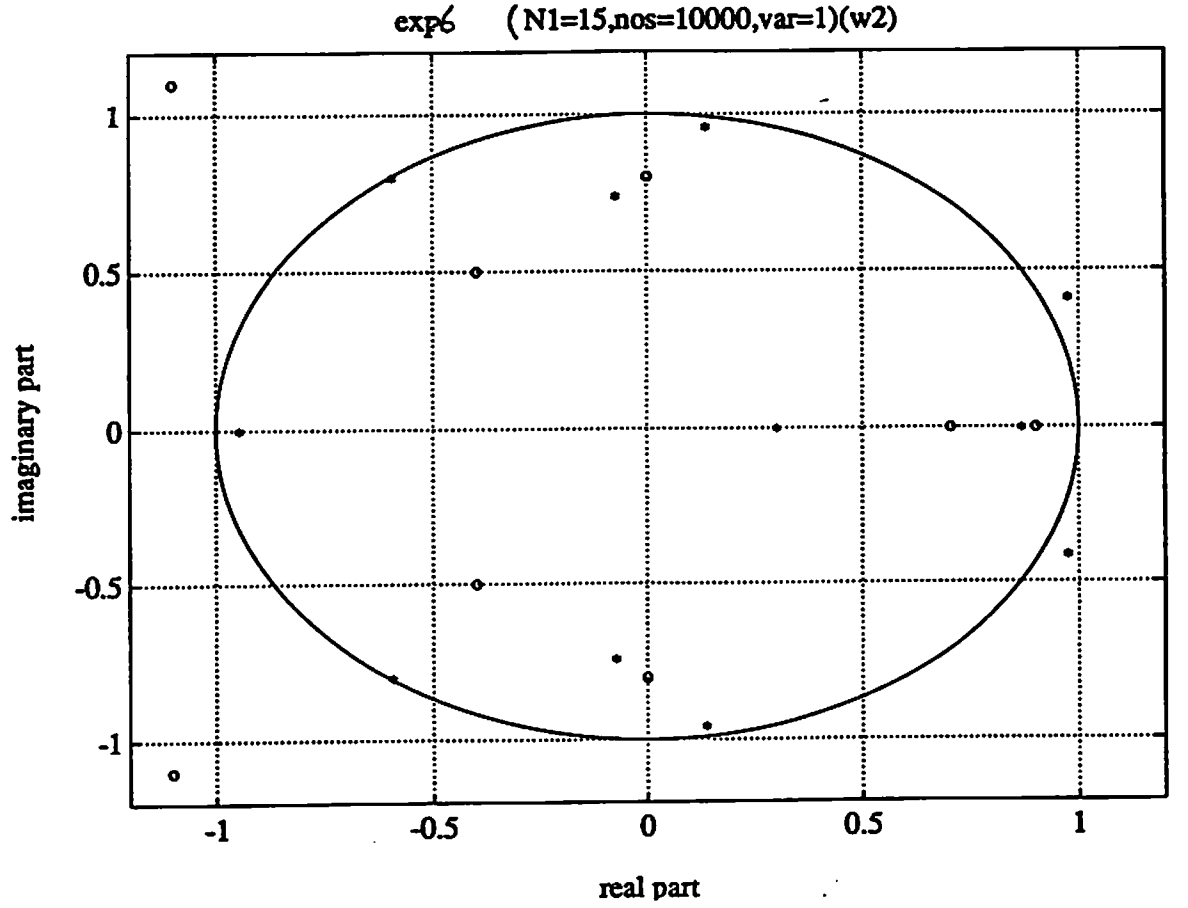

Figure 27: Adaptive channel root locations obtained by EVAM (using q_3) for SNR $\approx$ 10dB. (a) channel-1, (b) channel-2.

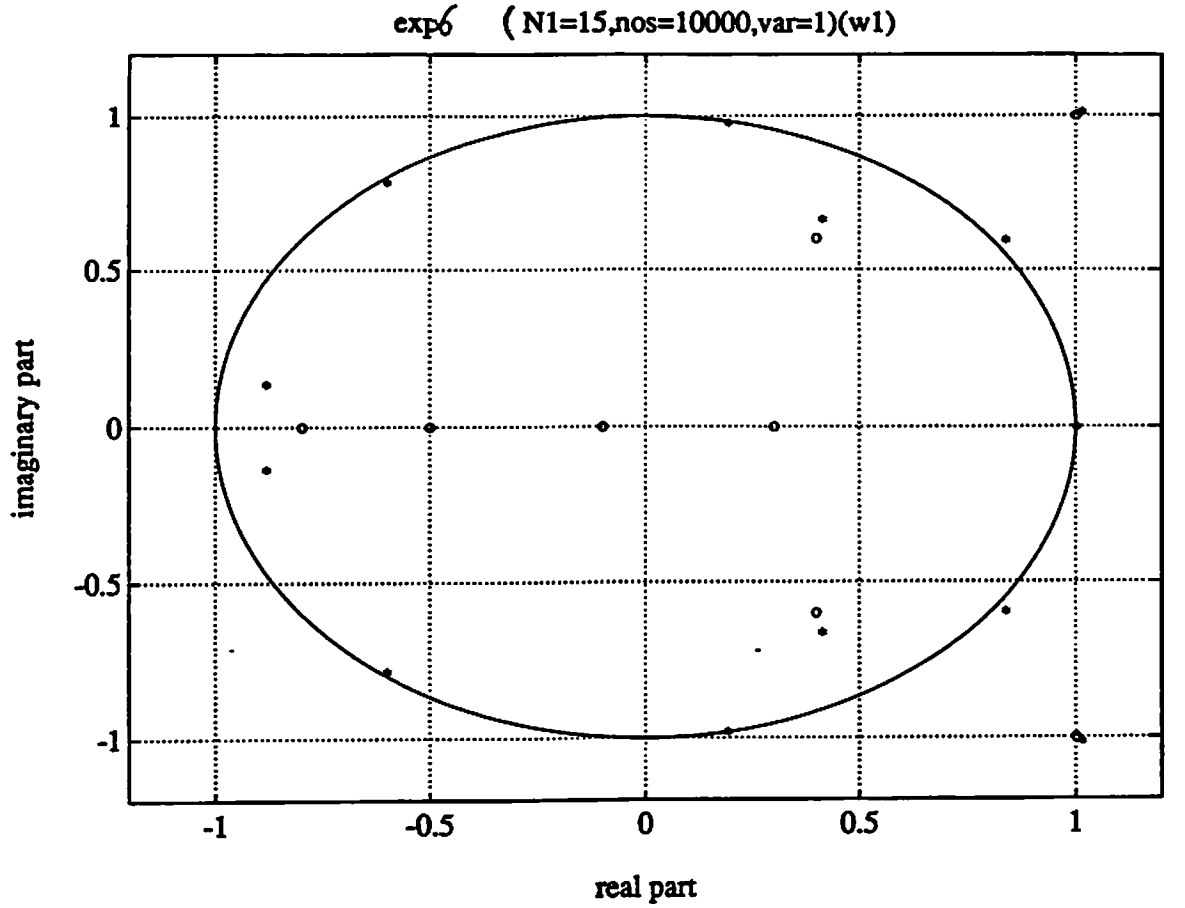

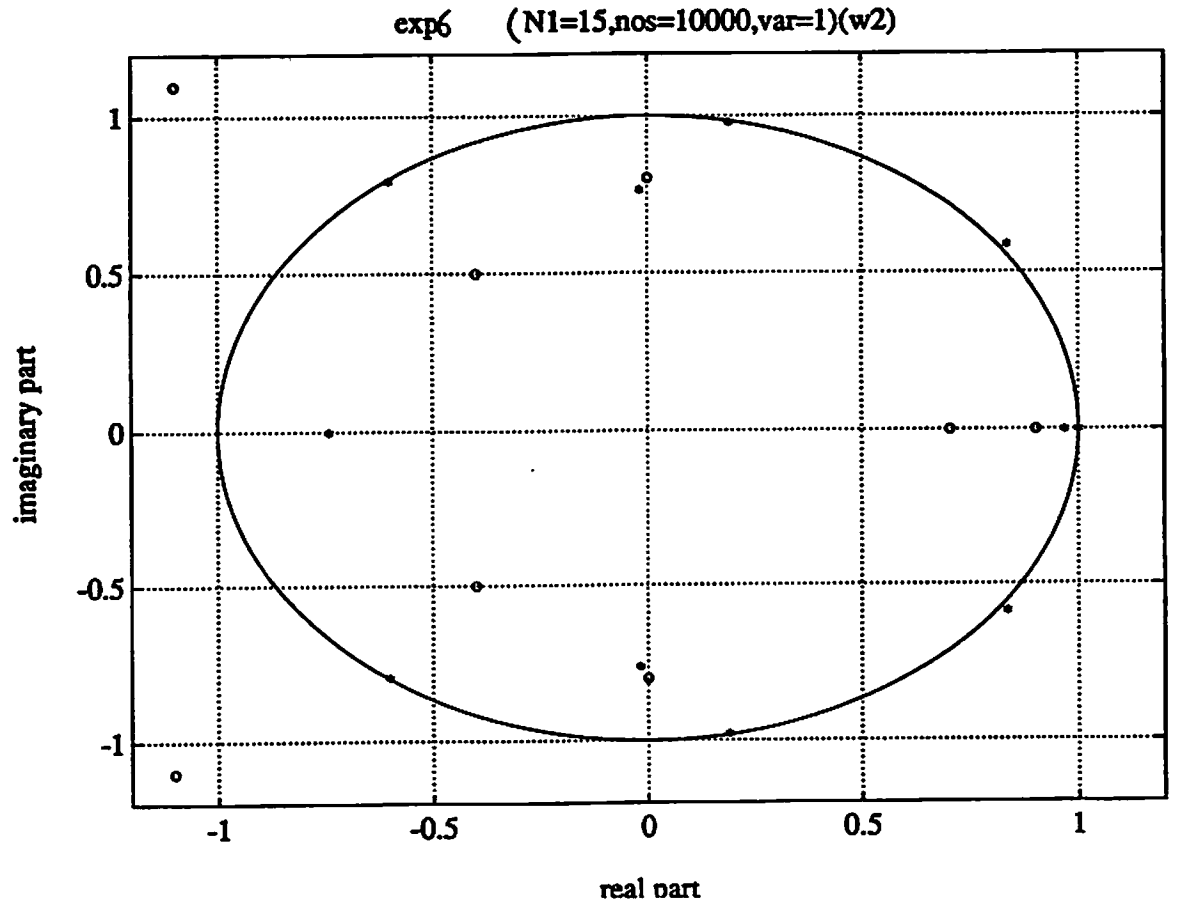

Figure 28: Adaptive channel root locations obtained by EVAM (using q_1) for SNR $\approx$ 10dB. (a) channel-1, (b) channel-2.

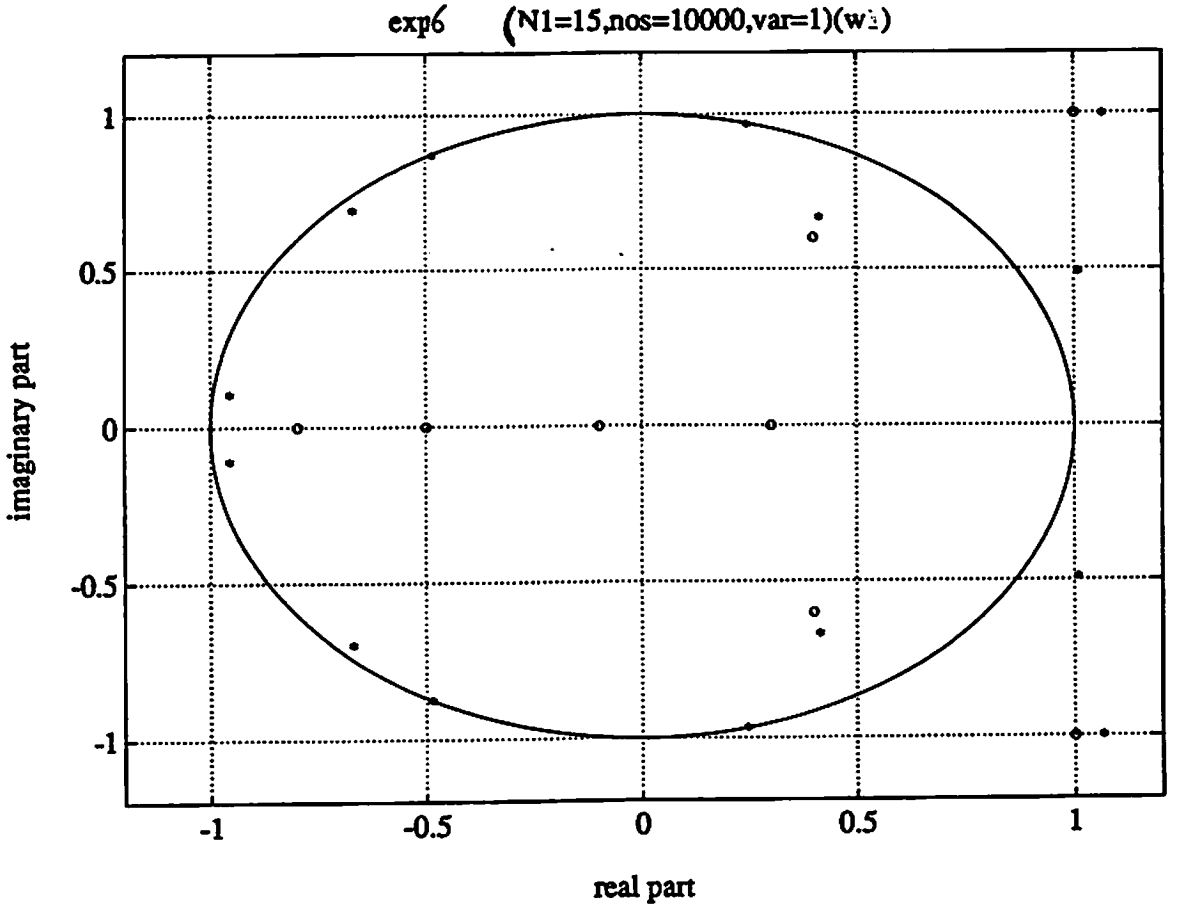

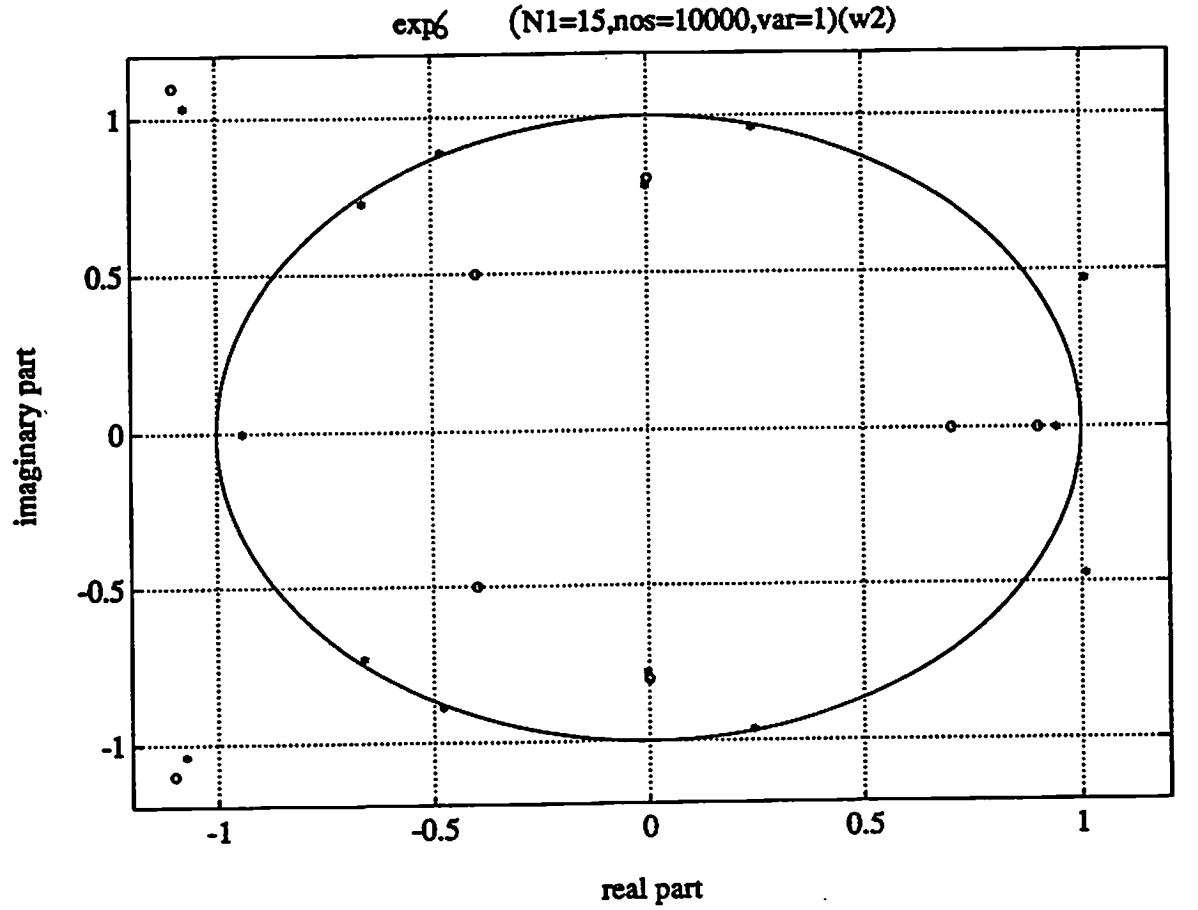

Figure 29: Adaptive channel root locations obtained by EVAM (using $\underline{q}_5$) for SNR $\approx$ 10dB. (a) channel-1, (b) channel-2.

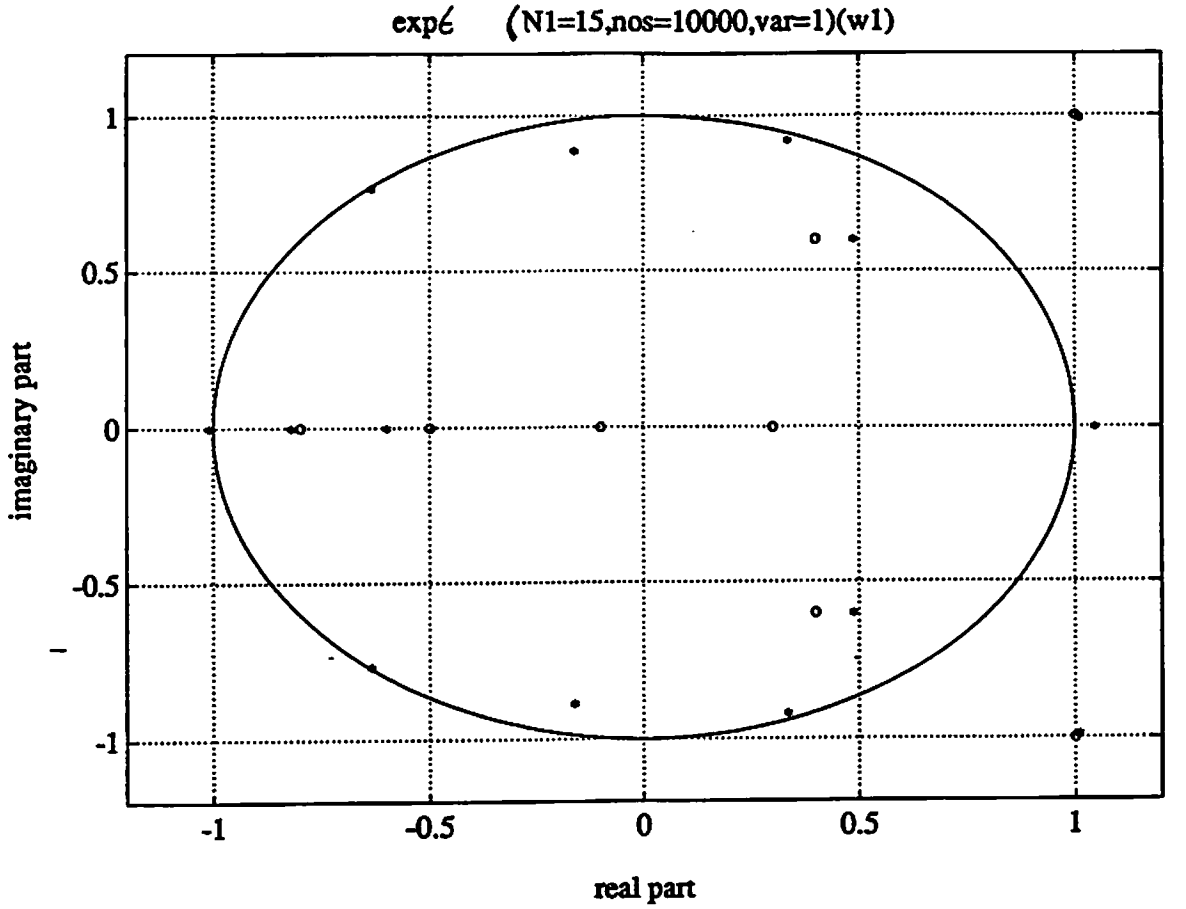

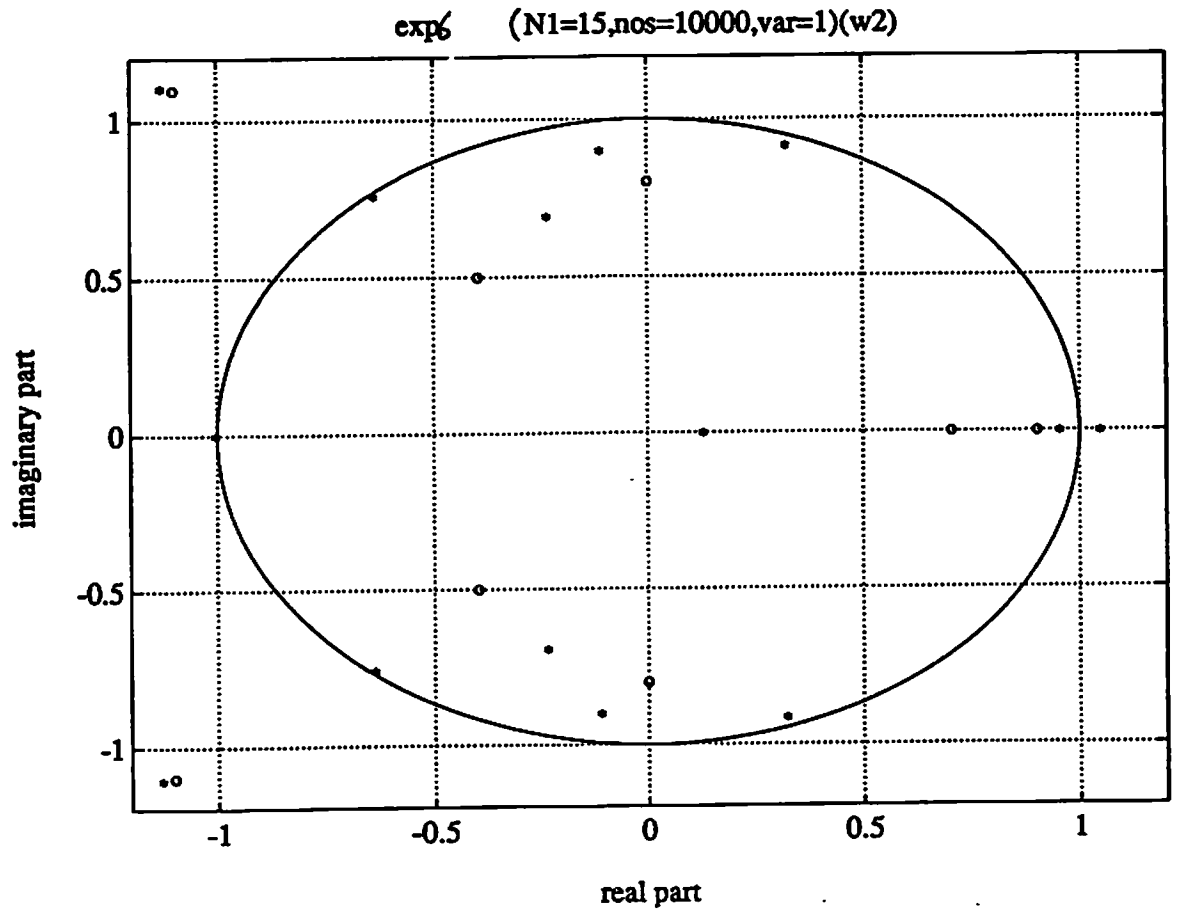

Figure 30: Adaptive channel root locations obtained by EVAM (using $\underline{q}_6$) for SNR $\approx$ 10dB. (a) channel-1, (b) channel-2.

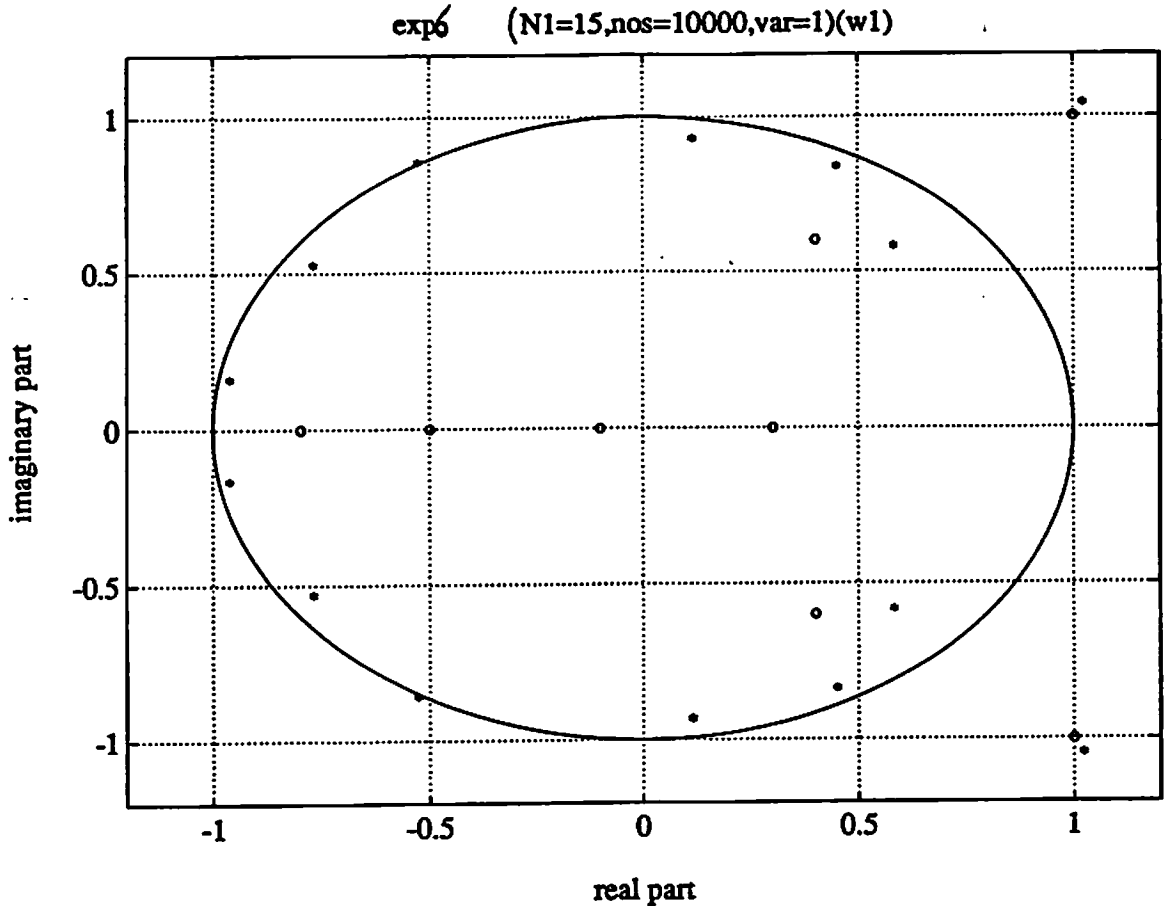

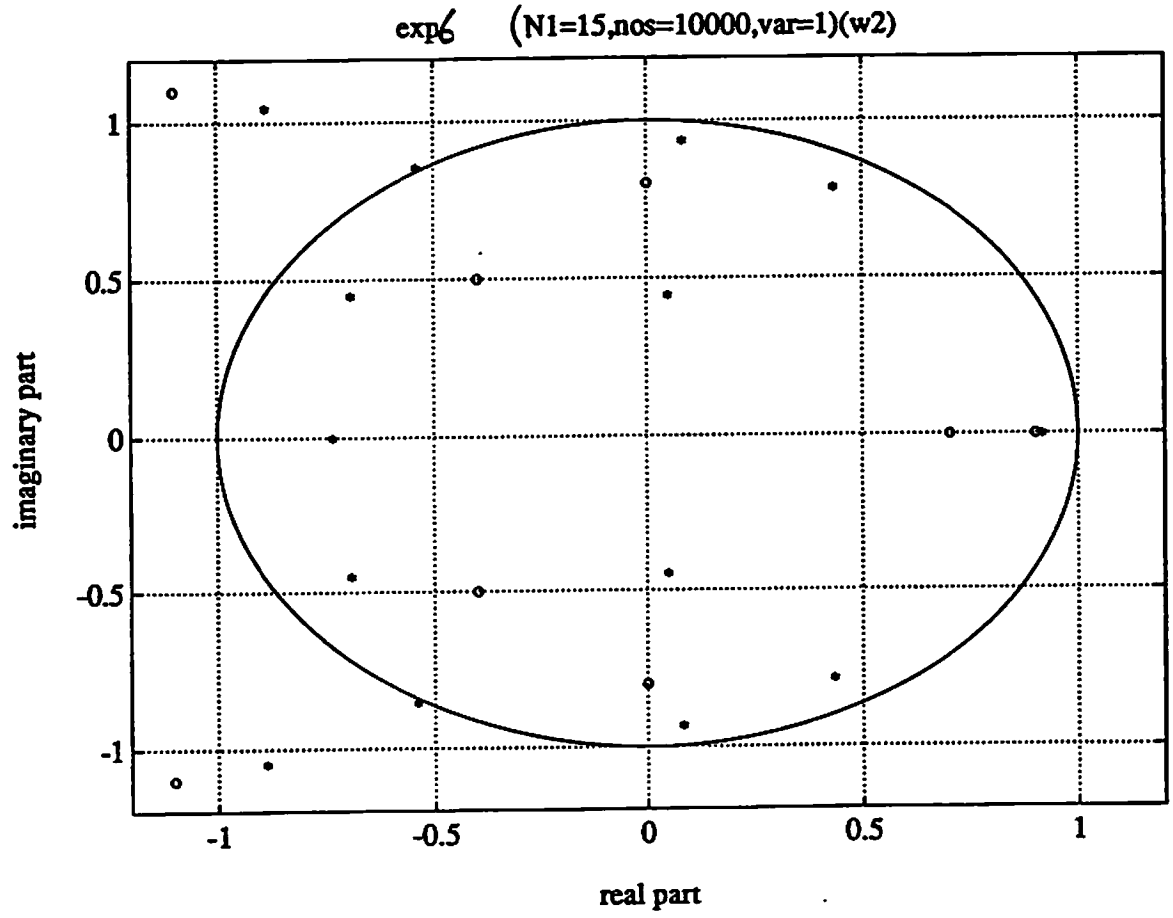

Figure 31: Adaptive channel root locations obtained by EVAM (using $\underline{q}_7$) for SNR $\approx$ 10dB. (a) channel-1. (b) channel-2.

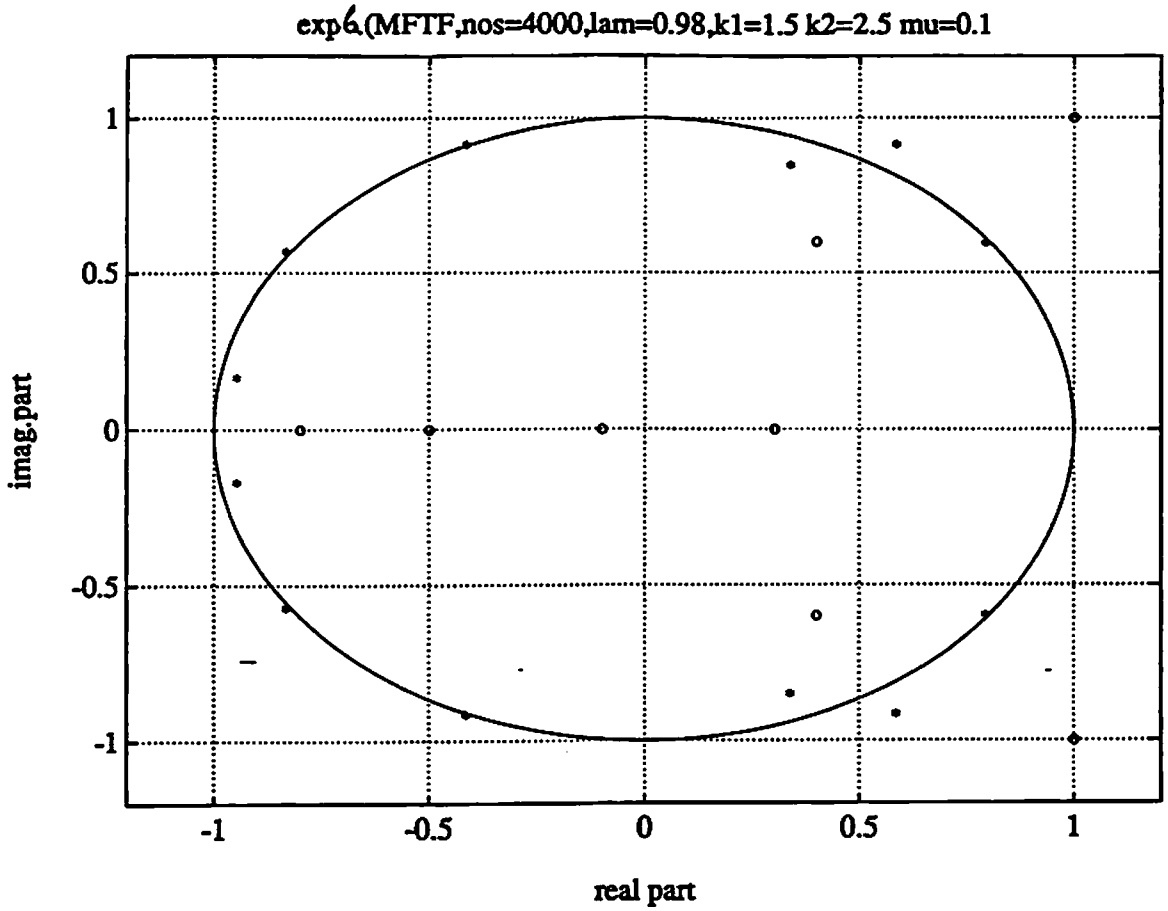

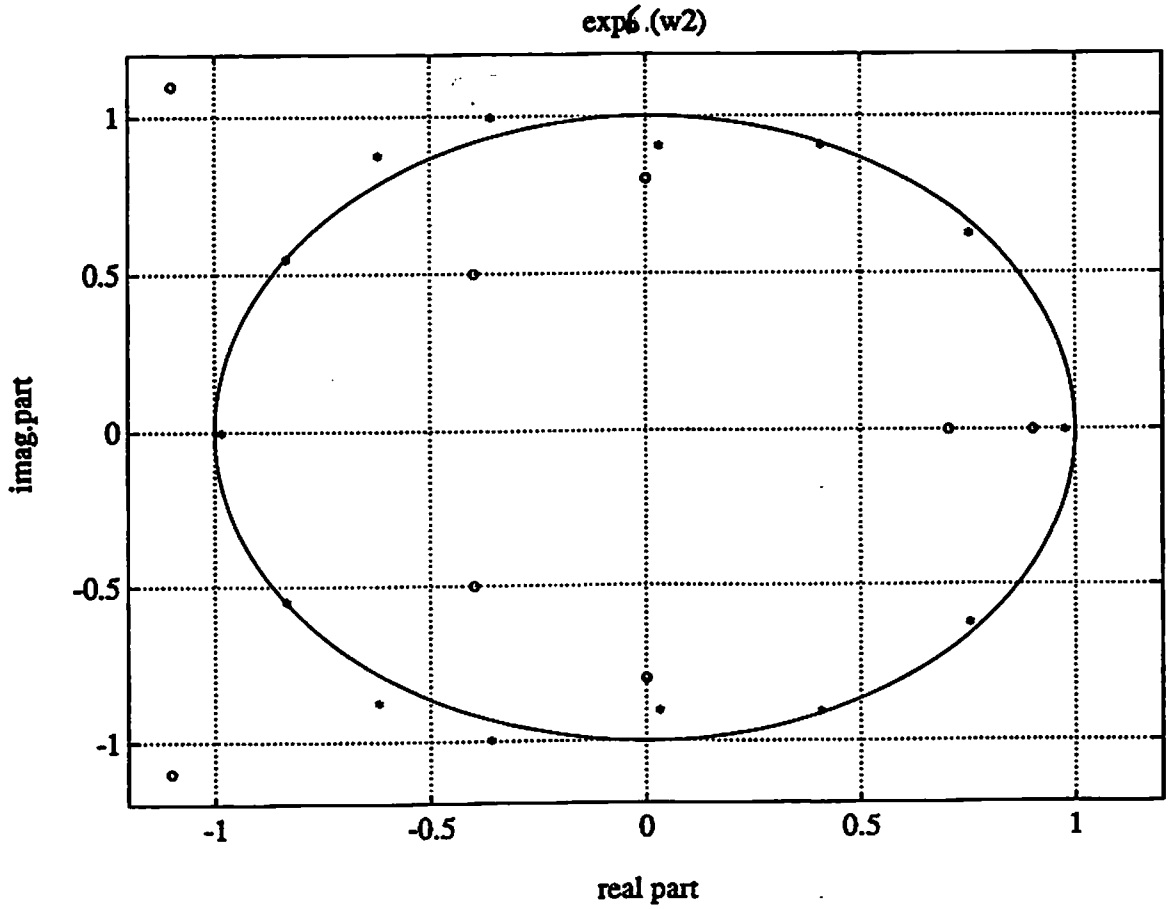

Figure 32: Adaptive channel root locations obtained by Modular RLS algorithm for SNR $\approx$ 10dB. (a) channel-1, (b) channel-2.